WESTERN DREDGING ASSOCIATION
(A Non-Profit Professional Organization)

Journal of Dredging Engineering

Volume 12, No. 1, January 2012
Official Journal of the Western Dredging Association

Dredging Flume at TU Delft

IN THIS ISSUE

AIMS & SCOPE OF THE JOURNAL

The *Journal of Dredging* is published by the Western Dredging Association (WEDA) to provide dissemination of technical and project information on dredging engineering topics. The peer-reviewed papers in this practice-oriented journal will present engineering solutions to dredging and placement problems, which are not normally available from traditional journals. Topics of interest include, but are not limited to, dredging techniques, hydrographic surveys, dredge automation, dredge safety, instrumentation, design aspects of dredging projects, dredged material placement, environmental and beneficial uses, contaminated sediments, litigation, economic aspects and case studies.

Produced and Printed by Anchor QEA, LLC on the behalf of the Western Dredging Association (WEDA)

CONSTRUCTING THE SHIELDS CURVE

PART A: FUNDAMENTALS OF THE SLIDING, ROLLING AND LIFTING MECHANISMS FOR THE ENTRAINMENT OF PARTICLES

S.A. Miedema[1]

ABSTRACT

Prediction of the entrainment of particles is an essential issue for the study of erosion phenomena in many applications. The original Shields curve describes the entrainment of many particles at many locations and is thought critical to general transport. The mechanisms involved in general are sliding, rolling and lifting, new models of which have been developed. I will introduce new concepts for the determination of the effective velocity and the acting point of the drag force, based on integration of the drag force over the cross section of the exposed particle (where earlier models were based on integration of the velocity), the behavior of turbulence intensity very close to the virtual bed level and the factor of simultaneous occurrence of the small turbulent eddies. The resulting values of the Shields parameter, based on practical and reasonable properties, are compared with data, resulting in the best correlation for the sliding mechanism with the data of many researchers. The Shields parameter found for rolling and lifting overestimates the measurements from literature. Sliding seems to be the mechanism moving the top layer of the particles, while rolling and lifting are much more mechanisms of individual particles. In the new model it is considered that in the laminar region entrainment is dominated by drag and the influence of small turbulent eddies, while in the turbulent region this is dominated by drag and lift. The transition region is modeled based on sophisticated interpolation. The model correlates very well with the original data of Shields (1936) and data of others and also matches the empirical relation of Soulsby & Whitehouse (1997) well. The model is suitable for incorporating exposure and protrusion levels and laminar main flow.

Part B of this publication gives a sensitivity analysis, describes the influence of exposure and protrusion levels and compares the model with data from different points of view like terminal settling velocity, shear stress, friction velocity, erosion flux and laminar main flow.

[1] Associate Professor & Educational Director, Offshore & Dredging Engineering, Delft University of Technology, Mekelweg 2, 2628CD Delft, The Netherlands. Email: s.a.miedema@tudelft.nl

INTRODUCTION

Erosion is displacement of solids (soil, mud, rock and other particles) usually by the agents of currents such as, wind, water, or ice by downward or down-slope movement in response to gravity (Wikipedia). Erosion can be induced by natural currents or by human intervention. The purpose of this research is to find a mechanistic, transparent mathematical formulation for the initiation of motion of particles in a flow field. This phenomenon is often referred to as erosion or scour, while also terms like threshold velocity, incipient motion and entrainment are used. A sub-goal of the research is to use as few as possible empirical coefficients (not proven by either fundamental science or scientific research) and to use practical and reasonable values for the different properties. To understand the influence of the physical phenomena involved, such as gravity, drag, lift and turbulence, a step by step approach is applied, each step adding an influence factor to the model, starting with gravity and drag, then adding lift and finally turbulence. This research is initiated out of scientific curiosity into the mechanistic background of the Shields curve.

PREVIOUS RESEARCH

Introduction

Erosion exists as long as the planet earth exists and it is one of the natural processes that has shaped or planet. In modern ages man tries to control nature and to be able to do so, man has to understand the physics behind these natural processes. Although there may have been others before, Shields (1936) was one of the first who managed to give some physical explanation to the erosion phenomena and to found this with experiments. The results of his research are shown in **Figure 1** together with the resulting theoretical curve from the current research. The original research as carried out by Shields in 1936 was based on a limited number of experiments and should be looked at in the context of the technology in that period. So it was and is a big achievement of Shields to find a relation for the initiation of motion of (spherical) particles that still holds today, although many have carried out additional research and tried to find a physical and mathematical explanation. These explanations usually incorporate phenomena such as gravity, drag, lift and turbulence and are based on sliding, rolling or lifting. Aspects such as, which velocity to use for the drag and the lift, where is the point of action of the drag force, the choice of the angle of repose and the pivoting angle are not always consistent. Especially the definition of incipient motion, is it when one particle starts moving, or many and then how many, is interpreted differently by different researchers. Some use sliding as the main mechanism, others rolling and a few lifting. Almost everybody uses the drag coefficient for spheres because many experiments are carried out for spheres, but real quarts grains have a larger drag coefficient especially at high Reynolds numbers. In general each of these models lacks one of these phenomena and/or aspects. The modeling usually stops, if a model has sufficient correlation with the data of many researchers (Buffington & Montgomery, 1997) and with the original Shields diagram (Shields, 1936).

Concept of Initiation of Motion

Dey distinguished 3 types of concepts for the definition of initiation of motion (Dey, 1999). The first type of concept is based on bed particle motion through visual observations. Kramer (1935) defined 4 different bed shear conditions, (1) no transport, (2) weak transport, (3) medium transport and (4) general transport. Although clear limits between these 4 levels do not exist, Kramer defined threshold shear stress to be the stress initiating general transport. Vanoni (1975) distinguished 5 levels, (1) no transport, (2) negligible transport, (3) small transport, (4) critical transport and (5) general transport. The Delft Hydraulics Laboratory carried out research in the sixties and seventies (DHL, 1972) and distinguished 7 levels of erosion, (1) occasional particle movement at some locations, (2) frequent particle movement at some locations, (3) frequent particle movement at many locations, (4) frequent particle movement at nearly all locations, (5) frequent particle movement at all locations, (6) permanent particle movement at all locations and (7) general transport. Graf and Pazis also distinguishes 4 levels of erosion but based it on the number of particles per unit area being entrained (Graf & Pazis, 1977), (1) N=1, (2) N=10, (3) N=100 and (4) N=1000. All the measurements show that the highest level (general transport) gives values in the Shields diagram slightly above the Shields curve. The Shields curve matches measurements between critical and general transport (Vanoni, 1975), between N=100 and N=1000 (Graf & Pazis, 1977) and between frequent particle movement at all locations and general transport (DHL, 1972).

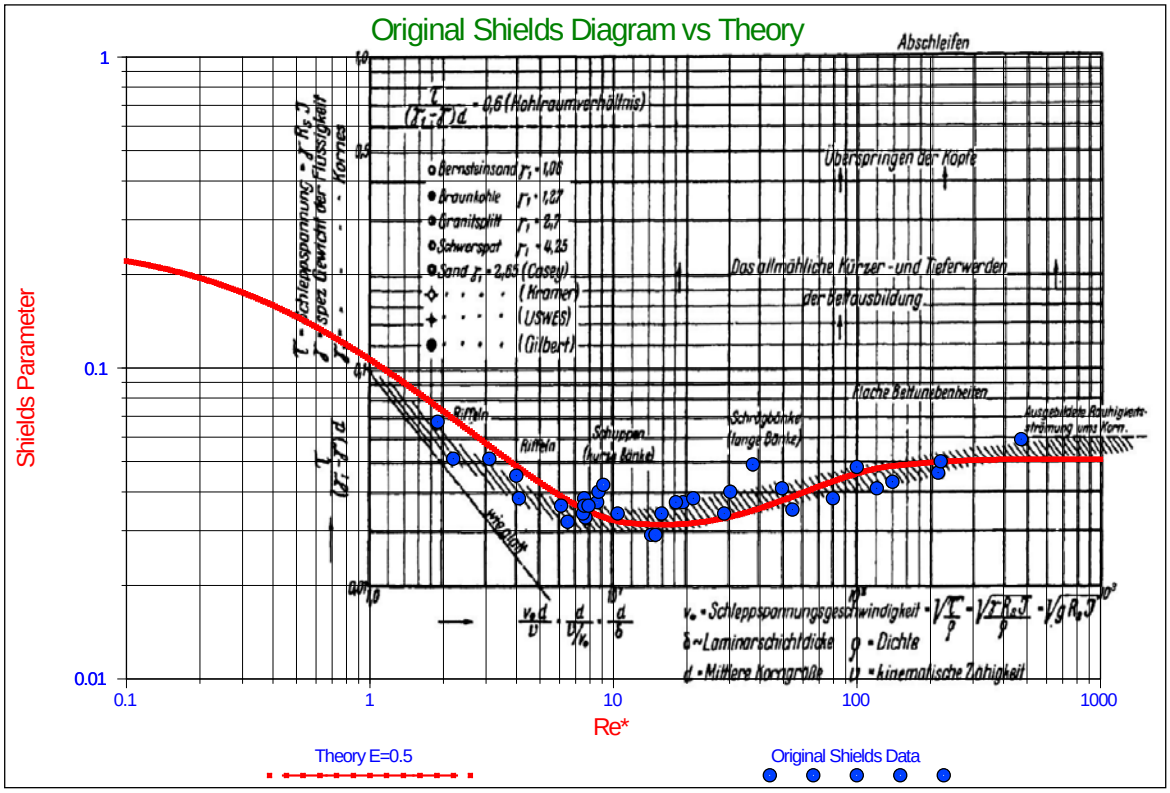

Figure 1: The original Shields diagram (Shields, 1936) and the resulting theoretical curve from the current research

The second type of concept is based on sediment flux in such a way that sediment threshold is the shear stress at which the extrapolated sediment flux becomes zero (Shields, 1936). USWES however set a concept of sediment threshold that tractive force results in a general motion of bed particles (USWES, 1936). Later this was changed to sediment threshold as a minimum flux.
The third type of concept is based on field measurements in marine environments.

Dey (and many others) concludes that the inconsistencies of these concepts lead to widely varying results (Dey, 1999), although the results of Vanoni (1975), Delft Hydraulics (1972) and Graf & Pazis (1977) show consistency. Maybe part of the scatter is caused by not understanding the physics of erosion completely. **Figure 2** gives an impression of the scatter of a collection of measurements found in Yalin & Karahan (1979) and used in publications of Julien (1995) and Zanke (2003), complemented with measurements from different sources.

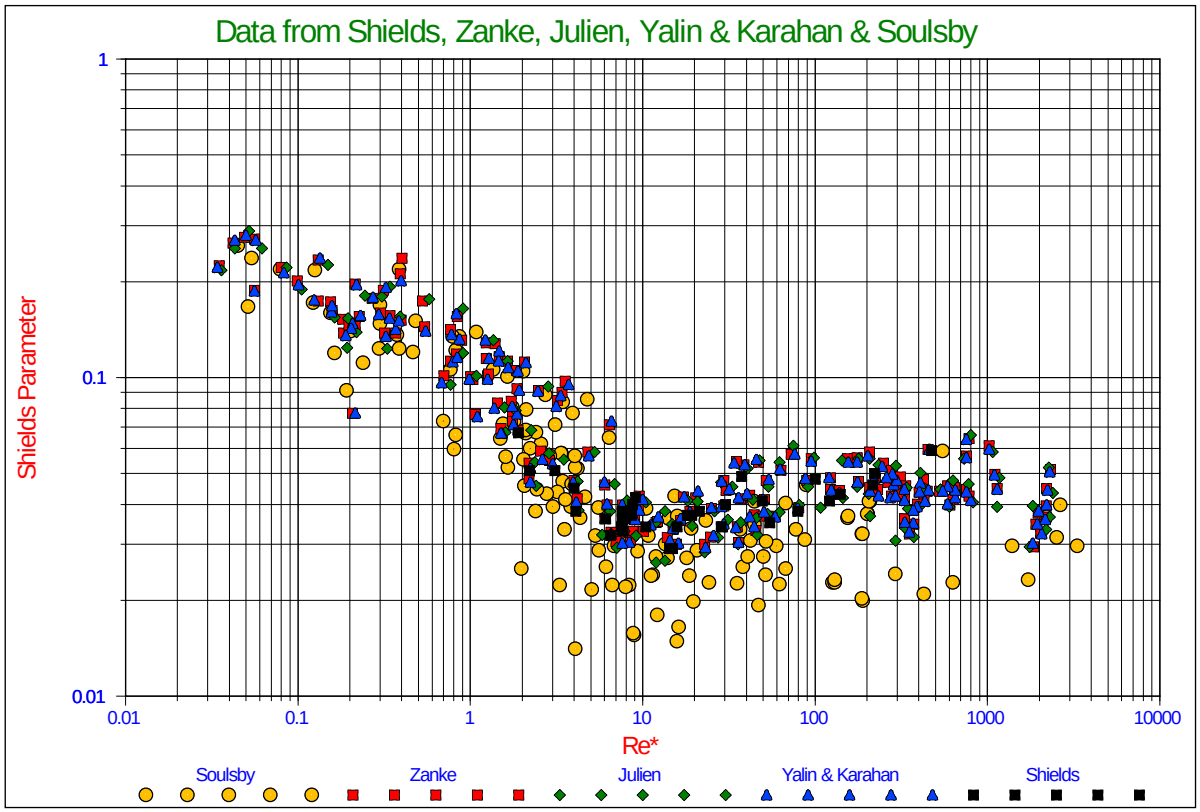

Figure 2: Data digitized and copied from Zanke (2003), Julien (1995), Yalin & Karahan (1979), Shields (1936) and others

Models on Sediment Threshold

Since there are many models available, only the most relevant ones, in the context of this paper, will be discussed. Shields (1936) introduced the fundamental concepts for initiation of motion and made a set of observations (see **Figure 1**) that have become legendary. From dimensional analysis and fluid mechanics considerations he deduced the relation between the ratio of the bed shear stress $\tau_b = \rho_f \cdot u_*^2$ and the gravitational force on a particle $(\rho_s - \rho_f) \cdot g \cdot d$ as a function of the boundary Reynolds number $Re_* = u_* \cdot d / \nu$. Based on curve fitting on his observations, the famous Shields curve was born. Later many experiments were carried out by numerous scientists of whom Buffington & Montgomery give a nice summary (Buffington & Montgomery, 1997). Buffington also gives critical analyses of the developments since Shields did his first findings (Buffington, 1999). In fact Shields did not derive a model or an equation, but published his findings as a graph (**Figure 1**). It is inconvenient that the Shields diagram is implicit; the friction velocity u_* appears in both the horizontal and the vertical axis. However with modern computers this should not be any problem.

Although less famous, Hjulstrom also carried out his research in the thirties (Hjulstrøm, 1935) and (Hjulstrøm, 1939). He presented his work in a graph showing the relation between the erosion velocity (average velocity above the bed) and the grain diameter. The graph, although explicit, depends on the water height, standard a height of 100 cm is used. For a certain water height, the Shields diagram can be converted to the Hjulstrom diagram. A mathematical description of the Hjulstrom diagram could not be found.
The equilibrium of a single particle resting on a granular bed was studied by White (1940). He obtained an expression for the threshold shear stress, but neglected the lift force. Later Kurihara (1948) extended the model and proposed some empirical equations for the estimation of threshold shear stress.

Egiazaroff (1965) found a relation between the threshold shear stress and the particle Reynolds number. He assumed that at the moment of incipient motion the velocity at a height of $0.63 \cdot d$ is equal to the terminal settling velocity of the particle. His results did not match the original Shields data quantitatively, although some relation will exist.

An extended Shields diagram was developed by Mantz (1977) followed by a graphical representation of a large volume of data by Yalin & Karahan (1979) (see also **Figure 2**)

The Ikeda-Coleman-Iwagaki model was presented by Ikeda (1982) and is based on the work of Iwagaki (1956) and Coleman (1967). The model is based on the assumption that the initiation of motion mechanism is sliding. Gravity, drag and lift are taken into account, but turbulence and grain placement are neglected. The zero level for the velocity profile is taken at the base of the grain exposed to the flow and the velocity used is at the center of the grain, so at $y = d/2$. This means that the grain is exposed to drag over the full height of the grain. For $d/\delta_v < 0.5$ the velocity profile of the viscous sub-layer is applied giving $F(Re_*) = u/u_* = u_* \cdot d/(2 \cdot \nu) = Re_*/2$, while for $d/\delta_v > 2$ the logarithmic velocity profile for rough boundaries is applied giving $F(Re_*) = u/u_* = 6.77$. In the transition area, $0.5 < d/\delta_v < 2$ the fit for the velocity profile

proposed by Swamee (1993) or Reichardt (1951) can be used by setting $y = d/2$ and $k_s = d$. This leads to the following equation for the Shields parameter:

$$\theta = \frac{4}{3} \cdot \frac{\mu}{C_D + \mu \cdot C_L} \cdot \frac{1}{F(Re_*)^2} \qquad \textbf{(1)}$$

This equation is valid for horizontal beds, but the effect of a slope can easily be incorporated. Considering two angles of internal friction (repose), $\phi = 40^\circ$, ($\mu = 0.84$) and $\phi = 60^\circ$, ($\mu = 1.73$) and further assuming that $k_s = 2 \cdot d$, $C_L = 0.85 \cdot C_D$ and using the standard relations for the drag coefficient for spheres, Garcia (2008) shows the resulting curves, compared with the original Shields (1936) data (fig. 2-17). The $\phi = 40^\circ$ curve underestimates the values of the Shields parameter compared with the original Shields data, while the $\phi = 60^\circ$ curve gets close, but still gives to small values. A $\phi = 60^\circ$ friction angle however is unreasonably high. The curve predicted follows the trend of Shields data, but is about a factor 1.6 smaller for the $\phi = 40^\circ$ case. A predecessor of this model was advanced by Egiazaroff (1965).

The Wiberg & Smith (1987A) model is based on the assumption that the initiation of motion mechanism is rolling. Gravity, drag and lift are taken into account and to some extend also turbulence. The equilibrium of moments around a pivot point is taken, where the location of the pivot point is defined as the contact point with an underlying particle under an angle ϕ_0 with the vertical. This angle is named the particle angle of repose or the dilatation angle. This angle differs from the internal friction angle, as used in the Ikeda-Coleman-Iwagaki model, because the internal friction angle (angle of natural repose) is a global soil mechanical parameter, where local variations are averaged out, while the pivot angle is a local angle matching a specific configuration of the grains. The resulting Wiberg-Smith equation is almost equal to the Ikeda-Coleman-Iwagaki equation apart from the difference between the internal friction angle (using the friction coefficient) in equation **(1)** and the pivot angle in equation **(2)**.

$$\theta = \frac{4}{3} \cdot \frac{\tan(\phi_0)}{C_D + \tan(\phi_0) \cdot C_L} \cdot \frac{1}{F(Re_*)^2} \qquad \textbf{(2)}$$

Wiberg & Smith (1987A) use the velocity profile as proposed by Reichardt (1951) providing a smooth transition between the viscous sub layer and the logarithmic profile. A lift coefficient of $C_L = 0.2$ is applied in the turbulent region, while it is assumed that particles residing completely in the viscous sub layer are not subject to lift. The calculations are carried out using $\phi_0 = 50^\circ$ and $\phi_0 = 60^\circ$ with $k_s = d$. In Wiberg & Smith (1987B) the average velocity on the particle is applied, giving $F(Re_*) = 6.0$ for the hydraulic rough region. The model matches the original Shields data well for the turbulent rough region for $\phi_0 = 60^\circ$, but overestimates the Shields data for the laminar flow in the viscous sub layer. The first conclusion does not come as a surprise, since $\phi_0 = 60^\circ$ is equal to $\mu = 1.73$ in the Ikeda-Coleman-Iwagaki model and Wiberg & Smith use a smaller lift

coefficient, resulting in a slightly higher curve. For the small Reynolds numbers the resulting curve overestimates the original Shields data. Wiberg & Smith (1987A) solve this by introducing turbulence. They state that periodic intrusions of high momentum fluid erode the viscous sub layer and produce locally higher boundary stresses. When the instantaneous boundary shear stress is sufficiently large, movement is more likely. To implement this, the thickness of the viscous sub layer is reduced to 60%, maintaining the momentum of the flow, resulting in higher instantaneous velocities by a factor 1.66. This lowers the curve in the lower Reynolds area and gives a good match with the Shields data. This effect of turbulence however is the same for the whole lower Reynolds area and influences the asymptotic value of the Shields curve going to a Reynolds number of zero.

Dey (1999) developed a detailed model based on rolling as the mechanism for incipient motion. The model includes gravity, drag and lift and even Magnus lift forces, but no turbulence. The Morsi & Alexander (1972) relation for the drag coefficient is used, while the Saffman (1965) approach for the lift force is followed. Additionally the lift due to the Magnus effect is used for large Reynolds numbers. Based on detailed mathematics the lever arms for the equilibrium of moments are derived. The average velocity acting on the sphere is determined by integration of the velocity over the actual surface of the sphere, depending on the virtual bed level. The Reichardt (1951) velocity profile is used. The resulting equation for the Shields parameter is similar to equation **(2)**, but much more detailed. There is an excellent agreement between the model developed by Dey and the experimental data used for a pivot angle of $\phi_0 = 32^\circ$. For the particle considered, a particle resting on top of 3 other particles in a dense 3D configuration, the exposure level would be near 1.0 and the protrusion level near 0.8. According to a detailed study of Luckner (2002) this would result in a pivot angle of about $\phi_0 = 20^\circ$.

Zanke (2001) and (2003) follows an approach different from all other researchers. Starting with a non-dimensional shear stress based on tilting a bed of particles and assuming that the shear stress exerted at the moment the top layer of the particles starts to move, he deducts the influences of turbulence and lift and finds a curve that is in good correlation with experimental data. The base non dimensional shear stress is set to $\theta = (1-n)\cdot\tan(\phi/1.5)$, where the porosity n is set to 0.3 and the friction angle to $\phi = 30^\circ$. This starting point can be disputed since the driving force when tilting a bed until the grains start to move is gravity, while the main influence in initiation of motion is flow. The way turbulence is incorporated, both in drag and in lift is very interesting. The basis of the turbulence influences is the equation formulated by Nezu & Nakagawa (1993) for the turbulence intensity parallel to the wall as a function to the distance to the wall. Close to the wall in the viscous sub layer the turbulence intensity is about $u^+_{r.m.s.} = 0.3\cdot y^+$, where the time averaged velocity profile is known to be $u^+ = 1\cdot y^+$. Taking $u^+_{total} = u^+ + 2.2\cdot u^+_{r.m.s.} = 1.66\cdot u^+$, should give the same result as Wiberg & Smith (1987A) found by reducing the thickness of the viscous sub layer to 60%. Zanke (2001) uses a factor of 1.8 instead of 2.2, but then his approach is completely different. Zanke (2001) must also have noticed that the asymptotic value of the curve for very low Reynolds numbers decreases when adding the influence of turbulence as stated above. Now it can be discussed whether the virtual bed level for the time averaged velocity and the turbulence intensity are exactly the same. By choosing a lower virtual bed level for the time averaged velocity, the ratio between the turbulence intensity and the time averaged velocity is zero at the virtual bed level for the turbulence intensity, resulting in an asymptotic value that is

not influenced by the turbulence. Another interesting addition in the model of Zanke (2001) is the influence of cohesion, although it is the question which fundamental forces are taken into account.

Stevenson, Thorpe & Davidson (2002) and Stevenson, Cabrejos & Thorpe (2002) look at the process of incipient motion from the perspective of chemical engineering and also incorporated the rolling resistance. For small Reynolds numbers (viscous sub layer) the lift force is neglected.
It should be noted that a number of fit equations to the Shields data exist in order to be able to calculate the Shields parameter. A well know equation is the equation of Brownlie (1981) based on the Bonneville (1963) parameter.

$$\theta = \frac{0.22}{D_*^{0.9}} + 0.06 \cdot e^{-17.77 \cdot D_*^{-0.9}} \qquad (3)$$

Soulsby & Whitehouse (1997) defined another fit equation, based on the Bonneville (1963) parameter. The two fit equations differ in the asymptotic values. Brownlie uses 0.06 for very large Reynolds numbers, while Soulsby & Whitehouse use 0.055. As we will see later, this difference is not very relevant. The asymptote for very small Reynolds values for the Brownlie equation is proportional to $Re^{-0.9}$, while Shields (1936) proposed $0.1 \cdot Re^{-1}$, but Soulsby & Whitehouse found a value of 0.3, matching the mechanistic models as shown in the equations **(1)** and **(2)**.

$$\theta = \frac{0.30}{(1 + 1.2 \cdot D_*)} + 0.055 \cdot \left(1 - e^{-0.02 \cdot D_*}\right) \qquad (4)$$

Often it is found that for real sands and gravels the values found for initiation of motion (depending on the definition of course) are smaller than the ones found with the models and with the above equations. For this reason it is proposed to divide these equations by 2 for engineering purposes. Later we will see that this matches using the C_D values for sands and gravels for large Reynolds numbers, but not for small Reynolds numbers.

Shortcomings of the Existing Models

The existing models have developed during the years and have become more and more detailed. Still some shortcomings have been found and there is space for improvement.

1. In general the exposure and protrusion levels used have not been well defined.
2. When rolling is chosen as the mechanism for the initiation of motion, there is a relation between the protrusion level and the pivot angle and this cannot be chosen freely.

3. The choice of rolling, sliding or lifting as the main mechanism for the initiation of motion has not been motivated well. It is very well possible that at high protrusion levels rolling will occur, while at low protrusion levels the mechanism is sliding and at protrusion levels around zero the mechanism is lifting. Looking at nature this does not sound unreasonable, since nature will choose the mechanism with the least resistance.
4. All models use the relations for the drag coefficient for spheres, which is reasonable realizing that many experiments are carried out for spheres, but in reality we have to deal with natural sands and gravel, so the drag coefficient for sand should be used.
5. The models do not incorporate rolling resistance which is reasonable since quarts is very hard and thus the rolling resistance is very low. Still it is interesting to investigate the influence of rolling resistance at very high protrusion levels.
6. The models are not based on lifting, which is also reasonable, since it can be proven mathematically that initiation of motion by lifting requires a higher shear stress than rolling or sliding, so sliding or rolling will already occur before lifting could occur. Unless the bed is fixed and one single grain is subjected to the flow at a very low protrusion level.
7. It is difficult to distinguish between the influence of drag and lift, since both are in the denominator of equations **(1)** and **(2)**. Considering full turbulent flow resulting in drag and lift, while turbulence is phased out due to the size of the particles in relation with the size of the small turbulent eddies and considering laminar flow resulting in drag and the influence of small turbulent eddies, enables us to tune the model on the different physical phenomena.
8. The models use the velocity at the centre of the sphere, the average velocity on the sphere or the surface averaged velocity on the sphere. Also the lever arms for rolling are sometimes chosen at the centre of the sphere or are determined by the surface averaged velocity. Since the forces on the sphere are determined by the square of the velocity in a linear or logarithmic velocity profile, the effective velocity should be determined by the surface averaged square of the velocity. This will give the actual acting point and lever arm.
9. The models are based on velocity profiles and not on the effect of the velocity on the forces on the sphere. Turbulence is a stochastic process and turbulence intensity should not be treated as a velocity profile.
10. The cross section for dragging and lifting is often chosen as the cross section of the sphere and thus chosen equal. The cross section for dragging sand lifting should depend on the protrusion and exposure levels and be different for dragging and lifting.
11. Using a velocity profile in the transition between laminar and turbulent flow is dangerous, since it is not only the velocity that changes, but also the contributions of lift and turbulence and for example the position of the acting point of the drag force.

KNOWNS AND UNKNOWNS

The models identified with equations **(1)** and **(2)** contain a number of known's and unknowns. The velocity profile and the drag coefficient can be determined theoretically or with semi-empirical equations. The viscosity (at a fixed temperature) and the Karman constant are known constants. The friction coefficient and the pivot angle can be found from many experiments or calculated geometrically. The main unknowns are the influence of turbulence and the influence of the lift coefficient. It is only useful to have different unknowns in a model if they can be isolated and measured independently. Looking at equations **(1)** and **(2)** we can see that both drag and lift are in the denominator and both drag and lift can be subject to the influence of turbulence, but then these influences cannot be isolated and measured separately. In general it can be assumed that lift does not occur in a laminar viscous flow, while the influence of small eddies is phased out for larger particles in a turbulent flow. So we will consider drag and turbulence for laminar viscous flow occurring at boundary Reynolds numbers below 5 and we will consider drag and lift for turbulent flow for boundary Reynolds numbers above 70. Since the drag based on the time averaged velocity profile is deterministic, this means that in the laminar viscous flow the only influence to make the model match the measurements is the turbulence, while in the turbulent flow the only influence to make the model match the measurements is the lift force. If there would be some lift force in the laminar viscous flow, the influence will be incorporated in the turbulence modelling, while a possible influence of turbulence in the turbulent region will be incorporated in the lift force modelling.

DEFINITIONS

Before starting with the model it is convenient to define a number of parameters as they are often used in literature.

The relative submerged specific density $\mathbf{R_d}$ is defined as:	$$\mathbf{R_d} = \frac{\rho_q - \rho_w}{\rho_w}$$	**(5)**
The term ***friction velocity*** comes from the fact that $\sqrt{\tau_b / \rho_w}$ has the same unit as velocity and it has something to do with the friction force. The bottom shear stress is often represented by friction velocity $\mathbf{u_*}$, defined by:	$$\mathbf{u_*} = \sqrt{\frac{\tau_b}{\rho_w}}$$	**(6)**
The Shields parameter θ is the ratio between the force resulting from the bottom shear stress and the force resulting from gravity:	$$\theta = \frac{\mathbf{u_*^2}}{\mathbf{R_d} \times \mathbf{g} \times \mathbf{d}}$$	**(7)**
The boundary Reynolds number:	$$\mathbf{Re_*} = \frac{\mathbf{u_*} \times \mathbf{d}}{\nu}$$	**(8)**

The roughness Reynolds number:	$\mathbf{k_s^+ = \frac{u_* \cdot k_s}{\nu}}$	**(9)**
The distance to the wall Reynolds number:	$\mathbf{y^+ = \frac{u_* \cdot y}{\nu}}$	**(10)**
The original Shields graph is not convenient to use, because both axis contain the shear velocity $\mathbf{u_*}$ and this is usually an unknown, this makes the graph an implicit graph. To make the graph explicit, the graph has to be transformed to another axis system. In literature often the dimensionless grain diameter $\mathbf{D_*}$ is used, also called the Bonneville (1963) parameter:	$\mathbf{D_* = d \cdot \sqrt[3]{\frac{R_d \cdot g}{\nu^2}}}$	**(11)**
The relation between the Shields parameter and the Bonneville parameter is:	$\mathbf{Re_* = \sqrt{\theta} \cdot D_*^{1.5}}$	**(12)**
So the Bonneville parameter is a function of the Shields number and the boundary Reynolds number according to:	$\mathbf{D_* = \left(\frac{Re_*}{\sqrt{\theta}} \right)^{2/3}}$	**(13)**
Another parameter that is often used for the horizontal axis is the so called Grant and Madsen (1976) parameter or sediment fluid parameter:	$\mathbf{S_* = \frac{D_*^{1.5}}{4} = \frac{Re_*}{4 \cdot \sqrt{\theta}}}$	**(14)**
The particle Reynolds number, which differs a factor 4 from the Grant and Madsen parameter:	$\mathbf{Re_p = D_*^{1.5} = \frac{Re_*}{\sqrt{\theta}}}$	**(15)**
The non-dimensional velocity	$\mathbf{u^+ = \frac{\overline{u(y)}}{u_*}}$	**(16)**
The non-dimensional laminar sub-layer thickness	$\mathbf{\delta_v^+ = \frac{\delta_v \cdot u_*}{\nu} = 11.6}$	**(17)**
The particle drag Reynolds number is the Reynolds number used to calculate the drag coefficient $\mathbf{C_D}$. This Reynolds number differs from the particle Reynolds number, using the effective velocity used to calculate the drag force on a particle.	$\mathbf{Re_D = \ell \cdot \alpha \cdot Re_*}$	**(18)**

VELOCITY DISTRIBUTIONS

Scientific Classification

Figure 3 shows the classification of flow layers. Starting from the bottom we have:

1. Viscous sub layer: a thin layer just above the bottom. In this layer there is almost no turbulence. Measurement shows that the viscous shear stress in this layer is constant. The flow is laminar. Above this layer the flow is turbulent.
2. Transition layer: also called buffer layer. Viscosity and turbulence are equally important.
3. Turbulent logarithmic layer: viscous shear stress can be neglected in this layer. Based on measurement, it is assumed that the turbulent shear stress is constant and equal to bottom shear stress. It is in this layer where Prandtl introduced the mixing length concept and derived the logarithmic velocity profile.
4. Turbulent outer layer: velocities are almost constant because of the presence of large eddies which produce strong mixing of the flow.

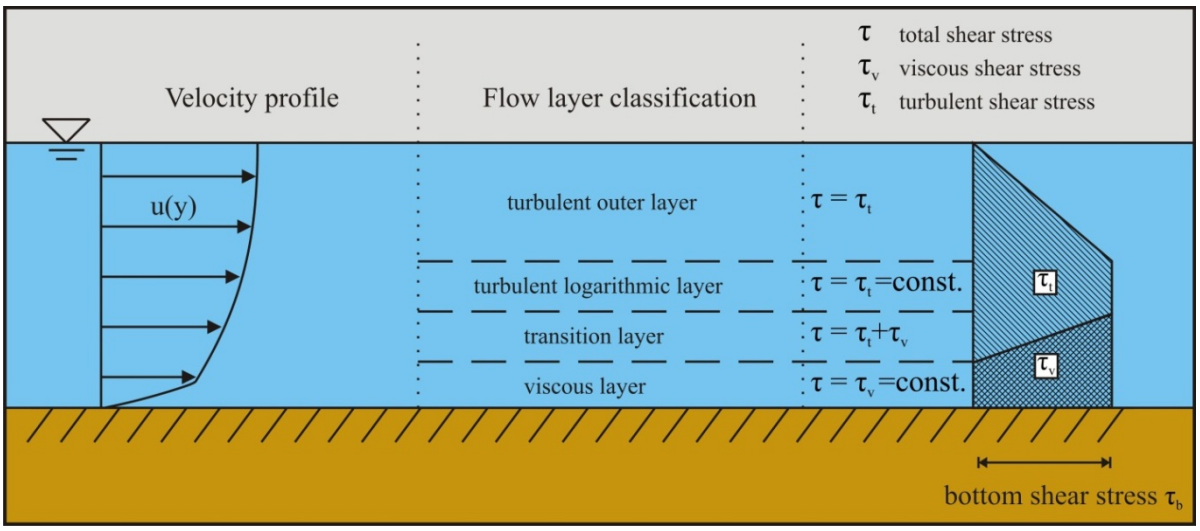

Figure 3: Scientific classification of flow region (Layer thickness is not to scale, turbulent outer layer accounts for 80% - 90% of the region) (Liu Z. , 2001)

Engineering Classification

In the turbulent logarithmic layer the measurements show that the turbulent shear stress is constant and equal to the bottom shear stress. By assuming that the mixing length is proportional to the distance to the bottom (**ℓ=κy**), Prandtl obtained the logarithmic velocity profile. Various expressions have been proposed for the velocity distribution in the transitional layer and the turbulent outer layer. None of them are widely accepted. However, by the modification of the mixing length assumption, see next section, the logarithmic velocity profile applies also to the transitional layer and the turbulent outer layer. Measurement and computed velocities show reasonable agreement. Therefore in engineering point of view, a turbulent layer with the

logarithmic velocity profile covers the transitional layer, the turbulent logarithmic layer and the turbulent outer layer, see Figure 3.

As to the viscous sub layer. The effect of the bottom (or wall) roughness on the velocity distribution was first investigated for pipe flow by Nikuradse. He introduced the concept of equivalent grain roughness $\mathbf{k_s}$ (Nikuradse roughness, bed roughness). Based on experimental data, it was found that:

1. Hydraulically smooth flow for $\frac{u_* \cdot k_s}{\nu} \leq 5$, Bed roughness is much smaller than the thickness of viscous sub layer. Therefore, the bed roughness will not affect the velocity distribution.
2. Hydraulically rough flow for $\frac{u_* \cdot k_s}{\nu} \geq 70$, Bed roughness is so large that it produces eddies close to the bottom. A viscous sub layer does not exist and the flow velocity is not dependent on viscosity.
3. Hydraulically transitional flow for $5 \leq \frac{u_* \cdot k_s}{\nu} \leq 70$, The velocity distribution is affected by bed roughness and viscosity.

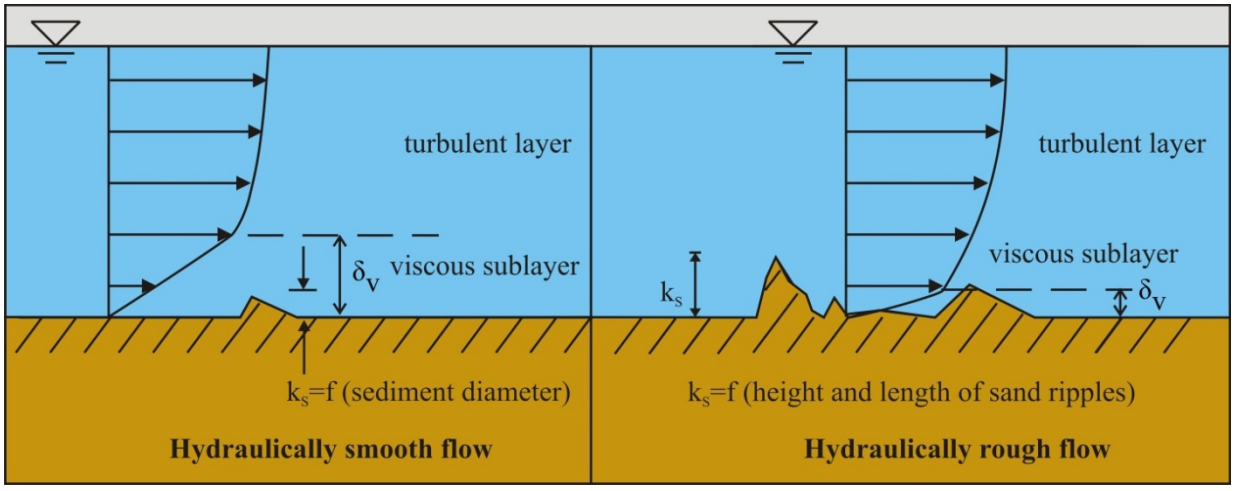

Figure 4: Engineering classification of flow region (Layer thickness is not to scale) (Liu Z. , 2001)

Turbulent Layer

In the turbulent layer the total shear stress contains only the turbulent shear stress. The total shear stress increases linearly with depth (equation **(19)** or **Figure 4**), i.e.

$$\tau_t(y) = \tau_b \cdot \left(1 - \frac{y}{h}\right) \qquad \textbf{(19)}$$

By Prandtl's mixing length theory:

$$\tau_t = \rho \cdot \ell^2 \left(\frac{du}{dy} \right)^2 \quad \textbf{(20)}$$

And assuming for the mixing length:

$$\ell = \kappa \cdot y \cdot \left(1 - \frac{y}{h} \right)^{0.5} \quad \textbf{(21)}$$

With **κ** the Von Karman constant (**κ=0.412**) and **h>>y**, we get:

$$\frac{du}{dy} = \frac{1}{\kappa \cdot y} \cdot \sqrt{\frac{\tau_b}{\rho}} = \frac{u_*}{\kappa \cdot y} \quad \textbf{(22)}$$

Integration of the equation gives the famous logarithmic velocity profile (law of the wall):

$$u(y) = \frac{u_*}{\kappa} \cdot \ln \left(\frac{y}{y_0} \right) \quad \textbf{(23)}$$

Where the integration constant y_0 is the elevation corresponding to zero velocity ($u_{y=y0}=0$), given by Nikuradse by the study of the pipe flows.

$$y_0 = 0.11 \cdot \frac{\nu}{u_*} \qquad \text{Hydraulically smooth flow} \qquad \frac{u_* \cdot k_s}{\nu} \le 5 \quad \textbf{(24)}$$

$$y_0 = 0.033 \cdot k_s \qquad \text{Hydraulically rough flow} \qquad \frac{u_* \cdot k_s}{\nu} \ge 70 \quad \textbf{(25)}$$

$$\frac{y_0}{k_s} = \frac{1}{9 \cdot k_s^+} + \frac{1}{30} \cdot \left(1 - e^{-\frac{k_s^+}{26}} \right) \qquad \text{Hydraulically transition flow} \qquad 5 < \frac{u_* \cdot k_s}{\nu} < 70 \quad \textbf{(26)}$$

It is interesting to note that the value of the friction velocity u_*, which, by definition, has nothing to do with velocity, is the value of the flow velocity at the elevation $y=y_0.e^{\kappa}$, thus:

$$u_{y=y_0 \cdot e^{\kappa}} = u_* \quad \textbf{(27)}$$

Viscous Sub Layer

In the case of hydraulically smooth flow there is a viscous sub layer. Viscous shear stress is constant in this layer and equal to the bottom shear stress, i.e.

$$\tau_\nu = \rho \cdot \nu \cdot \frac{du}{dy} = \tau_b \tag{28}$$

Integrating and applying $\mathbf{u_{y=0}=0}$ gives:

$$u(y) = \frac{\tau_b}{\rho} \cdot \frac{y}{\nu} = \frac{u_*^2}{\nu} \cdot y = y^+ \cdot u_* \tag{29}$$

Thus, there is a linear velocity distribution in the viscous sub layer. The linear velocity distribution intersects with the logarithmic velocity distribution at the elevation $y = 11.6 \cdot \nu / u_*$, yielding a theoretical viscous sub layer thickness δ_ν:

$$\delta_\nu = 11.6 \cdot \frac{\nu}{u_*} \tag{30}$$

The velocity profile is illustrated in **Figure 6**, with the detailed description of the fluid velocity near the bottom.

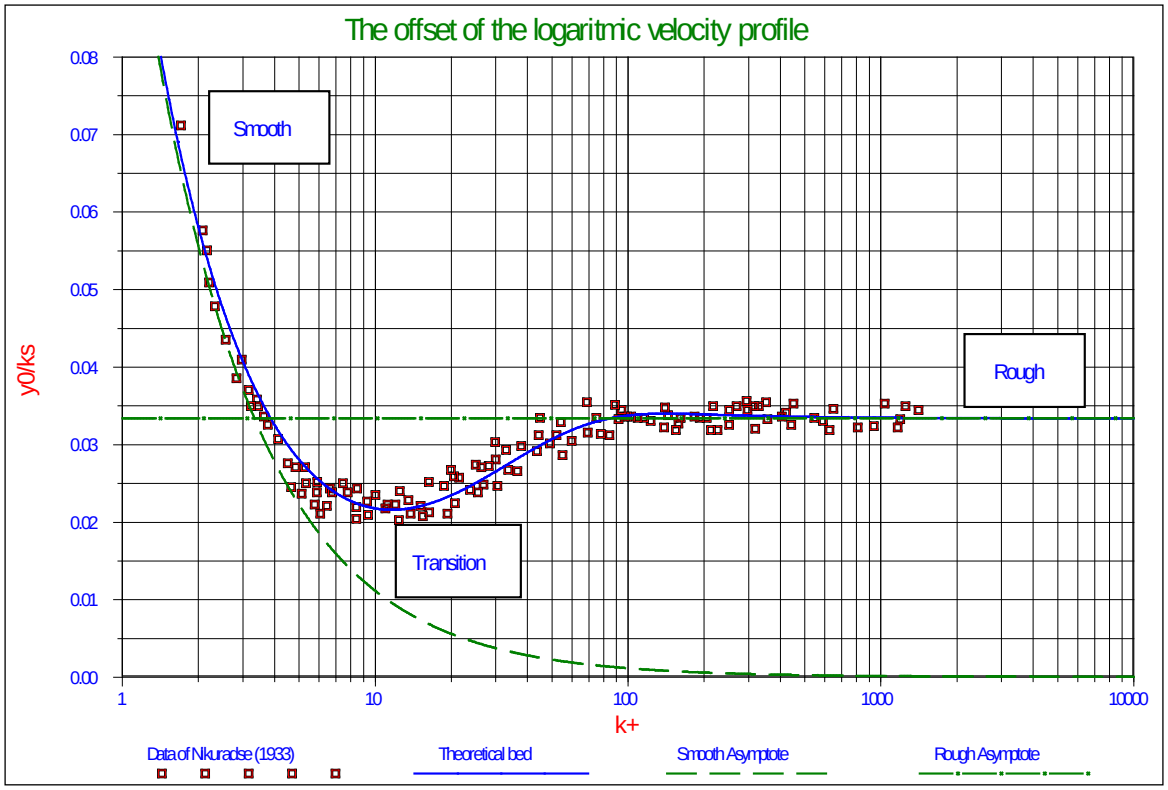

Figure 5: The transition smooth-rough (Guo & Julien, 2007)

Bed Roughness

The bed roughness $\mathbf{k_s}$ is also called the equivalent Nikuradse grain roughness, because it was originally introduced by Nikuradse in his pipe flow experiments, where grains are glued to the smooth wall of the pipes. The only situation where we can directly obtain the bed roughness is a flatbed consisting of uniform spheres, where $\mathbf{k_s}$ = diameter of sphere. But in nature the bed is composed of grains with different size. Moreover, the bed is not flat, various bed forms, e.g. sand ripples or dunes, will appear depending on grain size and current. In that case the bed roughness can be obtained indirectly by the velocity measurement.

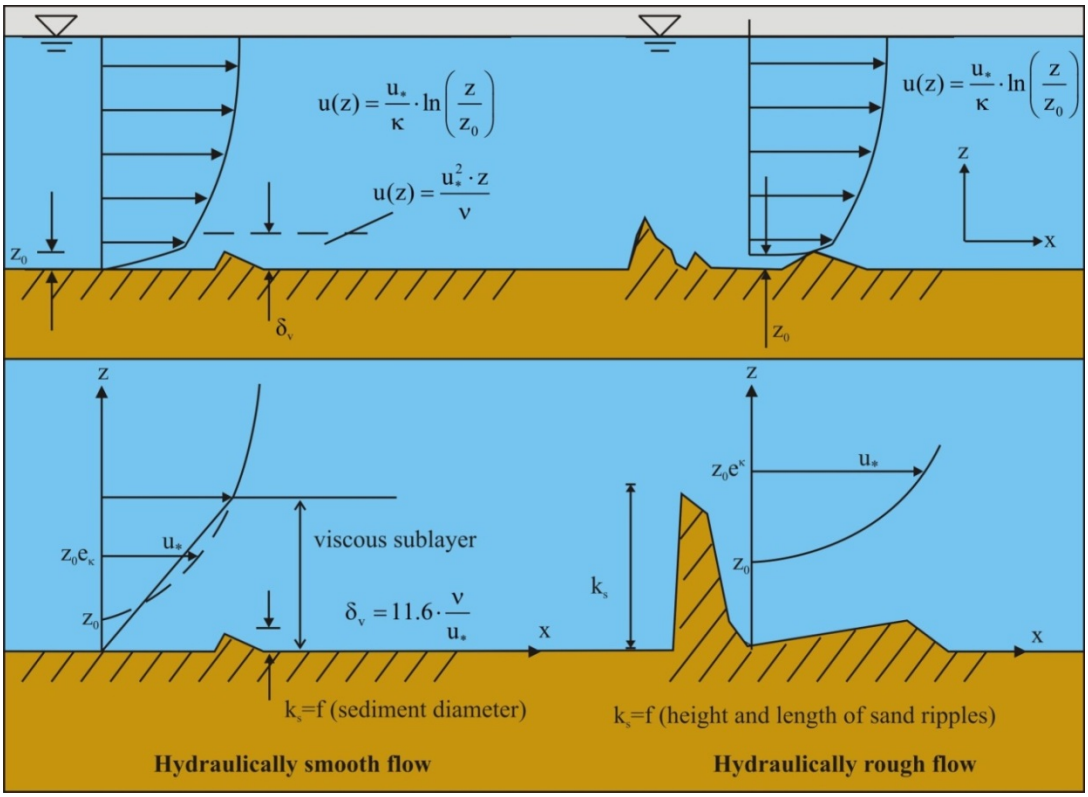

Figure 6: Illustration of the velocity profile in hydraulically smooth and rough flows (Liu Z. , 2001)

The Transition Laminar-Turbulent

Reichardt (1951) derived an equation for the velocity that describes a laminar linear profile up to an $\mathbf{y^+}$ value of about 5, a turbulent logarithmic profile from an $\mathbf{y^+}$ value of about 40 and a transition velocity profile from 5 to 40 that is in excellent agreement with measurements made in that zone (see Schlichting (1968), p. 601). Equation **(31)** and **Figure 7** show this velocity profile. Wiberg & Smith (1987A) and others also use this velocity profile.

$$\frac{u(y)}{u_*} = \frac{\ln(1+\kappa\cdot y^+)}{\kappa} - \frac{\ln(1/9)+\ln(\kappa)}{\kappa}\cdot\left(1-e^{-\frac{y^+}{11.6}} - \frac{y^+}{11.6}e^{-0.33\cdot y^+}\right) \qquad (31)$$

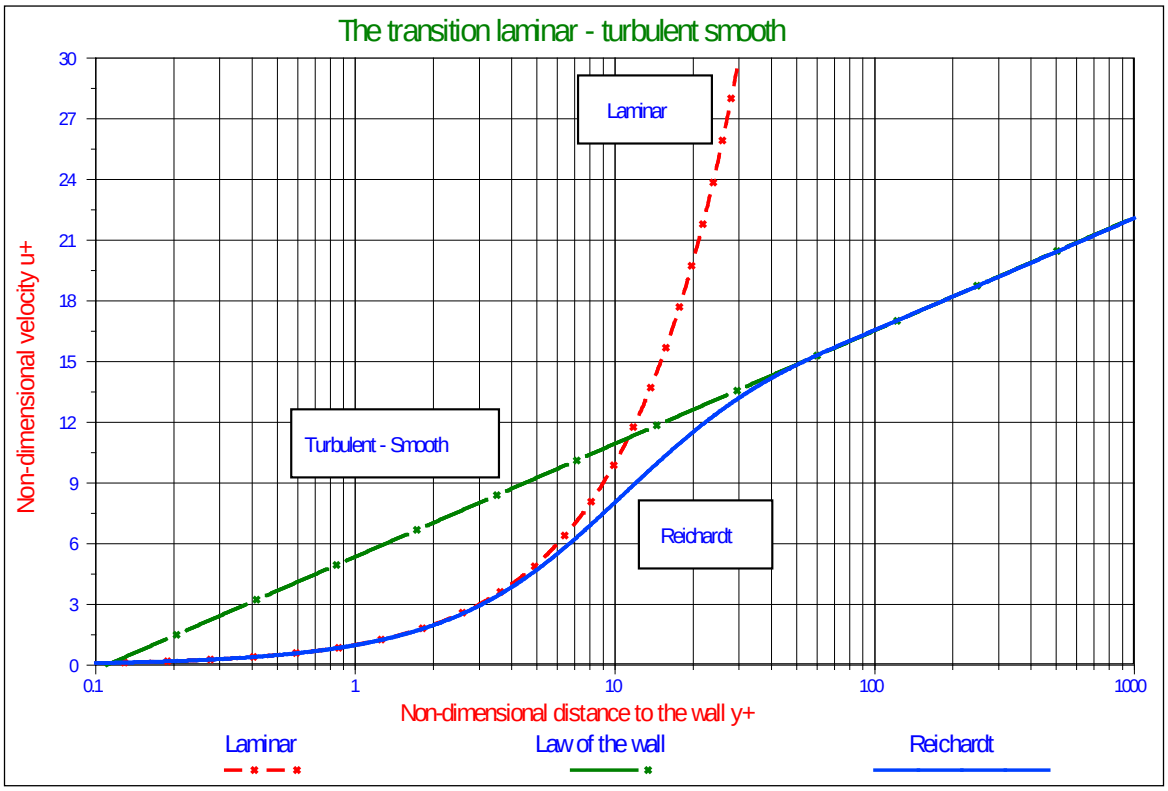

Figure 7: The velocity profile from laminar to smooth-turbulent

The Transition Smooth-Rough

The transition between hydraulic smooth and rough flow can be approximated in many ways, but the resulting equation should match measurements like shown in Garcia (2008) (fig. 2.3). The following equations (derived by the author), give a very good approximation of this transition, where the distance to the wall equals the roughness. Equation (32) gives the velocity as a function of the non-dimensional distance to the wall $\mathbf{y^+}$ (equation (10)) and the non-dimensional roughness $\mathbf{k_s^+}$ (equation (9)).

$$\frac{\bar{u}(y^+)}{u_*} = \frac{1}{\kappa}\cdot\ln\left(\frac{y^+}{0.11}\right)\cdot e^{-0.95\cdot\frac{k_s^+}{11.6}} + \frac{1}{\kappa}\cdot\ln\left(\frac{y^+}{0.033\cdot k_s^+}\right)\cdot\left(1-e^{-0.95\cdot\frac{k_s^+}{11.6}}\right) \qquad (32)$$

Since $11.6 = \delta_v\cdot u_*/\nu = \delta_v^+$ and $0.11 = 0.11\cdot\delta_v\cdot u_*/\nu/11.6 = 0.0095\cdot\delta_v^+$ and the influence of the second right hand term (giving 95 instead of 105), equation **(32)** can be written as:

$$\frac{\bar{u}(y^+)}{u_*} = \frac{1}{\kappa}\cdot\ln\left(95\cdot\frac{y^+}{\delta_v^+}\right)\cdot e^{-0.95\cdot\frac{k_s^+}{\delta_v^+}} + \frac{1}{\kappa}\cdot\ln\left(30\cdot\frac{y^+}{k_s^+}\right)\cdot\left(1-e^{-0.95\cdot\frac{k_s^+}{\delta_v^+}}\right) \qquad (33)$$

In terms of the dimensional parameters for the distance to the wall $\mathbf{y}$, the roughness $\mathbf{k_s}$ and thickness of the laminar layer $\boldsymbol{\delta_v}$ this gives:

$$\frac{\bar{u}(y)}{u_*} = \frac{1}{\kappa}\cdot\ln\left(95\cdot\frac{y}{\delta_v}\right)\cdot e^{-0.95\cdot\frac{k_s}{\delta_v}} + \frac{1}{\kappa}\cdot\ln\left(30\cdot\frac{y}{k_s}\right)\cdot\left(1-e^{-0.95\cdot\frac{k_s}{\delta_v}}\right) \qquad (34)$$

Figure 8 shows the non-dimensional velocity $\mathbf{u^+}$ at distances $\mathbf{y=k_s}$, $\mathbf{y=0.9k_s}$, $\mathbf{y=0.8k_s}$, $\mathbf{y=0.7k_s}$, $\mathbf{y=0.6k_s}$, $\mathbf{y=0.5k_s}$ and, $\mathbf{y=0.4k_s}$ from the wall. Up to a Reynolds number of 20 and above a Reynolds number of 70 equation (33) matches the measurements very well, between 20 and 70 the equation underestimates the measured values, but overall the resemblance is very good.

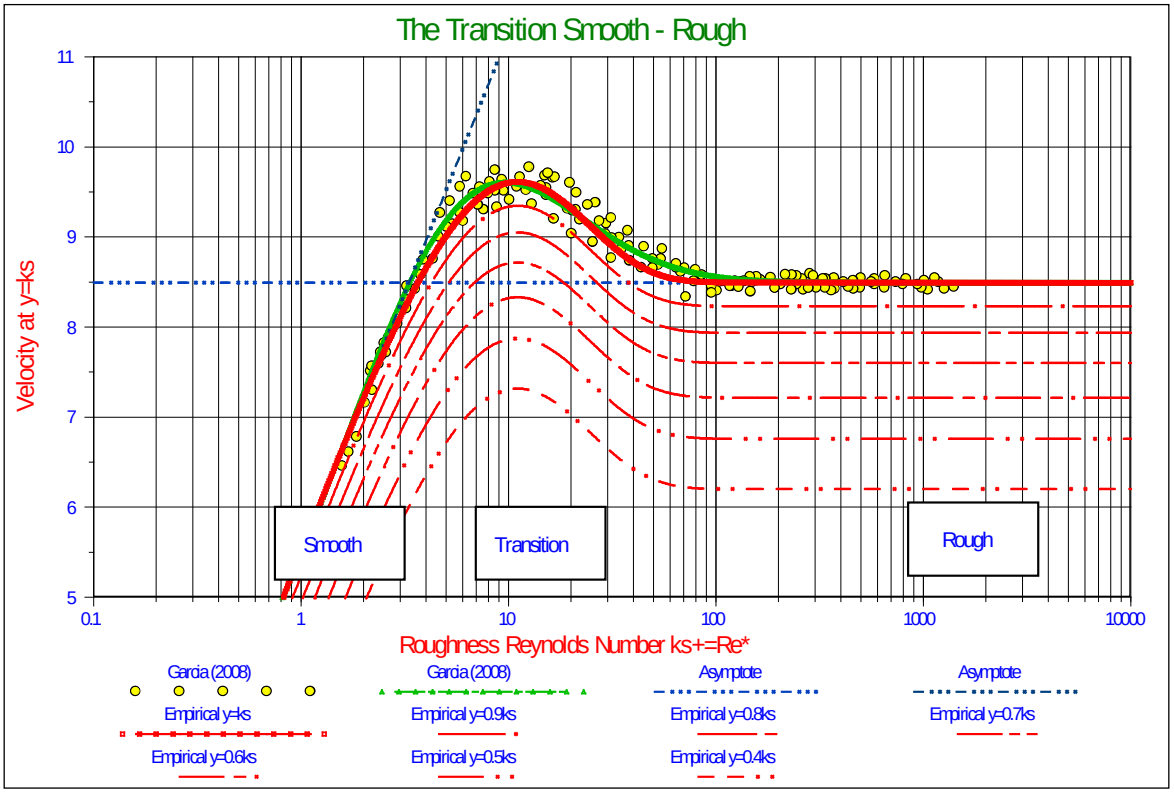

Figure 8: The transition smooth-rough for a number of distances to the wall

THE ANGLE OF INTERNAL FRICTION/THE FRICTION COEFFICIENT

When the mechanism for the initiation of motion is sliding, friction is involved. The angle of repose of granular material is often referred to as the angle of internal friction of the material in a loose condition. By rotating a bed until the top layer of particles starts to move (slide or roll) the angle of repose is determined, which is the slope angle at that point. Another way of determining this angle is to poor the particles on a surface and measure the slope angle of the cone shaped heap of particles that is formed. In literature a value between $\mathbf{30° - 35°}$ is mentioned for natural sands. Naden (1987) distinguishes between the friction angle ϕ, the dilatation angle ψ and the friction angle at zero dilatation ϕ_0. Where $\phi = \psi + \phi_0$, with values of $\phi = 35°$, $\psi = 30°$ and $\phi_0 = 5°$ (Kirkby & Statham, 1975). The value of ϕ_0 deals with the sliding of a quarts sphere on a quarts surface, so Coulomb friction, and could be related to rolling resistance. **Figure 9** shows the angle of repose for different materials and grain sizes. The relation between the friction coefficient and the angle of repose is:

$$\mu = \tan(\phi) \qquad \textbf{(35)}$$

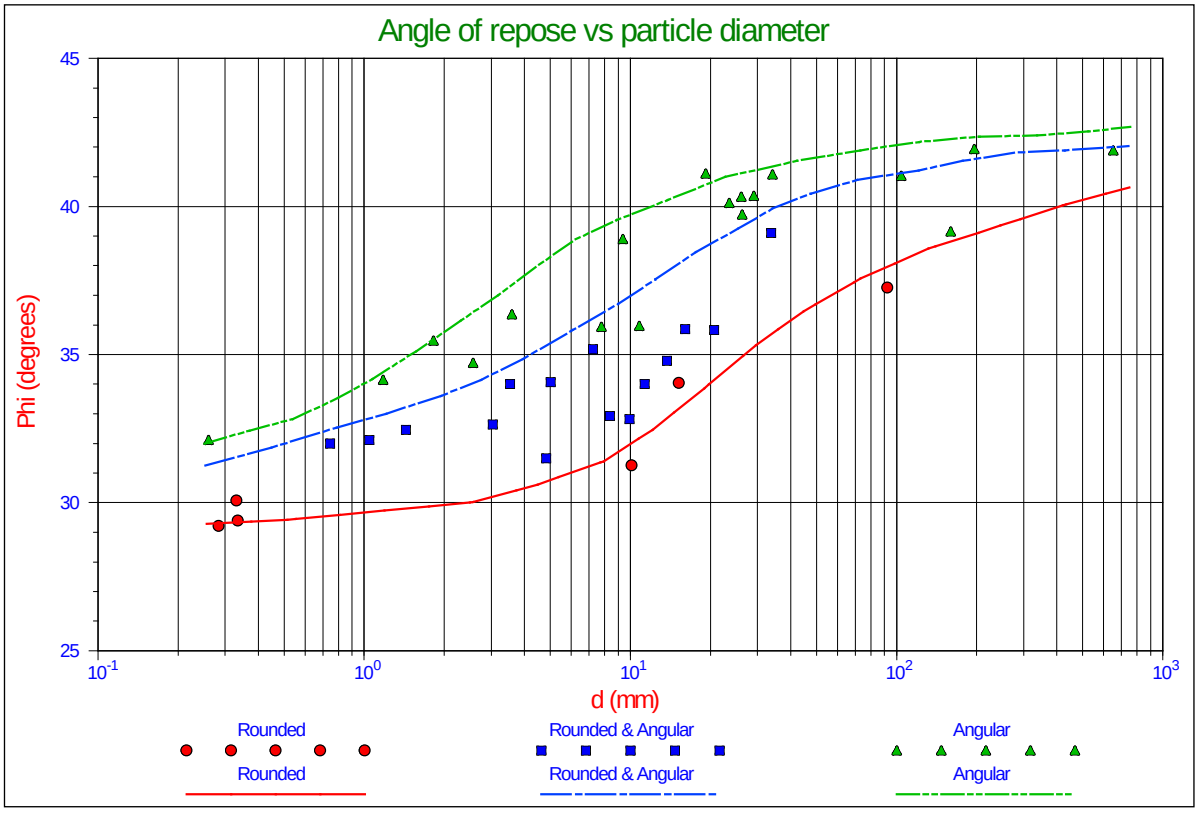

Figure 9: Angle of repose for granular material (Simons, 1957)

It should be noted that the angle of repose, in this context, is a global soil mechanical parameter, which can be used as an average value when the whole top layer starts to move. Individual

particles may encounter a different value. It should also be noted that the angle of repose is related to friction, which always has to do with the dissipation of energy, so it should not be mixed up with the pivot or dilatation angle which is related to resistance but not to the dissipation of energy.

THE PIVOT ANGLE/THE DILATATION ANGLE

When the mechanism for the initiation of motion is rolling, a pivot angle is involved. For spheres there is a geometrical relation between the pivot angle and the protrusion level. The pivot angle is sometimes referred to as the dilatation angle, which however is a global soil mechanical parameter and it is preferred not to use it as a local parameter, so we will use the term pivot angle. Luckner (2002) (page 18) determined the pivot angle for 3D sphere configurations, from protrusion levels ranging from 0% to 82%. In fact the maximum protrusion level of a sphere on top of other spheres in a 3D configuration is 82%. At a protrusion level of 0%, meaning the sphere is in between and at the same level as the surrounding spheres, the pivot angle is $\psi = \mathbf{90°}$. At a protrusion level of 30% the pivot angle is $\psi = \mathbf{59°}$, at 80% about $\psi = \mathbf{20°}$, at 90% about $\psi = \mathbf{12°}$ and of course at 100% $\psi = \mathbf{0°}$. In between these values a linear interpolation can be carried out. It is obvious that one is not free to choose the pivot angle, since it is related to the protrusion level.

THE MODEL

Before developing the model a number of assumptions have to be made in order to have starting points for the modeling to match the Shields curve and the measurements from literature . These assumptions have to be reasonable, matching literature and practice. These assumptions are:

1. The bed consists of spheres with one diameter **d**.
2. The virtual bed level is chosen at $\mathbf{0.2 \cdot d}$ below the top of the bed.
3. The criterion for initiation of motion is chosen to be between critical transport and general transport according to Vanoni (1975), Delft Hydraulics (1972) and Graf & Pazis (1977).
4. The exposure level **E** is chosen as $\mathbf{0.5 \cdot d}$, resulting in a protrusion level of $\mathbf{0.3 \cdot d}$, meaning that the standard sphere is exposed to the flow for 50% and reaches above the other spheres in the bed for 30%, based on Fenton & Abbot (1977) and Chin & Chiew (1993).
5. For the model an internal friction angle (angle of natural repose) of $\phi = \mathbf{30°}$ is chosen (for the sliding mechanism), which matches spheres and rounded particles of natural sands and gravel (see Figure 9).
6. For the model a pivot angle of $\psi = \mathbf{59°}$ is chosen (for the rolling mechanism), which matches a protrusion level of $\mathbf{0.3 \cdot d}$, based on Luckner (2002).
7. First full laminar flow will be considered up to a boundary/roughness Reynolds number of 11.6 and full turbulent flow above 11.6. The laminar flow is described with equation (31) and the turbulent flow with equation (33).

8. Later a transition area is introduced with full laminar flow up to a boundary/roughness Reynolds number of 5, a transition zone from 5 to 70 and a full turbulent flow above 70, with logarithmic interpolation in the transition zone.
9. For the laminar flow, the velocity at the top of the sphere is $\mathbf{0.5 \cdot Re_* \cdot u_*}$, resulting in an acting point at $\ell_{\mathbf{Drag}} = \mathbf{0.5}$, meaning at 50% of the flow field (see equation **(31)**). This also means the acting point is at $\mathbf{0.25 \cdot d}$ above the centre of the sphere (based on a surface averaged square of the velocity).
10. For the turbulent flow, the velocity at the top of the sphere is $\frac{\ln(\frac{0.5}{0.033})}{\kappa} \cdot \mathbf{u_*} = \mathbf{6.6 \cdot u_*}$, resulting in an acting point at $\ell_{\mathbf{Drag}} = \mathbf{0.655}$, meaning at 65.5% of the flow field (see equation **(33)**). This also means the acting point is at $\mathbf{0.327 \cdot d}$ above the centre of the sphere (based on a surface averaged square of the velocity).

DRAG INDUCED SLIDING AND ROLLING

To analyze the initiation of motion, the different physical phenomena will be taken into account one by one, starting with the drag force. Figure 10 shows the different forces (A) and moments (B) that play a role in drag induced motions.

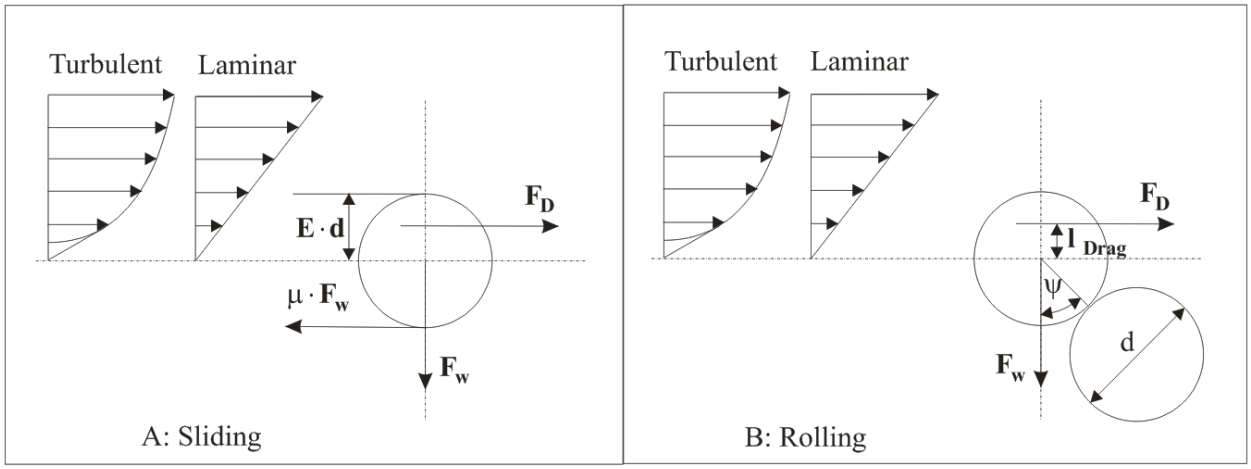

Figure 10: Drag induced sliding (A) and rolling (B)

Drag Induced Sliding

Let us consider a steady flow over a bed composed of cohesion less grains. The driving force is the flow drag force on the grain, assuming that part of the surface of the particle is hiding behind other particles and only a fraction E (the exposure level) is subject to drag:

$$\mathbf{F_D = C_D \cdot \tfrac{1}{2} \cdot \rho_w \cdot \left(\ell_{Drag} \cdot \alpha \cdot u_* \right)^2 \cdot f_D \cdot \frac{\pi \cdot d^2}{4}} \qquad \mathbf{(36)}$$

The velocity $\alpha \cdot \mathbf{u}_*$ is the actual velocity at the top of the sphere, so for an exposure level of 0.5 in a laminar flow, this would be equal to $\mathbf{0.5 \cdot Re_* \cdot u_*}$, assuming the roughness is equal to the sphere diameter (see equation **(30)**). In a turbulent flow this gives $\mathbf{\ln(0.5/0.033)/\kappa \cdot u_* = 6.6 \cdot u_*}$ (see equation **(33)**). The velocity $\ell_{\mathbf{Drag}} \cdot \alpha \cdot \mathbf{u}_*$ is the effective velocity resulting from integration of the velocity squared over the part of the sphere that is subject to flow. For an exposure level of 0.5 in a laminar flow the factor $\ell_{\mathbf{Drag}} = \mathbf{0.5}$. In a turbulent flow $\ell_{\mathbf{Drag}} = \mathbf{0.655}$. In fact the factor $\ell_{\mathbf{Drag}}$ gives the point of action of the drag force related to the exposure level **E**. The factor $\mathbf{f_D}$ is the fraction of the cross section being subject to drag and this factor is 0.5 for an exposure level of 0.5.

The submerged weight of the particle is:

$$\mathbf{F_w = (\rho_q - \rho_w) \cdot g \cdot \frac{\pi \cdot d^3}{6}} \qquad \mathbf{(37)}$$

At equilibrium the drag force is equal to the friction force:

$$\mathbf{F_D = \mu \cdot F_w} \qquad \mathbf{(38)}$$

By substituting equation **(36)** and equation **(37)** in equation **(38)**, this can be written as:

$$\mathbf{C_D \cdot \tfrac{1}{2} \cdot \rho_w \cdot (\ell_{Drag} \cdot \alpha \cdot u_*)^2 \cdot f_D \cdot \frac{\pi \cdot d^2}{4} = \mu \cdot (\rho_q - \rho_w) \cdot g \cdot \frac{\pi \cdot d^3}{6}} \qquad \mathbf{(39)}$$

Which can be re-arranged into (showing the Shields parameter):

$$\mathbf{\theta = \frac{u_*^2}{R_d \cdot g \cdot d} = \frac{4}{3} \cdot \frac{1}{\alpha^2} \cdot \frac{\mu}{\ell_{Drag}^2 \cdot f_D \cdot C_D}} \qquad \mathbf{(40)}$$

Drag Induced Rolling

In the case of rolling the sphere will pivot around the contact point with a sphere below, which has an angle with the vertical named the pivot angle ψ. There may be some rolling resistance which can be taken into account by introducing the friction angle for rolling $\phi_{\mathbf{Roll}}$. This friction will be very small for quarts-quarts rolling and is taken $\mathbf{1°}$ in the calculations. The equilibrium equation for rolling is:

$$\mathbf{F_D \cdot (\ell_{Lever} + \cos(\psi + \phi_{Roll})) \cdot R = F_w \cdot \sin(\psi + \phi_{Roll}) \cdot R} \qquad \mathbf{(41)}$$

With $\ell_{\mathbf{Lever}}$ the distance of the acting point of the drag force above the centre of the sphere. This distance is $\ell_{\mathbf{Lever}} = \mathbf{0.5}$ for laminar flow and $\ell_{\mathbf{Lever}} = \mathbf{0.655}$ for turbulent flow. Substituting equations **(36)** and **(37)** in equation (**41**) gives the following equilibrium equation.

$$\mathbf{C_D \cdot \tfrac{1}{2} \cdot \rho_w \cdot (\ell_{Drag} \cdot \alpha \cdot u_*)^2 \cdot f_D \cdot \frac{\pi \cdot d^2}{4} \cdot (\ell_{Lever} + \cos(\psi + \phi_{Roll})) \cdot R} = \mathbf{(\rho_q - \rho_w) \cdot g \cdot \frac{\pi \cdot d^3}{6} \cdot \sin(\psi + \phi_{Roll}) \cdot R} \quad \textbf{(42)}$$

$$\ell_{\mathbf{Lever}} = \mathbf{1 - 2 \cdot E \cdot (1 - \ell_{Drag})} \quad \textbf{(43)}$$

Which can be re-arranged into (showing the Shields parameter):

$$\theta = \frac{u_*^2}{R \cdot g \cdot d} = \frac{4}{3} \cdot \frac{1}{\alpha^2} \cdot \frac{\sin(\psi + \phi_{Roll})}{\ell_{Drag}^2 \cdot f_D \cdot C_D \cdot (\ell_{Lever} + \cos(\psi + \phi_{Roll}))} \quad \textbf{(44)}$$

The Drag Coefficient

Equations **(40)** and **(44)** contain the drag coefficient, which is one of the mainly experimental determined coefficients influencing the value of the Shields parameter. In 1851 Stokes theoretically derived the drag coefficient for spherical particles in a laminar flow and found that (for $\mathbf{Re_p < 0.5}$):

$$C_D = \frac{24}{Re_p} \quad \textbf{(45)}$$

For large Reynolds numbers the drag coefficient of spheres is a fixed number for which often the value of 0.445 is used. In the intermediate range of Reynolds numbers many fit functions are known. A good fit function for the transitional region has been derived by Turton & Levenspiel (1986), which is a 5 parameter fit function to the data as shown in **Figure 11**:

$$C_D = \frac{24}{Re_D} \cdot (1 + 0.173 \cdot Re_D^{0.657}) + \frac{0.413}{1 + 16300 \cdot Re_D^{-1.09}} \quad \textbf{(46)}$$

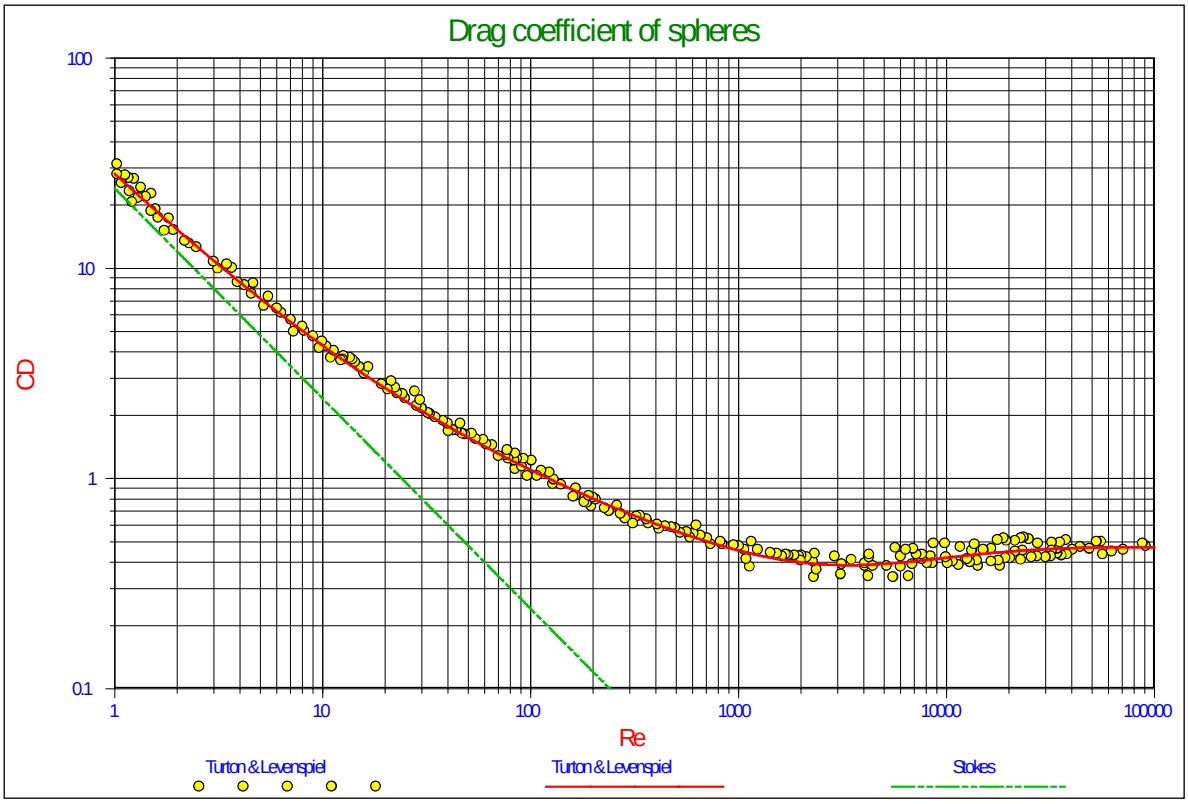

Figure 11: Experimental data for drag coefficients of spheres as a function of the Reynolds number (Turton & Levenspiel, 1986)

The models derived to describe the Shields curve use the drag coefficient of spheres and hardly any discussion about this has been found in literature, although it is known that for sands and gravels the drag coefficients, especially at large Reynolds numbers, are larger than the drag coefficient for spheres. Engelund & Hansen (1967) found the following equation based on measurements and found it best suited for natural sands and gravels (Julien, 1995):

$$C_D = \frac{24}{Re_D} + 1.5 \qquad (47)$$

It must be noted here that in general the drag coefficients are determined based on the terminal settling velocity of the particles. Wu & Wang (2006) recently gave an overview of drag coefficients and terminal settling velocities for different particle Corey shape factors. The result of their research is reflected in **Figure 12** and **Figure 13**. **Figure 12** shows the drag coefficients as a function of the Reynolds number and as a function of the Corey shape factor. **Figure 13** shows the drag coefficient for natural sands and gravels. The asymptotic value for large Reynolds numbers is about 1, while equation **(47)** shows an asymptotic value of 1.5. To emphasise the effect of the natural sands and gravels, equation **(47)** will be used in the model for natural sands and gravels, while equation **(46)** is used for spheres.

The Reynolds number used to calculate the drag coefficient is based on the velocity determined by the actual surface averaged velocity squared, according to equation (18).

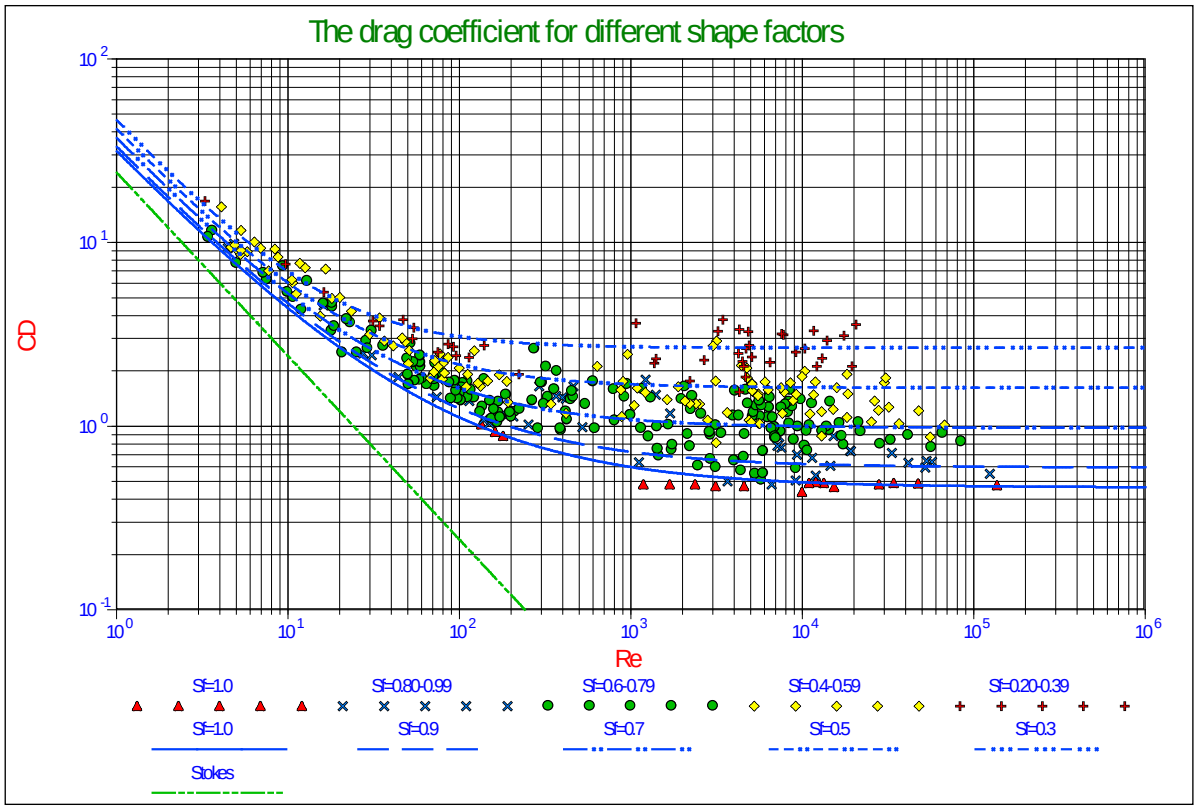

Figure 12: Drag coefficient as a function of the particle shape (Wu & Wang, 2006)

Figure 14 shows the results of equation **(40)** for sliding and equation **(44)** for rolling. It is obvious from this figure that the Shields parameter found as a function of the boundary Reynolds number overestimates with regards to the measurements, except for very small Reynolds numbers, so there must be other phenomena that have to be taken into account, like lift forces and turbulence. It is also clear from this figure that the curve for rolling is higher than the curve for sliding, out of which the conclusion can be drawn that the general mechanism of initiation of motion for critical to general transport is sliding and not rolling. The asymptotic value of the curve for sliding at very small Reynolds numbers is about 0.26, matching the asymptotic value of Soulsby & Whitehouse of 0.3 given in equation **(4)**. The minimum at a Reynolds number of 23.2 is caused by the fact that, at that Reynolds number, the top of the sphere reaches the top of the viscous sub layer, so at lower Reynolds numbers laminar viscous flow is considered and at higher Reynolds numbers turbulent flow.

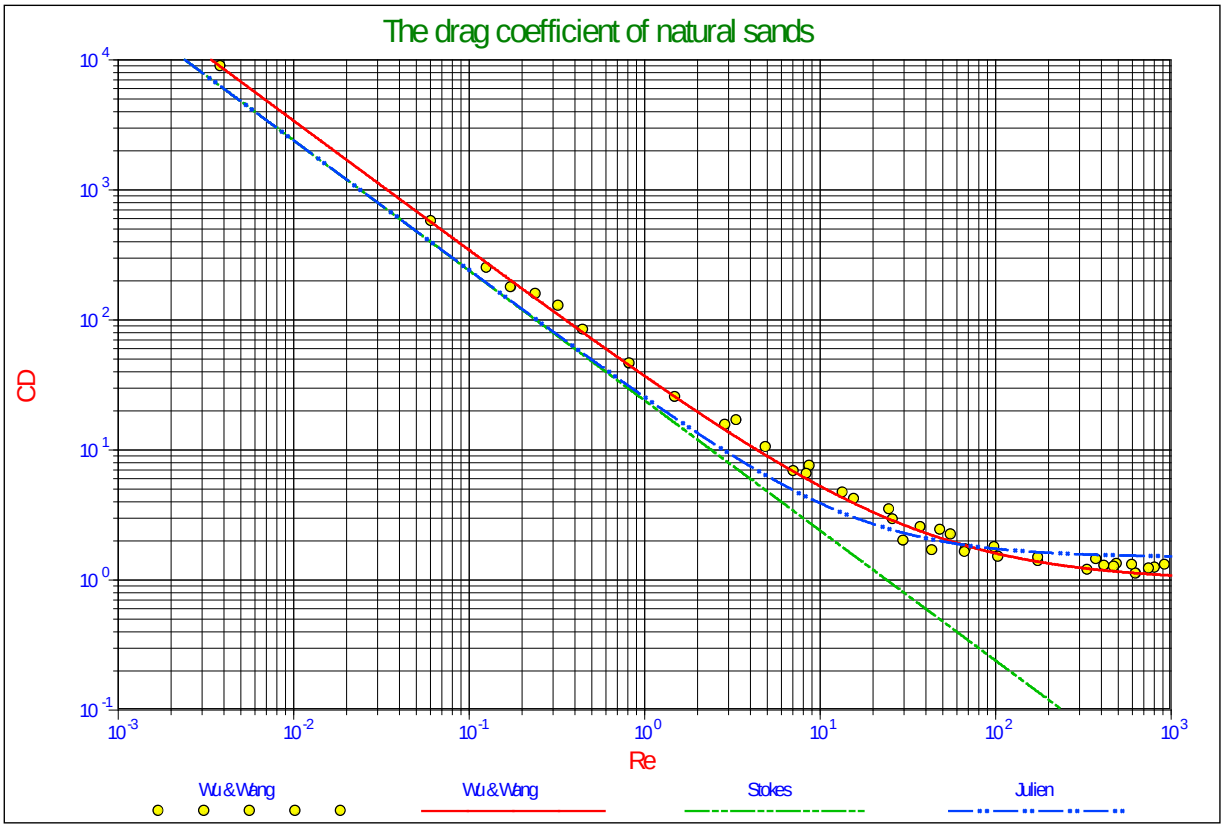

Figure 13: Drag coefficient for natural sediments (S_f=0.7) (Wu & Wang, 2006)

Pilotti & Menduni (2001) also derived a model based on drag and gravity only, for laminar main flow up to boundary Reynolds numbers of about 100. They assume that the sphericity of the grains is such that the drag coefficient of spheres can be applied. Using almost uniform grains in the range of 0.08 to 3 mm, the boundary Reynolds number was also varied by using a water glucose mixture with different densities, resulting in viscosities varying from $\mathbf{1.01 \cdot 10^{-6}}$ to $\mathbf{2.81 \cdot 10^{-4}}$ in m^2/sec. Turbulence is not taken into account in the model. The mechanism for initiation of motion was rolling of individual particles with pivot angles of $\mathbf{35°}$, $\mathbf{40°}$ and $\mathbf{45°}$. The resulting curves (only for the laminar region) have the same shape as the curves in **Figure 14** with asymptotic values of 0.13, 0.19 and 0.27 for the 3 pivot angles. The measured values of the Shields parameter are comparable with the data in **Figure 14** for the very low Reynolds numbers ($\mathbf{Re_* < 1}$), but higher in the intermediate range ($\mathbf{1 < Re_* < 100}$), matching the curve for sliding. It is difficult to compare the results exactly with **Figure 14**, since the exposure level of the model of Pilotti & Menduni (2001) is not known. In Part B of this publication these measurements are analyzed in relation with laminar (turbulence free) main flow.

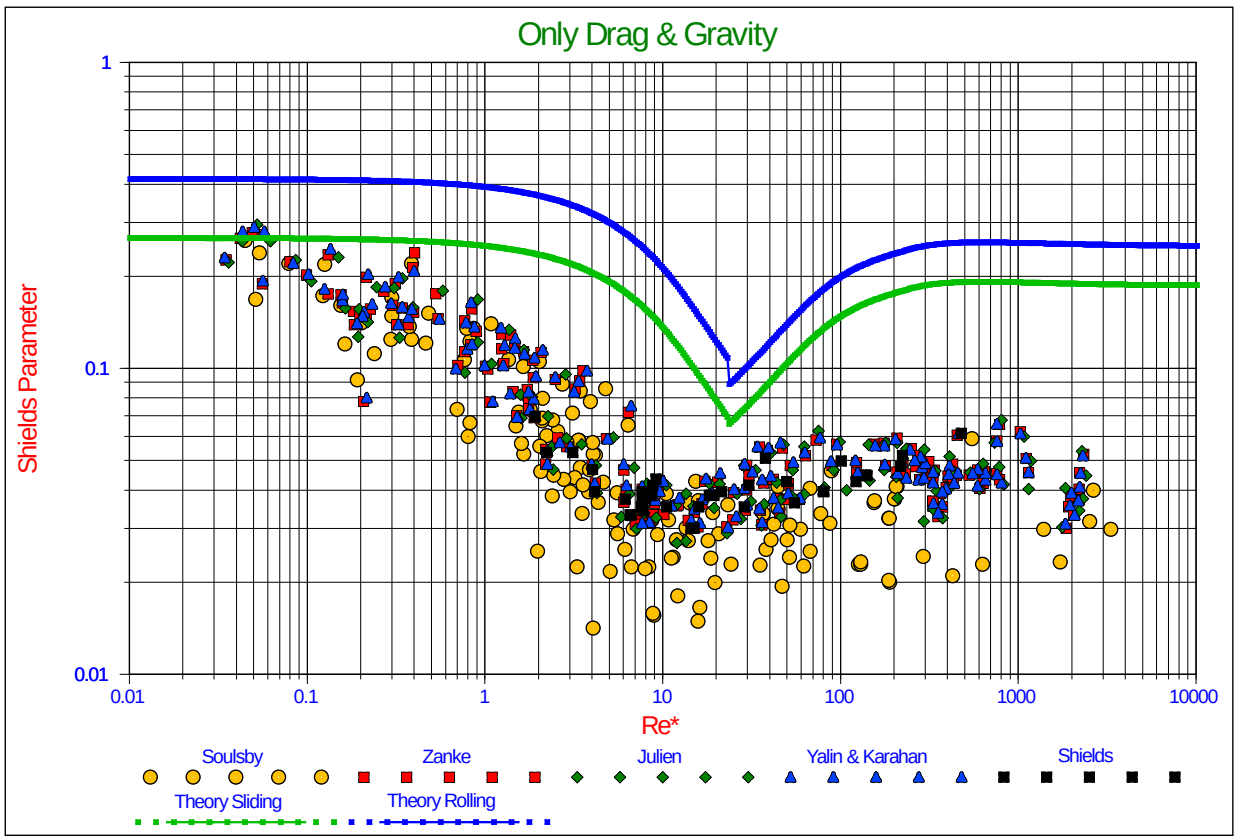

Figure 14: Drag induced initiation of motion

DRAG AND LIFT INDUCED SLIDING, ROLLING AND LIFTING

Drag induced sliding and rolling overestimates the Shields parameter compared with the measurements, so there must be other influences. The first influence considered is lift as is shown in Figure 15. The lift force is assumed to be upwards directed. Based on literature and theory, lift is assumed to occur in the turbulent region only.

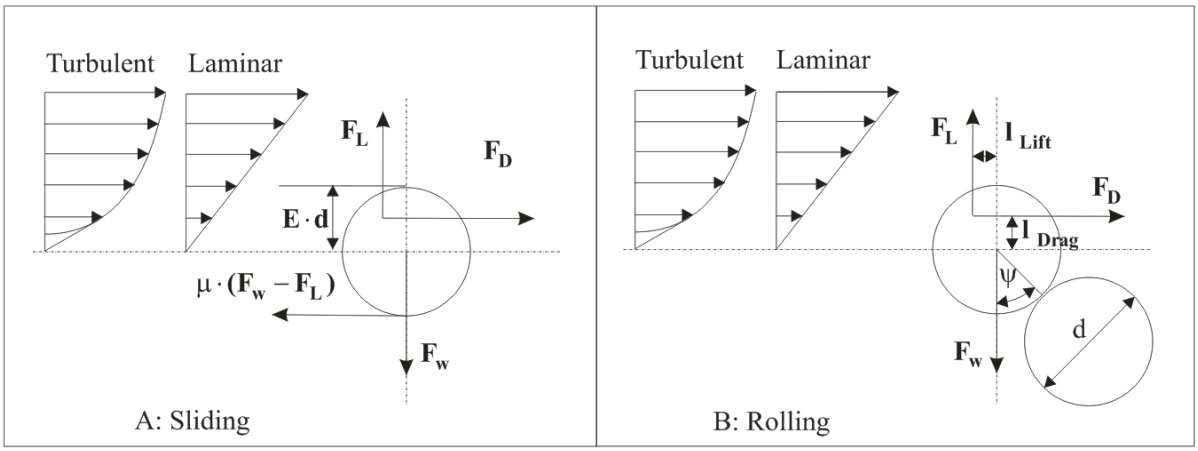

Figure 15: Drag and lift induced sliding (A) and rolling (B)

Drag and Lift Induced Sliding

Let us consider the steady flow over a bed composed of cohesion less grains. The driving forces are the flow drag and lift forces on the grain, assuming that part of the surface of the particle is hiding behind other particles and only a fraction E (the exposure level) is subject to drag and lift. This gives the following equation for the drag force:

$$\mathbf{F_D = C_D \cdot \tfrac{1}{2} \cdot \rho_w \cdot \left(\ell_{Drag} \cdot \alpha \cdot u_* \right)^2 \cdot f_D \cdot \frac{\pi \cdot d^2}{4}} \qquad \mathbf{(48)}$$

The lift force is written in the same way, but it is assumed that the lift force is determined by the velocity difference between the top and the bottom of the particle and the surface that is subject to lift is the projected horizontal cross section subject to the flow, this factor $\mathbf{f_L = 1}$ for an exposure level $\mathbf{E = 0.5}$, while the factor for drag $\mathbf{f_D = 0.5}$ in this case:

$$\mathbf{F_L = C_L \cdot \tfrac{1}{2} \cdot \rho_w \cdot (\alpha \cdot u_*)^2 \cdot f_L \cdot \frac{\pi \cdot d^2}{4}} \qquad \mathbf{(49)}$$

The submerged weight of the particle is:

$$\mathbf{F_w = (\rho_q - \rho_w) \cdot g \cdot \frac{\pi \cdot d^3}{6}} \qquad \mathbf{(50)}$$

At equilibrium the drag force and the friction force are equal (note that the friction force is reduced by the lift):

$$\mathbf{F_D = \mu \cdot (F_w - F_L)} \qquad \mathbf{(51)}$$

Substituting the equations **(48)**, **(49)** and **(50)** into **(51)** results in the following equation:

$$\mathbf{C_D \cdot \tfrac{1}{2} \cdot \rho_w \cdot (\ell_{Drag} \cdot \alpha \cdot u_*)^2 \cdot f_D \cdot \frac{\pi \cdot d^2}{4} = \mu \cdot \left((\rho_q - \rho_w) \cdot g \cdot \frac{\pi \cdot d^3}{6} - C_L \cdot \tfrac{1}{2} \cdot \rho_w \cdot (\alpha \cdot u_*)^2 \cdot f_L \cdot \frac{\pi \cdot d^2}{4} \right)} \qquad \mathbf{(52)}$$

Which can be re-arranged into (showing the Shields parameter):

$$\mathbf{\theta = \frac{u_*^2}{R_d \cdot g \cdot d} = \frac{4}{3} \cdot \frac{1}{\alpha^2} \cdot \frac{\mu}{\ell_{Drag}^2 \cdot f_D \cdot C_D + \mu \cdot f_L \cdot C_L}} \qquad \mathbf{(53)}$$

Drag and Lift Induced Rolling

The equilibrium equation for rolling is:

$$\mathbf{F_D \cdot (\ell_{Lever-D} + \cos(\psi + \phi_{Roll})) \cdot R + F_L \cdot (\ell_{Lever-L} + \sin(\psi + \phi_{Roll})) \cdot R = F_w \cdot \sin(\psi + \phi_{Roll}) \cdot R} \quad (54)$$

Substituting the equations **(48)**, **(49)** and **(50)** into (**54**) gives:

$$\mathbf{C_D \cdot \tfrac{1}{2} \cdot \rho_w \cdot (\ell_{Drag} \cdot \alpha \cdot u_*)^2 \cdot f_D \cdot \frac{\pi \cdot d^2}{4} \cdot (\ell_{Lever-D} + \cos(\psi + \phi_{Roll})) \cdot R}$$
$$\mathbf{+ C_L \cdot \tfrac{1}{2} \cdot \rho_w \cdot (\alpha \cdot u_*)^2 \cdot f_L \cdot \frac{\pi \cdot d^2}{4} \cdot (\ell_{Lever-L} + \sin(\psi + \phi_{Roll})) \cdot R}$$
$$\mathbf{= (\rho_q - \rho_w) \cdot g \cdot \frac{\pi \cdot d^3}{6} \cdot \sin(\psi + \phi_{Roll}) \cdot R} \quad \mathbf{(55)}$$

With the additional lever arms for drag and lift :

$$\mathbf{\ell_{Lever-D} = 1 - 2 \cdot E \cdot (1 - \ell_{Drag})}$$
$$\mathbf{\ell_{Lever-L} = 0} \quad \mathbf{(56)}$$

Which can be re-arranged into the Shields parameter:

$$\mathbf{\theta = \frac{u_*^2}{R_d \cdot g \cdot d} = \frac{4}{3} \cdot \frac{1}{\alpha^2} \cdot \frac{\sin(\psi + \phi_{Roll})}{\ell_{Drag}^2 \cdot f_D \cdot C_D \cdot (\ell_{Lever-D} + \cos(\psi + \phi_{Roll})) + f_L \cdot C_L \cdot (\ell_{Lever-L} + \sin(\psi + \phi_{Roll}))}} \quad \mathbf{(57)}$$

Lift Induced Lifting

A third possible mechanism for the initiation of motion is pure lifting. This will occur if the lift force is equal to the gravity force according to:

$$\mathbf{F_w = F_L} \quad \mathbf{(58)}$$

Substituting the equations **(48)** and **(50)** into equation **(58)** gives:

$$\mathbf{(\rho_q - \rho_w) \cdot g \cdot \frac{\pi \cdot d^3}{6} = C_L \cdot \tfrac{1}{2} \cdot \rho_w \cdot (\alpha \cdot u_*)^2 \cdot f_L \cdot \frac{\pi \cdot d^2}{4}} \quad (59)$$

Which can be re-arranged into the Shields parameter:

$$\theta = \frac{u_*^2}{R_d \cdot g \cdot d} = \frac{4}{3}\frac{1}{\alpha^2 \cdot C_L \cdot f_L} \qquad (60)$$

Since it is assumed that lift only occurs in turbulent flow and not in laminar flow, this mechanism only applies for boundary Reynolds numbers higher than 70. For an exposure level of 0.5, the factor $\alpha = 6.6$, the surface coefficient $f_L = 1$ and a lift coefficient of $C_L = 0.423$ is applied, which will be explained in the next paragraph. This results in a Shields parameter of 0.0726 for large boundary Reynolds numbers. How this relates to rolling and sliding will be discussed in the next paragraph.

The Lift Coefficient

The choice of the lift coefficient is a discussion in many of the models and many different values are found. Sometimes the lift coefficient is expressed as a fraction of the drag coefficient and sometimes as a constant. In most models however lift is present in the turbulent flow, but not in the laminar viscous sub layer. In this model also the choice is made to neglect lift in the laminar region, so for boundary Reynolds numbers below 5. Wiberg & Smith (1987A), Dey (1999), Pilotti & Menduni (2001), Stevenson, Thorpe & Davidson (2002) and others support this assumption. For the turbulent region different values are used for the lift coefficient.

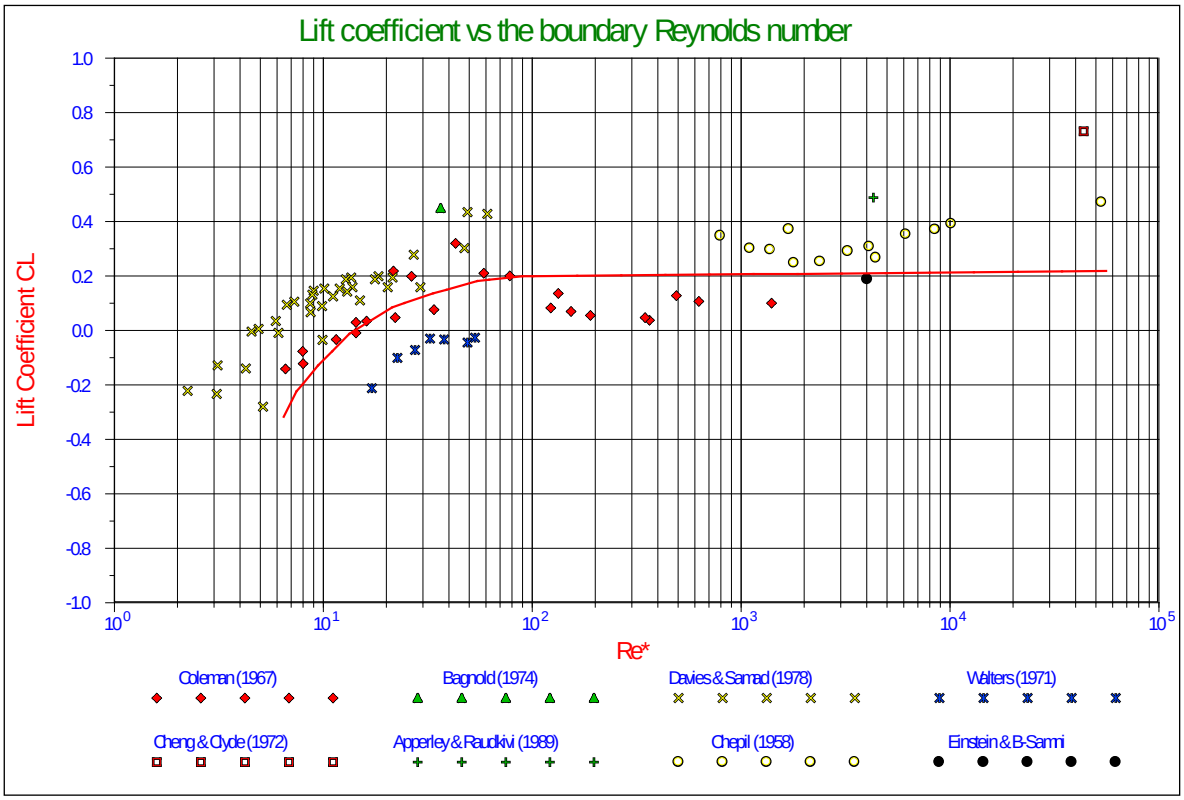

Figure 16: The lift coefficient as a function of the particle Reynolds number

Wiberg & Smith (1987A) use a value of 0.2, while using $\mathbf{0.85 \cdot C_D}$ in (Wiberg & Smith, 1987B) inspired by the work of Chepil (1958). Marsh, Western & Grayson (2004) compared 4 models, but also evaluated the lift coefficient as found by a number of researchers as is shown in **Figure 16**. For large Reynolds numbers an average value of 0.2 is found, while for small Reynolds numbers the lift coefficient can even become negative. Luckner (2002) found a relation where the lift coefficient is about $\mathbf{1.9 \cdot E \cdot C_D}$ (including the effect of turbulence), which matches the findings of Dittrich, Nestmann & Ergenzinger (1996). For an exposure level of 0.5 this gives $\mathbf{0.95 \cdot C_D}$, which is close to the findings of Chepil (1958). Using a lift coefficient of $\mathbf{0.95 \cdot C_D = 0.423}$ for boundary Reynolds numbers above 70, results in Shields curves as shown in **Figure 17**. The resulting curves for boundary Reynolds numbers below 23.2 have not changed, but the curves for boundary Reynolds numbers above 23.2 have lowered to a level of about 0.058 for rolling and 0.052 for sliding for very large boundary Reynolds numbers. This implies that sliding will also be the main mechanism for the initiation of motion when lift is included in the model. Comparing the values of 0.052 for sliding and 0.058 for rolling with the value of 0.0726 for pure lift, gives the conclusion that pure lift will not play an important role in the initiation of motion for an exposure level of 0.5, independent of the choice of the lift coefficient, since the lift coefficient is involved in all 3 mechanisms. The curve found for sliding matches the data, although it is high for large boundary Reynolds numbers, but then some of the experiments were carried out in sand where a different drag coefficient should be used as will be shown later. Compared with Shields (1936) and many other researchers, a value of 0.052 for large boundary Reynolds numbers is in the range of what should be expected.

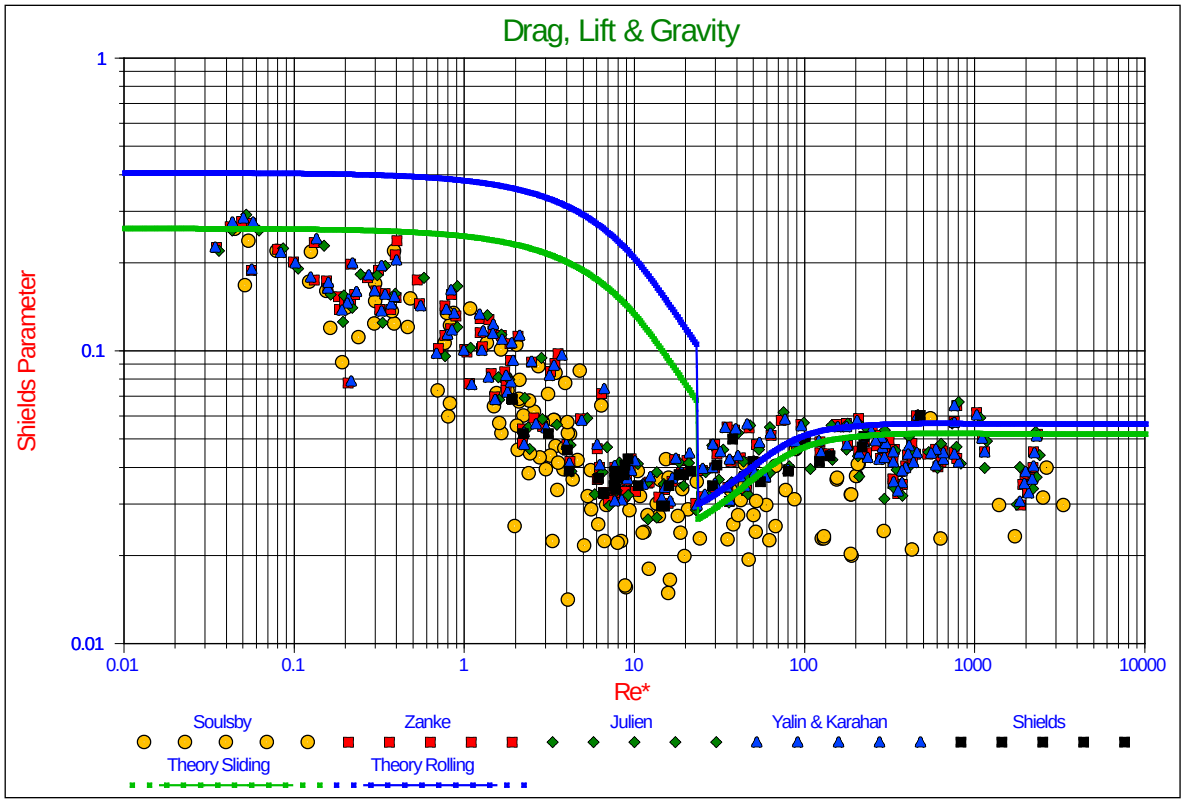

Figure 17: Drag and lift induced initiation of motion.

TURBULENCE

Turbulence describes the stochastic non-deterministic velocity fluctuations in a flow and although coherent structures exist in the occurrence of turbulence, turbulence has no long term memory. The implication of this is that turbulence cannot be described by a velocity profile, but instead it can be described by statistical properties. In general it is described by the turbulence intensity of the horizontal and vertical velocity and the intensity of the Reynolds stress. These intensities reflect the so called r.m.s. (root mean square) values of the velocity fluctuations. Assuming the velocity fluctuations are according to a normal or Gaussian distribution, the time and surface averaged velocity profiles represent the mean value of the distribution, as used in equations **(31)** and **(33)**, while the standard deviation is represented by the r.m.s. value, also called the first moment of the distribution. The second moment and third moment correspond to two times and three times the r.m.s. value. The probability of having an instantaneous velocity higher than the standard deviation in the direction of the mean velocity is 14.9%, for the second moment this is 2.3% and for the third moment 0.13%. Wiberg & Smith (1987A) reduce the height of the viscous sub layer to 60%, resulting in an increase of 1/0.6=1.66 of the velocity in the viscous sub layer. Assuming a turbulence intensity of $\mathbf{0.3 \cdot y^+ \cdot u_*}$ (Nezu & Nakagawa, 1993) and a mean velocity of $\mathbf{y^+ \cdot u_*}$, implicitly this means adding 2.2 times the turbulence intensity to the mean velocity. Since Wiberg & Smith only apply this for low boundary Reynolds numbers where the particles are small with regard to the height of the viscous sub layer, implicitly this means adding a turbulence effect to small boundary Reynolds numbers (smooth boundaries) and not to large boundary Reynolds numbers (rough boundaries). Hofland (2005) in his PhD thesis states that fluctuations created by smaller eddies are negligible for larger particles due to phase cancellations when integrated over the surface of a stone. Zanke (2001) and later Luckner (2002) apply turbulent velocity fluctuations both for small and large boundary Reynolds numbers and add 1.8 times the turbulence intensity to the mean velocity. Nezu & Nakagawa (1977) and (1993) and Nezu & Rodi (1986) found the following relation for the turbulence intensity parallel to the wall.

$$\frac{\mathbf{u_{r.m.s.}}}{\mathbf{u_*}} = \mathbf{0.3 \cdot y^+ \cdot e^{-\frac{y^+}{10}} + 2.26 \cdot e^{-\frac{y}{h}} \cdot \left(1 - e^{-\frac{y^+}{10}} \right)} \qquad \textbf{(61)}$$

The asymptotic value of the ratio between the turbulence intensity and the time and surface averaged velocity is 0.3. Measurements of this ratio, carried out by Eckelman (Hinze, 1975) on smooth walls as a function of the distance to the wall $\mathbf{y^+}$, show a small increase near the wall to a value of 0.38 at $\mathbf{y^+ = 4}$. Approaching the wall further shows a decrease to a value of 0.24, but the measurements do not contradict the assumption of having a ratio at the wall of zero. Kim, Moin and Moser (1987) confirm these findings, but state that additional measurements show a finite value at the wall, although the measurements in their paper do not contradict a value of zero. Zanke (2003) assumes a ratio of zero at the wall and achieves this by shifting the time averaged velocity with respect to the distance to the wall. In fact implicitly this means that the virtual bed level for the time averaged velocity (which is chosen at $\mathbf{0.2 \cdot d}$ below the top of the

spheres in this paper) is located lower than the virtual bed level for the turbulence intensity. Considering that the measurements of Eckelman and later Kim, Moin & Moser were carried out on a smooth wall where the wall is the virtual bed level, while here we consider a bed of grains or spheres where a virtual bed level has to be defined, resulting in a correct drag force on the spheres, there is no reason why the two virtual bed levels should be the same. The solution of Zanke, choosing two different virtual bed levels is one way of solving this problem. One can also choose one virtual bed level for both, the time averaged velocity and the turbulence intensity, but consider that below the top of the spheres, the turbulence intensity is decreased, due to the shadow effect of the spheres. Assuming the turbulence intensity to be zero at the virtual bed level and increasing proportional to the square of the distance to the wall, very close to the wall between the grains, and proportional to the distance to the wall above the grains, this can be represented with the following equation:

$$\frac{u'_{r.m.s.}}{u_*} = \frac{u_{r.m.s.}}{u_*} \cdot \left(1 - e^{-y^+}\right) \qquad \textbf{(62)}$$

Another reason for assuming a ratio of zero at the virtual bed level is the fact that the asymptotic value found for the Shields curve for the boundary Reynolds number approaching zero matches the measurements (see **Figure 14** and **Figure 17**). Any ratio larger than zero would lower the curves found. **Figure 18**C shows the turbulence intensity according to equation **(61)**, while **Figure 18**A shows the turbulence intensity very close to the wall. **Figure 18**B shows the difference between equation **(61)** and applying damping on the turbulence intensity very close to the wall according to equation **(62)**. The turbulence intensity profile according to equation **(62)** does not contradict the findings of Nezu and Nakagawa (1993), Eckelman (Hinze, 1975) and Kim, Moin & Moser (1987) and matches the findings of Zanke (2003). Now it is the question how many times the standard deviation of the turbulence intensity should be used. Wiberg & Smith (1987A) implicitly used a factor 2.2 and Zanke (2003) used a factor 1.8 explicitly. Since we consider the initiation of motion, particles or spheres will start to entrain if there is one moment when the condition for entrainment is satisfied. On the other hand the Shields curve falls somewhere between critical and general transport, meaning that already many particles at many locations entrain. A factor of 3 will be chosen here, meaning that the probability of having a higher instantaneous velocity is only 0.13%, so about 1 out of 1000 occurrences of turbulent eddies. The factor n in equation **(63)**, the turbulence intensity factor, is chosen 3.

$$\frac{u'_{n\cdot r.m.s.}}{u_*} = n \cdot \frac{u'_{r.m.s.}}{u_*} \qquad \textbf{(63)}$$

The resulting turbulence intensity profile should not be interpreted as a velocity distribution, since it describes the intensity of stochastic turbulent velocity fluctuations. This means that the influence of these fluctuations on the drag force can be derived by integrating the fluctuations over the height of a particle and in fact this should be added to the mean velocity and then the surface averaged value of the square of the total velocity should be determined. Taking the square root of this velocity and deducting the time averaged velocity gives the contribution of the turbulence. Since at one location the turbulent velocity fluctuations will be positive, while at the same time at other locations they will be negative, the probability that at one moment in time the

turbulent velocity fluctuations over the height of the particle are unidirectional in the direction of the time averaged velocity is almost zero. For very small particles having a diameter smaller than or equal to the size of the small turbulent eddies, this may still be the case, but with increasing diameter the influence of the eddies will decrease due to the fact that they cancel each other out. For very large particles the influence of this turbulence will reduce to zero. It is proposed to name this effect the probability of simultaneous occurrence effect and the factor determining the turbulent velocity that should be added to the time averaged velocity, the factor of simultaneous occurrence. The point of action of the resulting surface averaged square of the velocity is assumed not to change, although there is no reason for that. With the height $y^+ = E \cdot Re_*$ at the top of a particle with exposure level **E,** equation **(64)** is proposed for the factor of simultaneous occurrence and this is shown in **Figure 18**D. The resulting effective velocity profile is shown in **Figure 18**C and **Figure 18**A and used to calculate the resulting Shields curve as shown in **Figure 19**.

$$\frac{u_{eff}}{u_*} = \frac{u'_{n\cdot r.m.s.}}{u_*} \cdot e^{-\left(\frac{y^+}{10}\right)^2} \qquad \textbf{(64)}$$

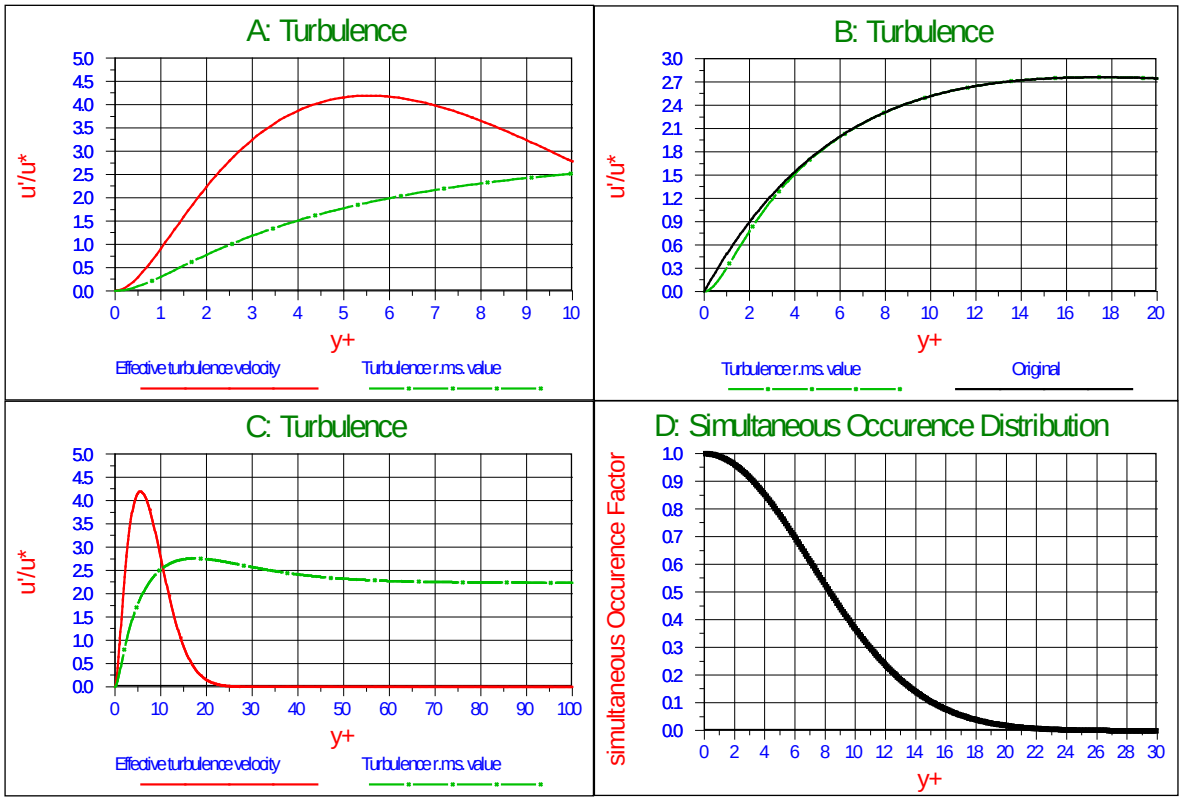

Figure 18: The contribution of turbulence to the velocity

From **Figure 19** it can be concluded that the resulting curve matches the measurements very well for sliding, while the curve for rolling still overestimates the values of the Shields parameter. The transition point for the boundary Reynolds number is at 23.2, because the laminar regime extends to the point where the top of a grain reaches the thickness of the viscous sub layer. The two regions, laminar and turbulent do not connect very well, due to different physics and different conditions. In the laminar region drag and turbulence determine the values and the shape of the curves, while drag and lift determine this in the turbulent region. It should be noted here that having a smooth or a rough wall, is not the same as having laminar or turbulent flow around a particle. Smooth or rough depends on the relative roughness of the wall and this is represented by the boundary Reynolds number, which is equal to the roughness Reynolds number if the roughness is represented by the particle diameter, while laminar or turbulent flow is determined by the height of the particle exposed to the flow in relation to the height of the viscous sub layer.

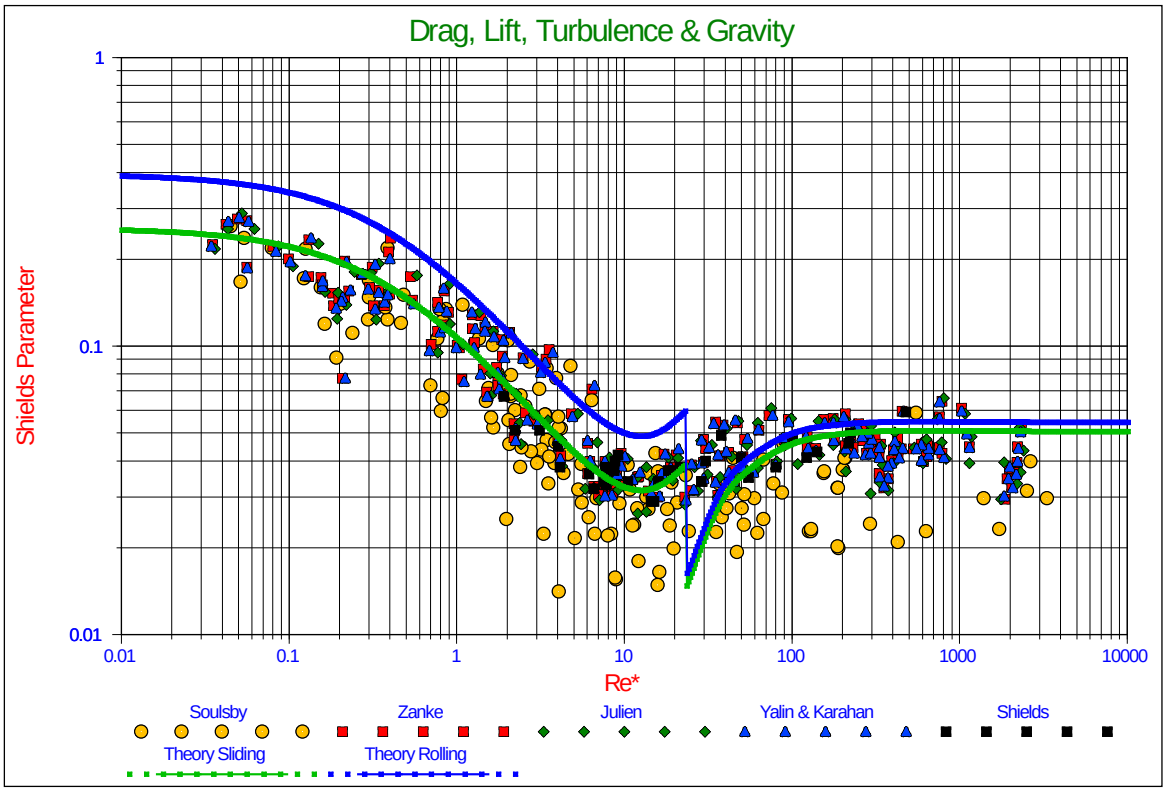

Figure 19: Drag, lift and turbulence induced initiation of motion

THE TRANSITION ZONE

The transition zone covers the transition from a laminar regime to a turbulent regime. This does not just involve the velocity profile. In the laminar regime, $y^+ < 5$, the velocity profile is considered to be linear, but also the influence of small turbulent eddies is considerable, while in the turbulent regime, $y^+ > 70$, the velocity profile is logaritmic and the lift force has a considerable influence. If we would carry out an interpolation between the linear and logaritmic velocity profiles only, like Wiberg & Smith (1987) and others did, we would neglect the fact that in the laminar regime we have the influence of snall turbulent eddies, while in the turbulent

regime they are phased out, and in the turbulent regime we have the lift force, while in the laminar regime this can be neglected. Also the point of action of the drag force changes considerably going from laminar to turbulent. So the interpolation has to be carried out on the Shields parameter itself, in order to take into account all the parameters that play a role. Since the Shields diagram is drawn in double logaritmic coordinates, the interpolation is carried out the following way. First the distance to the wall as a function of the coordinate on the horizontal axis is determined according to:

$$\xi = y^+ = \frac{u_* \cdot E \cdot d}{\nu} = E \cdot Re_* \tag{65}$$

A straight line in the double logarithmic diagram can be represented by:

$$\ln(\theta) = A + \ln(\xi) \cdot \left[\frac{\partial \ln(\theta)}{\partial \ln(\xi)}\right] \tag{66}$$

A non dimensional distance of 5 is chosen as the limit of pure laminar flow in the viscous sub layer. At higher values there is a deviation of the linear velocity profile. The derevative of the Shields parameter with respect to the distance to the wall in the laminar region is:

$$\left[\frac{\partial \ln(\theta)}{\partial \ln(\xi)}\right]_{Lam} = \frac{\ln(\theta_5) - \ln(\theta_{5-\Delta\xi})}{\ln(5) - \ln(5-\Delta\xi)} \tag{67}$$

Now the constant A can be determined according to:

$$A_{Lam} = \ln(\theta_5) - \left[\frac{\partial \ln(\theta)}{\partial \ln(\xi)}\right]_{Lam} \cdot \ln(5) \tag{68}$$

This results in the equation for the Shields parameter given by a straight line going to the right at a non dimensional distance from the wall above 5.

$$\ln(\theta_{Lam}) = A_{Lam} + \ln(\xi) \cdot \left[\frac{\partial \ln(\theta)}{\partial \ln(\xi)}\right]_{Lam} \tag{69}$$

For the turbulent region the same procedure is applied, but at a non dimensional distance from the wall of 70. The derevative of the Shields parameter with respect to the distance to the wall in the laminar region is:

$$\left[\frac{\partial \ln(\theta)}{\partial \ln(\xi)}\right]_{Turb} = \frac{\ln(\theta_{70}) - \ln(\theta_{70+\Delta\xi})}{\ln(70) - \ln(70+\Delta\xi)} \tag{70}$$

Now the constant A can be determined according to:

$$\mathbf{A_{Turb} = \ln(\theta_{70}) - \left[\frac{\partial \ln(\theta)}{\partial \ln(\xi)}\right]_{Turb} \cdot \ln(70)} \quad \mathbf{(71)}$$

This results in the equation for the Shields parameter according to a straight line going to the right at a non dimensional distance to the wall below 70.

$$\mathbf{\ln(\theta_{Turb}) = A_{Turb} + \ln(\xi) \cdot \left[\frac{\partial \ln(\theta)}{\partial \ln(\xi)}\right]_{Turb}} \quad \mathbf{(72)}$$

The location in between the non dimensional distances to the wall of 5 and 70 is determined logaritmically according to:

$$\mathbf{Q = \frac{\ln(\xi) - \ln(5)}{\ln(70) - \ln(5)}} \quad \mathbf{(73)}$$

So at 5 the value of **Q** is zero and at 70 the value is one. To ensure a smooth transition between the laminar and turbulent region, a sine shaped probability is introduced, giving a probability of one for Q at a non dimensional distance of 5 and zero at 70, according to:

$$\mathbf{P = 1 - \frac{\left(1 + \sin\left(\frac{\pi}{2} \cdot (2 * Q - 1)\right)\right)}{2}} \quad \mathbf{(74)}$$

Now the values of the Shields parameter can be determined in the transition zone, based on the values and the direction of the curves found in the transition points at the non dimensional distances to the wall of 5 and 70. It should be noted that for an exposure level of 0.5, this is at values of the boundary Reynolds number of 10 and 140.

$$\mathbf{\theta(\xi) = Exp\left(\left(A_{Lam} + \ln(\xi) \cdot \left[\frac{\partial \ln(\theta)}{\partial \ln(\xi)}\right]_{Lam}\right) \cdot P + \left(A_{Turb} + \ln(\xi) \cdot \left[\frac{\partial \ln(\theta)}{\partial \ln(\xi)}\right]_{Turb}\right) \cdot (1 - P)\right)} \quad \mathbf{(75)}$$

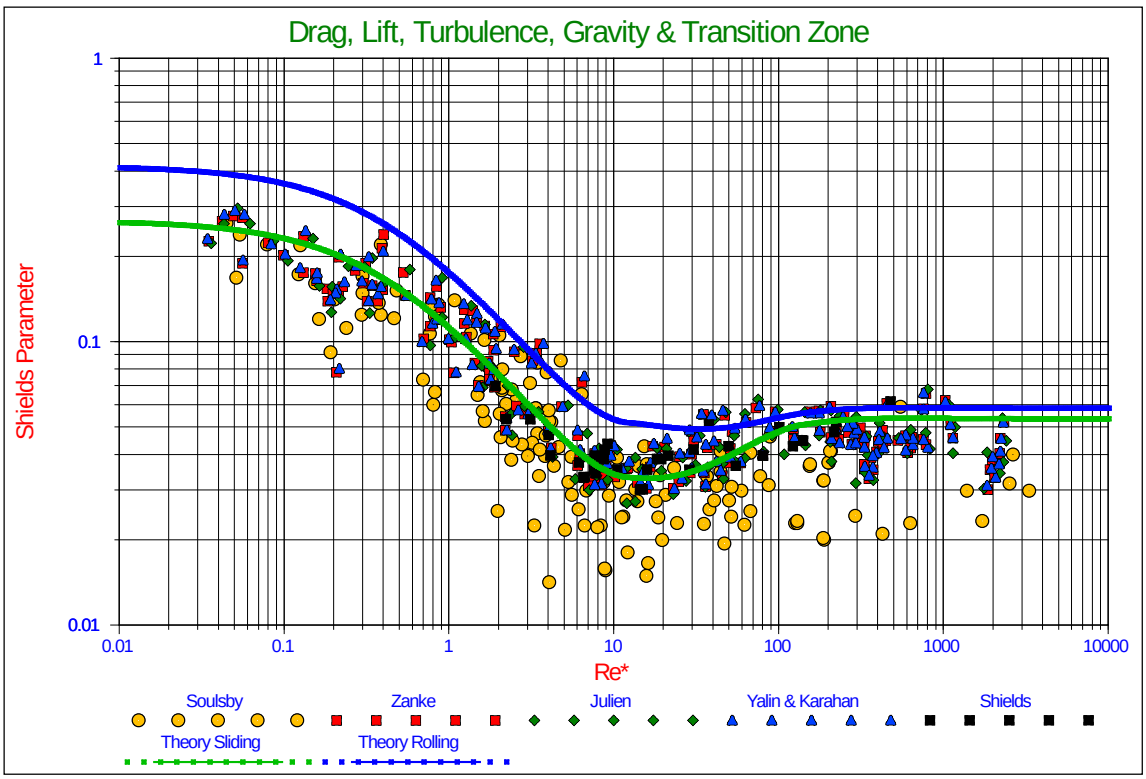

Figure 20: Drag, lift and turbulence induced initiation of motion with transition interpolation

The resulting curves for sliding and rolling are shown in **Figure 20**. The curve for sliding is still the lowest of the two curves and matches the data very well. The difference between sliding and rolling is small in the turbulent region and bigger in the laminar region. The main mode of entrainment is sliding, which makes sense, since many particles at many locations are entrained. Sliding seems to be the mechanism for making the whole top layer starting to move, while rolling is much more the mechanism of individual particles.

CONCLUSIONS AND DISCUSSION

A model to explain the Shields curve has been developed based on realistic values of the properties involved. The model correlates well with the original data of Shields (1936) (see **Figure 1**), the data collected by Yalin & Karahan (1979) and the data of others. Sliding, rolling and lifting are considered as the mechanism for entrainment, where sliding correlated the best with the data. Rolling gives higher values than sliding for the Shields parameter, while pure lift only occurs in the turbulent region at even higher values of the Shields parameter than rolling. Since sliding correlates the best and the fact that the original Shields data match critical to general transport, meaning that many particles at many locations are entrained, the main mechanism is sliding. Rolling and lifting are much more mechanisms of individual particles, while sliding may mobilize the whole top layer of the particles. Rolling by pivoting can only

occur if a pivot point exists, but when most particles in the top layer start to move, there often is no next particle, creating a pivot point. It can be expected however that particles having a higher exposure level than the 0.5 considered, will start to roll at lower values of the Shields parameter then predicted with the model.

Some new concepts have been introduced, comparing the model developed with already existing models. First of all the definition of the exposure and protrusion level in relation with the flow field and the use of the acting velocity and lever arm. The acting velocity and lever arm are not estimated, but determined based on taking the square root of the surface averaged square of the velocity integrated over the cross section of the particle exposed to the flow. It is surprising that previous researchers choose an average velocity or surface averaged velocity, since we are dealing with forces. To find the acting point of a stress or pressure, the stress or pressure has to be integrated over the cross section exposed to the flow in order to determine the acting point and the effective value. The introduction of the influence of turbulence is not new, but the introduction of the effective turbulence influence, based on the factor of simultaneous occurrence is. Also here, it is not about a velocity distribution or turbulence intensity distribution, but it is about the probability of the resulting force on a particle taking into account the phase cancellations of the small eddies. The original turbulence intensity profile as proposed by Nezu & Nakagawa (1993) has been modified slightly, so not only the turbulence intensity at the virtual bed is zero, but also the derivative with respect to the distance to the wall. The laminar region is dominated by drag and small eddy turbulence, while the turbulent region is dominated by drag and lift. A transition zone is chosen for non-dimensional particle exposure heights from 5 to 70 and a sophisticated interpolation method is used.

Finally, the virtual bed level is chosen at $\mathbf{0.2 \cdot d}$ below to top of the bed. In literature different values are used for the virtual bed level. Van Rijn (1984) and later Dey (1999) for example used $\mathbf{0.25 \cdot d}$. To interpret the value of the virtual bed level we have to consider that it is a value used to justify the velocity profile above the bed. Most probably, the velocity profile between the top of the grains will not follow the theoretical velocity profile, but most probably there will already be velocity at lower levels than the assumed virtual bed level. This implies that at very low exposure levels, resulting in negative protrusion levels, the velocity distribution should be corrected with respect to the theoretical profile. This also implies that the virtual bed levels for the time averaged velocities and the turbulence intensity do not necessarily have to be the same, justifying the modified turbulence intensity, but also the assumptions made by Zanke (2003). The fact that the model developed correlates very well with the data for very common values for the different properties, including the virtual bed level, proves that the model gives a good description of reality, without having the presumption of being reality.

LIST OF SYMBOLS USED

$\mathbf{A}$	Surface or cross section	m^2
$\mathbf{A_{Lam}}$	Interpolation constant for the laminar region	-
$\mathbf{A_{Turb}}$	Interpolation constant for the turbulent region	-
$\mathbf{C_D}$	Drag coefficient	-
$\mathbf{C_L}$	Lift coefficient	-
$\mathbf{d}$	Sphere, particle or grain diameter	m
$\mathbf{D_*}$	The Bonneville parameter or non-dimensional grain diameter	-
$\mathbf{E}$	Exposure level	-
$\mathbf{f_D, f_{Drag}}$	Fraction of cross section exposed to drag	-
$\mathbf{f_L, f_{Lift}}$	Fraction of top surface exposed to lift	-
$\mathbf{F_D}$	Drag force	N
$\mathbf{F_L}$	Lift force	N
$\mathbf{F_w}$	Weight of a particle	N
$\mathbf{g}$	Gravitational constant	9.81 m/sec^2
$\mathbf{h}$	Thickness of the layer of water	m
$\mathbf{k_s}$	Roughness often chosen equal to the particle diameter	m
$\mathbf{k_s^+}$	The non-dimensional roughness or roughness Reynolds number	-
ℓ	The point of action of the drag force	-
ℓ	Mixing length	m
$\ell_{\mathbf{Drag}}$	Drag point of action	-
$\ell_{\mathbf{Lift}}$	Lift point of action	-

$\ell_{\mathbf{Lever-D}}$	Additional lever arm for drag	-
$\ell_{\mathbf{Lever-L}}$	Additional lever arm for lift	-
n	Turbulence intensity factor	-
P	Probability used in interpolation	-
p/d	Relative protrusion level	-
Q	Factor used in interpolation	-
R	Radius of sphere, particle or grain	m
$\mathbf{R_d}$	The relative submerged specific density	-
$\mathbf{Re_D}$	The particle drag Reynolds number	-
$\mathbf{Re_*}$	Boundary Reynolds number	-
$\mathbf{Re_p}$	The particle Reynolds number	-
$\mathbf{S_*}$	The Grant & Madsen parameter	-
u	Time and surface averaged velocity	m/sec
$\mathbf{u_*}$	Friction velocity	m/sec
$\mathbf{u^+}$	Non dimensional time and surface averaged velocity	-
$\mathbf{u_{r.m.s.}}$	Turbulence intensity	m/sec
$\mathbf{u'_{r.m.s.}}$	Modified turbulence intensity	m/sec
$\mathbf{u'_{n\cdot r.m.s.}}$	The n^{th} moment of the modified turbulence intensity	m/sec
$\mathbf{u_{eff.}}$	The effective modified turbulence intensity	m/sec
$\mathbf{u^+_{r.m.s.}}$	Non dimensional turbulence intensity	-
$\mathbf{u^+_{total}}$	Non dimensional total velocity	-
V	Volume	m^3

y	Distance to the wall or virtual bed level	m
y_0	Integration constant	m
y^+	Non dimensional distance to the wall (Reynolds number)	-
α	The velocity factor at a certain exposure level	-
δ_v	Thickness of the viscous sub layer	m
δ_v^+	The non dimensional thickness of the viscous sub layer	11.6
κ	Von Karman constant	0.412
ρ	Fluid density	kg/m^3
ρ_f	Fluid density	kg/m^3
ρ_s	Solids density	kg/m^3
ρ_w	The density of water or fluids	kg/m^3
ρ_q	The density of quarts or solids	kg/m^3
ϕ	Internal friction angle/angle of repose	°
ϕ_0	The Coulomb friction angle quarts-quarts	°
ϕ_0	Pivot angle in Wiberg & Smith (1987A)	°
ϕ_{Roll}	Friction angle for rolling resistance	°
Ψ	The dilatation angle	°
Ψ	The pivot angle	°
θ	The Shields parameter or non-dimensional shear stress	-
θ_5	The Shields parameter for $\xi = 5$	-
θ_{70}	The Shields parameter for $\xi = 70$	-
τ	Total shear stress	Pa

τ_t	Turbulent shear stress	Pa
τ_v	Viscous shear stress	Pa
τ_b	Bed shear stress	Pa
ν	Kinematic viscosity	m^2/sec
μ	Friction coefficient usually the tangent of the internal friction angle	-
μ_{Roll}	Equivalent friction coefficient for rolling	-
ξ	The non-dimensional distance of the top of the sphere to the virtual bed level	-

REFERENCES

Bonneville, R. (1963). *essais de synthese des lois debut d'entrainment des sediment sous l'action d'un courant en regime uniform.* Chatou: Bulletin Du CREC, No. 5.

Brownlie, W. (1981). *Compilation of alluvial channel data: laboratory and field, Technical Report KH-R-43B.* Pasadena, California, USA: California Institute of Technology.

Buffington, J. M. (1999). The legend of A.F. Shields. *Journal of Hydraulic Engineering, 125*, 376–387.

Buffington, J. M., & Montgomery, D. R. (1997). A systematic analysis of eight decades of incipient motion studies, with special reference to gravel-bedded rivers. *Water Resources Research, 33*, 1993-2029.

Charru, F., Mouilleron, H., & Eiff, O. (2004). Erosion and deposition of particles on a bed sheared by a viscous flow. *Journal of fluid mechanics, Vol. 519.*, 55-80.

Chepil, W. (1958). The use of evenly spaced hemispheres to evaluate aerodynamic force on a soil failure. *Transaction of the American Geophysics Union, Vol. 39(3)*, 397-404.

Chin, C. O., & Chiew, Y. M. (1993). Effect of bed surface structure on spherical particle stability. *Journal of Waterway, Port, Coastal and Ocean Engineering, 119(3)*, 231–242.

Coleman, N. L. (1967). A theoretical and experimental study of drag and lift forces acting on a sphere resting on a hypothetical stream bed. *International Association for Hydraulic Research,12th Congress, 3*, pp. 185-192.

Coleman, N. L., & Ellis, W. M. (1976). Model study of the drag coefficient of a streambed particle. *Federal Interagency Sedimentation Conference*, (pp. 4-12). Denver, Colorado.

Dey, S. (1999). Sediment threshold. *Applied Mathematical Modelling*, 399-417.

Dey, S., & Raikar, R. (2007). Characteristics of loose rough boundary streams at near threshold. *Journal of Hydraulic Engineering, ASCE.*, 288-304.

DHL. (1972). *Systematic Investigation of Two Dimensional and Three Dimensional Scour, Report M648/M863.* Delft, Netherlands: Delft Hydraulics Laboratory.

Dittrich, A., Nestmann, F., & Ergenzinger, P. (1996). Ratio of lift and shear forces over rough surfaces. *Coherent flow structures in open channels.*, 126-146.

Egiazarof, I. (1965). Calculation of non-uniform sediment concentrations. *Journal of the Hydraulic Division, ASCE, 91(HY4)*, 225-247.

Engelund, F., & Hansen, E. (1967). A monograph on sediment transport to alluvial streams. *Copenhagen: Technik Vorlag*.

Everts, C. (1973). Particle overpassing on flat granular boundaries. *Journal of Waterways, Harbors, & Coastal Engineering, ASCE Vol. 99(WW4).*, 425-438.

Fenton, J. D., & Abbott, J. E. (1977). Initial movement of grains on a stream bed: The effect of relative protrusion. *Proceedings of Royal Society, 352(A)*, pp. 523–537. London.

Garcia, M. H. (2008). *Sedimentation Engineering* (Vol. 110). ASCE Manuals & Reports on Engineering Practise No. 110.

Govers, G. (1987). Initiation of motion in overland flow. *Sedimentology (34)*, 1157-1164.

Graf, W. H., & Pazis, G. C. (1977). Les phenomenes de deposition et d'erosion dans un canal alluvionnaire. *Journal of Hydraulic Research, 15*, 151-165.

Grass, A. J. (1970). The initial instability of fine bed sand. *Journal of Hydraulic Division, ASCE, 96(3)*, 619-632.

Guo, J., & Julien, P. (2007). Buffer law and transitional roughness effects in turbulent open-channel flows. *5th International Symposium on Environmental Hydraulics, 4-7 December 2007.* Tempe, Arizona, USA: ISEH.

Hinze, J. (1975). *Turbulence.* McGraw Hill Book company.

Hjulstrøm, F. (1935). Studies of the morphological activity of rivers as illustrated by the River Fyris. *Bulletin of the Geological Institute, 25*, 221–527. University of Uppsala.

Hjulstrøm, F. (1939). Transportation of debris by moving water, in Trask, P.D., ed., Recent Marine Sediments. *A Symposium: Tulsa, Oklahoma, American Association of Petroleum Geologists*, (pp. 5-31). Tulsa, Oklahoma.

Hofland, B. (2005). *Rock & Roll.* Delft, The Netherlands: PhD Thesis, Delft University of Technology.

Ikeda, S. (1982). Incipient motion of sand particles on side slopes. *Journal of the Hydraulic division, ASCE, 108*(No. HY1).

Iwagaki, Y. (1956). Fundamental study on critical tractive force. *Transactions of the Japanese Society of Civil Engineers, Vol. 41*, 1-21.

Julien, P. (1995). Erosion and sedimentation. *Cambridge University Press*.

Kim, J., Moin, P., & Moser, R. (1987). Turbulence statistics in fully developed channel flow at low Reynolds number. *Journal of Fluid Mechanics, 177*, 133-166.

Kirkby, M., & Statham, I. (1975). Surface stone movement and scree formation. *Journal of Geology, Vol. 83.*, 349-362.

Kramer, H. (1935). Sand mixtures and sand movement in fluvial levels. *Transaction of ASCE 100.*, 798-838.

Kurihara, M. (1948). On the critical tractive force. *Research Institute for Hydraulic Engineering*, Report No. 3, Vol. 4.

Liu, H. (1957). Mechanics of sediment ripple formation. *Journal of the Hydraulics Division, Vol. 83, No. 2, March/April.*, 1-23.

Liu, Z. (2001). Sediment Transport. *Lecture notes*. Aalborg University.

Loiseleux, T., Gondret, P., Rabaud, M., & Doppler, D. (2005). Onset of erosion and avalanche for an inclined granular bed sheared by a continuous laminar flow. *Physics of fluids, Vol. 17*, 1-9.

Luckner, T. (2002). Zum Bewegungsbeginn von Sedimenten. *Dissertation.* Darmstadt, Germany: Technische Universitat Darmstadt.

Luckner, T., & Zanke, U. (2007). An analytical solution for calculating the initiation of sediment motion. *International Journal of sediment Research, Vol. 22, No. 2.*, 87-102.

Madsen, O., & Grant, W. (1976). *Sediment transport in the coastal environment.* Cambridge, Massachusetts, USA: Technical report 209, M.I.T.

Mantz, P. A. (1977). Incipient transport of fine grains and flakes by fluids—Extended Shields diagram. *Journal of Hydraulic Division, ASCE, 103(6)*, 601-615.

Marsh, N. A., Western, A. W., & Grayson, R. B. (2004, July 1). Comparison of Methods for Predicting Incipient Motion for Sand Beds. *Journal of Hydraulic Engineering, 130*(No. 7, July 1, 2004)).

Miedema, S. (2010A). Constructing the Shields Curve: Part A Fundamentals of the Sliding, Rolling and Lifting Mechanisms for the Entrainment of Particles. *Submitted to the Journal of Hydraulic Engineering*.

Miller, M., McCave, I., & Komar, P. (1977). Threshold of sediment motion under unidirectional currents. *Sedimentology, Vol. 24.*, 507-527.

Morsi, S., & Alexander, A. (1972). An investigation of particle trajectories in two-phase flow systems. *Journal of Fluid Mechanics, Vol. 55*, 193-208.

Naden, P. (1987). An erosion criterion for gravel bed rivers. *Earth Surface and Landforms, Vol. 12.*, 83-93.

Nakagawa, H., & Nezu, I. (1977). Prediction of the contribution to the Reynolds stress from the bursting events in open-channel flows. *Journal of Fluid Mechanics, 80*, 99–128.

Neil, C. (1967). Mean velocity criterion for scour of coarse uniform bed material. *Proceedings of the twelfth I.H.A.R. Congress.*, (pp. 46-54).

Nezu, I., & Nakagawa, H. (1993). *Turbulence in Open Channel Flows.* A. A. Balkema.

Nezu, I., & Rodi, W. (1986). Open-channel flow measurements with a laser Doppler anemometer. *Journal of Hydraulic Engineering . ASCE, 112*, 335–355.

Nino, Y., Lopez, F., & Garcia, M. (2003). Threshold of particle entrainment into suspension. *Sedimentology, Vol. 50.*, 247-263.

Ourimi, M., Aussillous, P., Medale, M., Peysson, Y., & Guazzelli, E. (2007). Determination of the critical Shields number for particle erosion in laminar flow. *Physics of fluids, Vol. 19.*, 1-4.

Paintal, A. S. (1971). Concept of critical shear stress in loose boundary open channels. *Journal of Hydraulic Research, 8*(1), 91-109.

Pilotti, M., & Menduni, G. (2001). Beginning of sediment transport of incoherent grains in shallow shear flows. *Journal of Hydraulic Research, Vol. 39, No. 2.*, 115-124.

Prager, E., Southard, J., & Vivoni-Gallart, E. (1996). Experiments on the entrainment threshold of well-sorted and poorly sorted carbonate sands. *Sedimentology, Vol. 43.*, 33-40.

Reichardt, H. (1951). Vollstandige Darstellung der Turbulenten Geswindigkeitsverteilung in Glatten Leitungen. *Zum Angew. Math. Mech., 3(7)*, 208-219.

Rijn, L. v. (1984). Sediment transport: Part I: Bed load transport. *Journal of Hydraulic Engineering, Vol. 110(10)*, 1431-1456.

Rijn, L. v. (1993). *Principles of sediment transport in rivers, estuaries and coastal seas.* Utrecht & Delft: Aqua Publications, The Netherlands.

Rijn, L. v. (2006). *Principles of sediment transport in rivers, estuaries and coastal areas, Part II: Supplement 2006.* Utrecht & Delft: Aqua Publications, The Netherlands.

Saffman, P. G. (1965). The lift on small sphere in a slow shear low. *Journal of Fluid Mechanics, 22*, 385-400.

Schlichting, H. (1968). *Boundary layer theory.* 6th ed. New York: McGraw-Hill.

Shields, A. (1936). Anwendung der Aehnlichkeitsmechanik und der Turbulenzforschung auf die Geschiebebewegung. *Mitteilung der Preussischen Versuchsanstalt fur Wasserbau und Schiffbau, Heft 26, Berlin.* Belin.

Simons, D. (1957). *Theory and design of stable channels in alluvial material.* PhD thesis: Colorado State University.

Soulsby, R., & Whitehouse, R. (1997). Threshold of sediment motion in coastal environment. *Proceedings Pacific Coasts and Ports.* (pp. 149-154). Christchurch, New Zealand: University of Canterbury.

Stevenson, P., Cabrejos, F. J., & Thorpe, R. B. (2002). Incipient motion of particles on a bed of like particles in hydraulic and pneumatic conveying. *Fourth World Congress of Particle Technology, Sydney, 21st–25th July (paper 400).* Sydney.

Stevenson, P., Thorpe, R. B., & Davidson, J. F. (2002). Incipient motion of a small particle in the viscous boundary-layer at a pipe wall. *Chemical Engineering Science, 57,* 4505–4520.

Sundborg, A. (1956). The River Klarålven: Chapter 2. The morphological activity of flowing water erosion of the stream bed. *Geografiska Annaler, 38,* 165-221.

Swamee, P. K. (1993). Critical depth equations for irrigation canals. *Journal of Irrigation and Drainage Engineering, ASCE.*, 400-409.

Tison, L. (1953). Studies of the critical tractive force of entrainment of bed materials. *Proceedings of the fifth I.A.H.R. Congress.*, (pp. 21-35).

Turton, R., & Levenspiel, O. (1986). A short note on the drag correlation for spheres. *Powder technology Vol. 47,* 83-85.

USWES. (1936). *Flume tests made to develop a synthetic sand which will not form ripples when used in movable bed models.* Vicksburg, Mississippi, USA: United States Waterways Experiment Station, tech. Memo 99-1.

Vanoni, V. A. (1975). *Sedimentation Engineering: American Society of Civil Engineers, Manuals and Reports on Engineering Practice. No. 54. P.745.*

White, C. M. (1940). The equilibrium of grains on the bed of a stream. *Proceedings Royal Society of London, A174,* pp. 322-338.

White, S. (1970). Plane bed thresholds of fine grained sediments. *Nature Vol. 228.*, 152-153.

Wiberg, P. L., & Smith, J. D. (1987A). Calculations of the critical shear stress for motion of uniform and heterogeneous sediments. *Water Resources Research, 23*(8), 1471–1480.

Wiberg, P., & Smith, J. (1987B). Initial motion of coarse sediment in streams of high gradient. *Proceedings of the Corvallis Symposium.* IAHS Publication No. 165.

Wikipedia. (n.d.). Retrieved from Wikipedia: http://en.wikipedia.org/wiki/Erosion

Wu, W., & Wang, S. (2006). Formulas for sediment porosity and settling velocity. *Journal of Hydraulic Engineering, 132(8),* 858-862.

Yalin, M. S., & Karahan, E. (1979). Inception of sediment transport. *ASCE Journal of the Hydraulic Division, 105,* 1433–1443.

Zanke, U. C. (2001). *Zum Einfluss der Turbulenz auf den Beginn der Sedimentbewegung.* Darmstadt, Germany: Mitteilungen des Instituts fur Wasserbau und Wasserwirtschaft der TU Darmstadt, Heft 120.

Zanke, U. C. (2003). On the influence of turbulence on the initiation of sediment motion. *International Journal of Sediment Research, 18*(1), 17–31.

Ziervogel, K. (2003). *Aggregation and transport behavour of sediment surface particles in Mecklenburg Bight, south western Baltic Sea affected by biogenic stickiness.* Rostock: PhD Thesis, Universitat Rostock, Germany.

CONSTRUCTING THE SHIELDS CURVE

PART B: SENSITIVITY ANALYSIS, EXPOSURE & PROTRUSION LEVELS, SETTLING VELOCITY, SHEAR STRESS & FRICTION VELOCITY, EROSION FLUX AND LAMINAR MAIN FLOW

S.A. Miedema[2]

ABSTRACT

The model developed in Part A is verified and validated from 6 points of view.

1. The traditional Shields diagram, a sensitivity analysis
2. Exposure and protrusion levels
3. Shear velocity and shear stress
4. The ratio between the friction velocity and the terminal settling velocity
5. Stages of entrainment
6. Laminar main flow

It is proposed to distinguish 4 different Shields curves:

1. The Shields curve based on spheres in a turbulent main flow.
2. The Shields curve based on natural sands and gravels in a turbulent main flow.
3. The Shields curve in a laminar main flow for spheres.
4. The Shields curve in a laminar main flow for natural sand and gravels.

The general conclusions of this research are:

- The basic Shields curve can be determined by applying the sliding entrainment mechanism, with a friction angle of 30°, an exposure level of 0.5 (protrusion level of 0.3), a turbulence intensity factor of n=3, a lift coefficient of 0.415 and the drag coefficient of spheres.
- Using a reasonable bandwidth for the properties, like friction angle, lift coefficient and turbulence intensity, most of the scatter in the data found, can be explained.
- For natural sands and gravels a modified drag coefficient should be applied, based on the angularity of the particles.
- In the laminar region entrainment is dominated by drag and turbulence, while in the turbulent region this is dominated by drag and lift.
- Up to an exposure level of 0.6 sliding is the main entrainment mechanism, while for higher exposure levels rolling will occur.
- Laminar and turbulent main flow result in two different entrainment curves, based on the presence of turbulence. For laminar main flow a turbulence intensity factor of 0.5 has been found to correlate well with the measurements.
- The model developed correlates well with datasets of many independent researchers.

[2] Associate Professor & Educational Director, Offshore & Dredging Engineering, Delft University of Technology, Mekelweg 2, 2628CD Delft, The Netherlands. Email: s.a.miedema@tudelft.nl

INTRODUCTION

In Part A, a model for the entrainment of particles as a result of fluid (or air) flow over a bed of particles has been developed. The model distinguishes sliding, rolling and lifting as the mechanisms of entrainment. Sliding is a mechanism that occurs when many particles are starting to move and it is based on the global soil mechanical parameter of internal friction. Both rolling and lifting are mechanisms of individual particles and they are based on local parameters such as the pivot angle and the exposure and protrusion rate. Equations **(76)**, **(77)** and **(78)** give the Shields parameter for these 3 mechanisms.

Sliding

$$\theta_{sliding} = \frac{u_*^2}{R_d \cdot g \cdot d} = \frac{4}{3} \cdot \frac{1}{\alpha^2} \cdot \frac{\mu}{\ell_{Drag}^2 \cdot f_D \cdot C_D + \mu \cdot f_L \cdot C_L} \quad \textbf{(76)}$$

Rolling

$$\theta_{rolling} = \frac{u_*^2}{R_d \cdot g \cdot d} = \frac{4}{3} \cdot \frac{1}{\alpha^2} \cdot \frac{\sin(\psi + \phi_{Roll})}{\ell_{Drag}^2 \cdot f_D \cdot C_D \cdot (\ell_{Lever-D} + \cos(\psi + \phi_{Roll})) + f_L \cdot C_L \cdot (\ell_{Lever-L} + \sin(\psi + \phi_{Roll}))} \quad \textbf{(77)}$$

Lifting

$$\theta_{lifting} = \frac{u_*^2}{R_d \cdot g \cdot d} = \frac{4}{3} \frac{1}{\alpha^2 \cdot C_L \cdot f_L} \quad \textbf{(78)}$$

Analysis

The additional lever arm for lifting $\ell_{Lever-L} = 0$, since there is no reason to assume that the lift force does not go through the center of the particle. Now an effective friction coefficient for rolling, μ_{Roll}, can be introduced:

$$\mu_{Roll} = \frac{\sin(\psi + \phi_{Roll})}{\ell_{Lever-D} + \cos(\psi + \phi_{Roll})} \quad \textbf{(79)}$$

Substituting equation **(79)** in to equation **(77)**, gives an equation for the Shields parameter for rolling, very similar to the equation for sliding. For very small values of the surface coefficient

$\mathbf{f_D}$ at low exposure and protrusion levels, both equations **(76)** and **(80)** reduce to equation **(78)**, meaning that at very low exposure and protrusion levels, the three mechanisms give the same Shields parameter. Using $\phi = 30°$ for sliding and $\psi + \phi_{Roll} = 60°$ for rolling, an exposure level of $E = 0.5$ and an additional lever arm for the drag force of $\ell_{Lever-D} = 0.5$ for laminar flow and $\ell_{Lever-D} = 0.655$ for turbulent flow, results in a friction coefficient for sliding of $\mu = 0.577$, for laminar rolling of $\mu_{Roll-Lam} = 0.866$ and for turbulent rolling of $\mu_{Roll-Turb} = 0.75$. This explains why the Shields parameter found for rolling is higher than the one for sliding, where the difference is bigger in the laminar region than in the turbulent region.

$$\theta_{rolling} = \frac{u_*^2}{R_d \cdot g \cdot d} = \frac{4}{3} \cdot \frac{1}{\alpha^2} \cdot \frac{\mu_{Roll}}{\ell_{Drag}^2 \cdot f_D \cdot C_D + \mu_{Roll} \cdot f_L \cdot C_L} \quad \textbf{(80)}$$

Laminar Region

For the laminar region (the viscous sub layer) the velocity profile of Reichardt (1951) is chosen. This velocity profile gives a smooth transition going from the viscous sub layer to the smooth turbulent layer.

$$u_{top}^+ = \frac{u(y_{top})}{u_*} = \frac{\ln(1 + \kappa \cdot y_{top}^+)}{\kappa} - \frac{\ln(1/9) + \ln(\kappa)}{\kappa} \cdot \left(1 - e^{-\frac{y_{top}^+}{11.6}} - \frac{y_{top}^+}{11.6} e^{-0.33 \cdot y_{top}^+} \right) \approx y_{top}^+ \quad \textbf{(81)}$$

For small values of the boundary Reynolds number and thus the height of a particle, the velocity profile can be made linear to:

$$y_{top}^+ = E \cdot Re_* = E \cdot k_s^+ \quad \textbf{(82)}$$

Adding the effective turbulent velocity to the time averaged velocity gives for the velocity function α_{Lam}:

$$\alpha_{Lam} = y_{top}^+ + u_{eff}^+(y_{top}^+) \quad \textbf{(83)}$$

Turbulent Region

Particles that extend much higher into the flow will be subject to the turbulent velocity profile. This turbulent velocity profile can be the result of either a smooth boundary or a rough boundary. Normally it is assumed that for boundary Reynolds numbers less than 5 a smooth boundary

exists, while for boundary Reynolds numbers larger than 70 a rough boundary exists. In between in the transition zone the probability of having a smooth boundary is:

$$P = e^{-0.95 \cdot \frac{Re_*}{11.6}} = e^{-0.95 \cdot \frac{k_s^+}{11.6}} \quad (84)$$

This gives for the velocity function α_{Turb} :

$$\alpha_{Turb} = \frac{1}{\kappa} \cdot \ln\left(\frac{E \cdot d}{0.11 \cdot \frac{\nu}{u_*}} + 1 \right) \cdot P + \frac{1}{\kappa} \cdot \ln\left(\frac{E \cdot d}{0.033 \cdot k_s} + 1 \right) \cdot (1 - P) \quad (85)$$

The velocity profile function has been modified slightly by adding 1 to the argument of the logarithm. Effectively this means that the velocity profile starts y_0 lower, meaning that the virtual bed level is chosen y_0 lower for the turbulent region. This does not have much effect on large exposure levels (just a few percent), but it does on exposure levels of 0.1 and 0.2. Not applying this would result in to high (not realistic) shear stresses at very low exposure levels.

Sensitivity Analysis

In the previous paragraphs a model for the determination of the Shields curve was developed, based on a number of assumptions. The exposure level was chosen as 0.5, giving a protrusion level of 0.3, assuming a virtual bed level at $0.2 \cdot d$ below the top of the bed of uniform spheres. For sliding a friction angle of $\phi = 30°$ and for rolling a pivot angle of $\psi = 59°$ were chosen. The drag coefficient for spheres is applied and the lift coefficient according to $C_L = 0.423$ for the turbulent region. Finally the influence of turbulence is modelled, using 3 times the r.m.s. value of the turbulence intensity. The resulting curve, matching the data the best, is the curve for sliding. Now the question is, how sensitive is this model for variations in these assumptions.

The Angle of Natural Repose/the Angle of Internal Friction

The angle of repose/the angle of internal friction has been chosen at $\phi = 30°$, but could be a bit smaller or bigger according to Miedema (2010A), so also values of $\phi = 25°$ and $\phi = 35°$ will be applied. **Figure 21** shows the resulting curves. From this figure it is obvious that the variation of the friction angle might explain some of the scatter in the laminar region, while the influence of this variation is very limited in the turbulent region.

Turbulence

In the model an influence of 3 times the r.m.s. value of the turbulence intensity was used. The question is, if this is the best option and how sensitive is the model for the influence of turbulence. To test this also turbulence intensity factors of 0, 1, 2 and 4 times the r.m.s. value of the turbulence intensity are applied. A factor of 0 means no turbulence, so laminar main flow. The results are shown in **Figure 22** and show that part of the scatter for boundary Reynolds numbers in the range between 1 and 20 can be explained. The relatively high values for the Shields parameter as found by Pilotti & Menduni (2001) could be explained by a different behavior of the turbulence intensity, due to the laminar flow used.

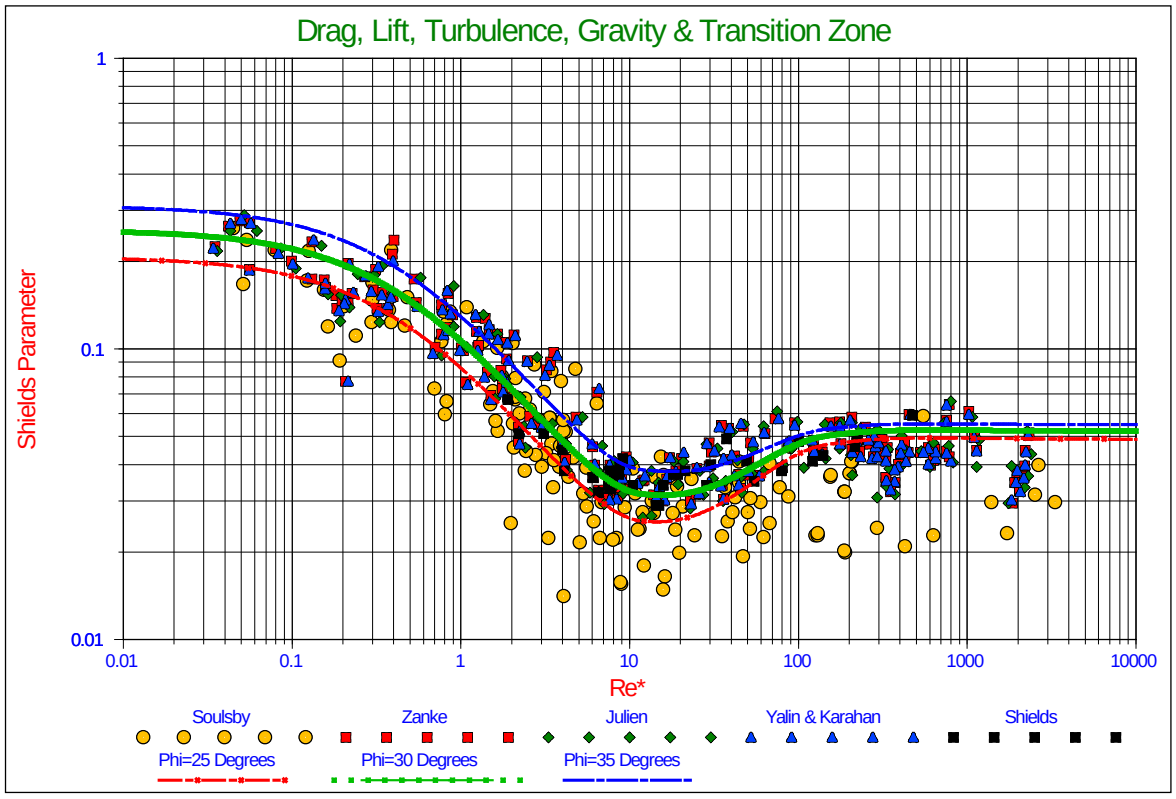

Figure 21: The Shields curve for sliding for friction angles of 25°, 30° and 35°

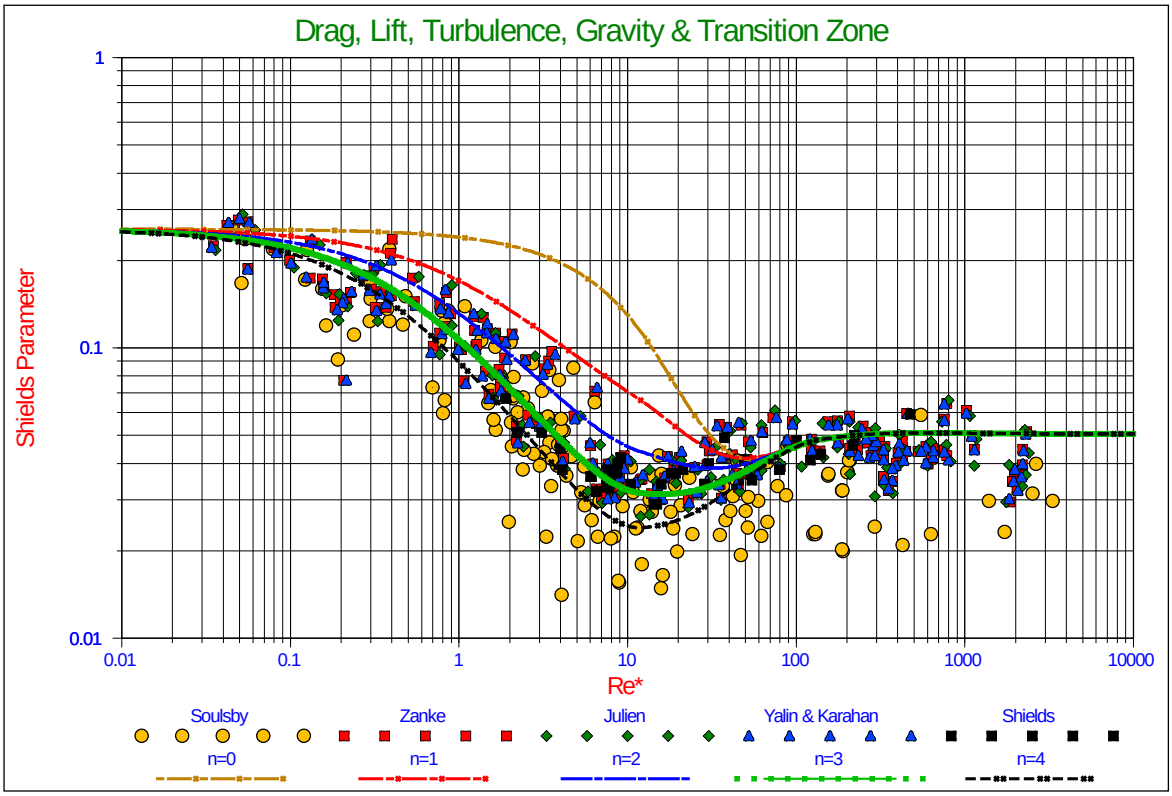

Figure 22: The Shields curve for sliding for different levels of turbulence

The Drag and the Lift Coefficient

The drag coefficient as known for spherical particles is used, like in the models found in literature, but it is known that non spherical particles encounter a higher drag coefficient, especially in the turbulent region. The lift coefficient is chosen at $\mathbf{C_L = 0.423}$, but what is the influence of a smaller lift coefficient, like the factor 0.2 as used by Wiberg & Smith (1987A). To investigate this calculations are carried out with the drag coefficient for sand, according to Miedema (2010A) and a lift coefficient of $\mathbf{C_L = 0.3}$. The results of these calculations are shown in **Figure 23**. Reduced lift may explain some scatter above the regular curve in the turbulent region, while using the drag coefficient for natural sand grains, explains a lot of the scatter below the regular curve in the turbulent region, especially since some of these data are achieved from experiments with natural sands. In the laminar region both lift and the drag coefficient have no effect, since lift is supposed to occur in the turbulent region only and the drag coefficient for spheres and natural sand grains does not differ much for very small particles.

Lower, Medium and Upper Levels and Real Sand Particles

From this sensitivity analysis a lower, medium (regular) and upper level for the Shields curve can be constructed. The lower level has a friction angle of $\mathbf{\phi = 25°}$, a turbulence intensity factor of 4 and a $\mathbf{C_L = 0.423}$. The medium or regular level has a friction angle of $\mathbf{\phi = 30°}$, a turbulence

intensity factor of 3 and a $\mathbf{C_L = 0.423}$. The upper level has a friction angle of $\boldsymbol{\phi = 35°}$, a turbulence intensity factor of 2 and a $\mathbf{C_L = 0.3}$. As a special case the lower level is also calculated with the drag coefficient for natural sands and gravels.

Figure 24 shows the results of these calculations. The upper level explains most of the scatter of the data above the regular or medium curve. The lower level explains most of the scatter in the laminar and transition region below the regular curve, but not in the turbulent region. However, applying the drag coefficient for natural sand grains also explains for the scatter below the regular curve in the turbulent region. Also the observation that in reality entrainment often occurs at values for the Shields parameter much lower than the original Shields curve and the proposal to take 50% for engineering purposes (Brownlie, 1981), can be explained by using the drag coefficient for natural sands and gravels. In the laminar region however the regular curve should be used up to boundary Reynolds numbers of about 5. In fact there should be two different Shields curves, one for spheres matching most of the experiments and one for natural sands and gravels using the appropriate drag coefficient. **Figure 25** explains for the influence of friction (or pivot angle), drag, lift and turbulence on the shape of the Shields curve. Increasing the friction coefficient will move the whole curve up, but more in the laminar region. Increasing the drag by using the drag coefficient for natural sands and gravels will move the turbulent and the transition region down. Increasing the lift will move the turbulent region down. Increasing the influence of turbulence will rotate the laminar region clockwise, while the asymptotic value for very small boundary Reynolds numbers will not change.

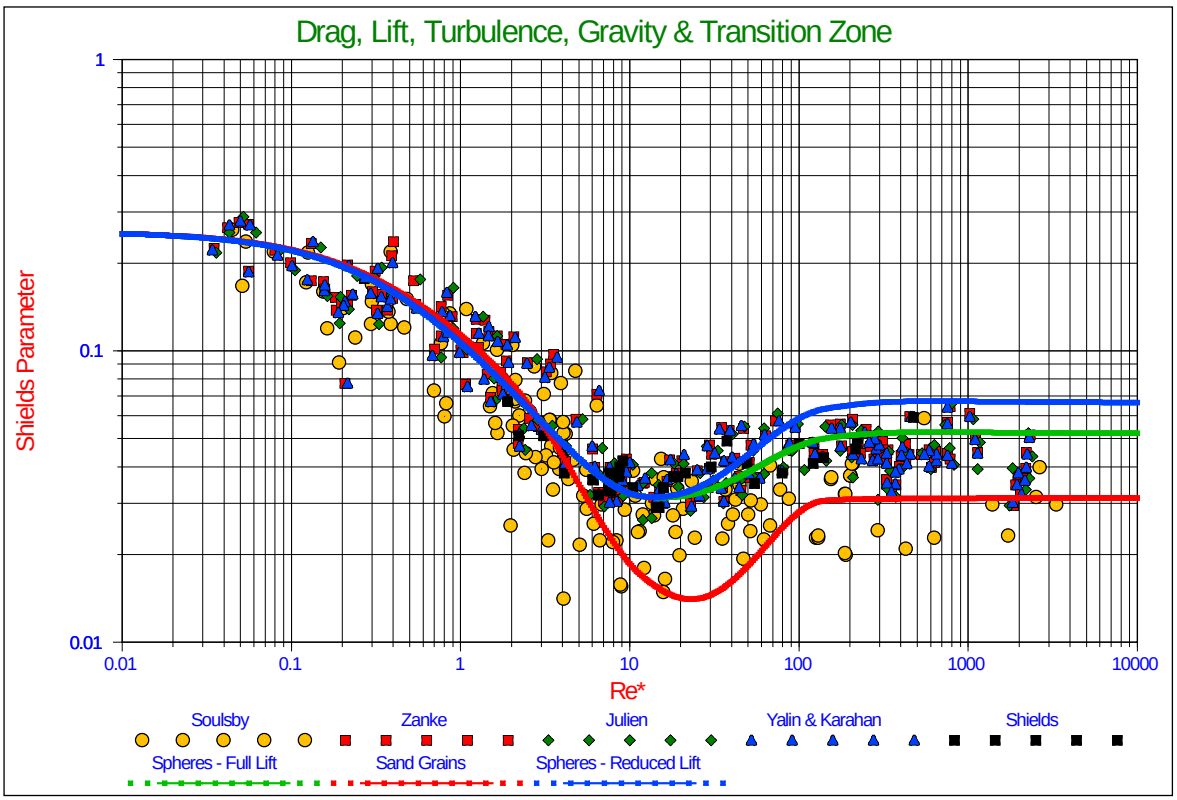

Figure 23: The Shields curve for spheres, sand grains and with reduced lift.)

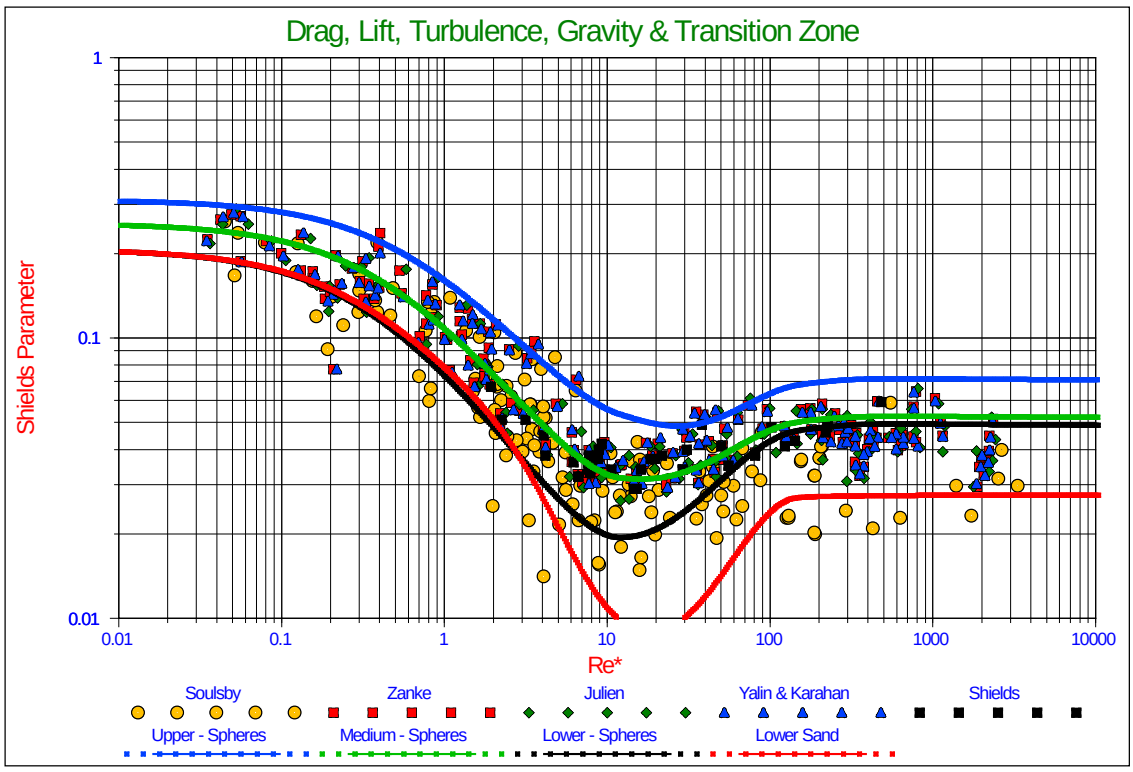

Figure 24: The medium (regular), lower and upper Shields curves for spheres and natural sand

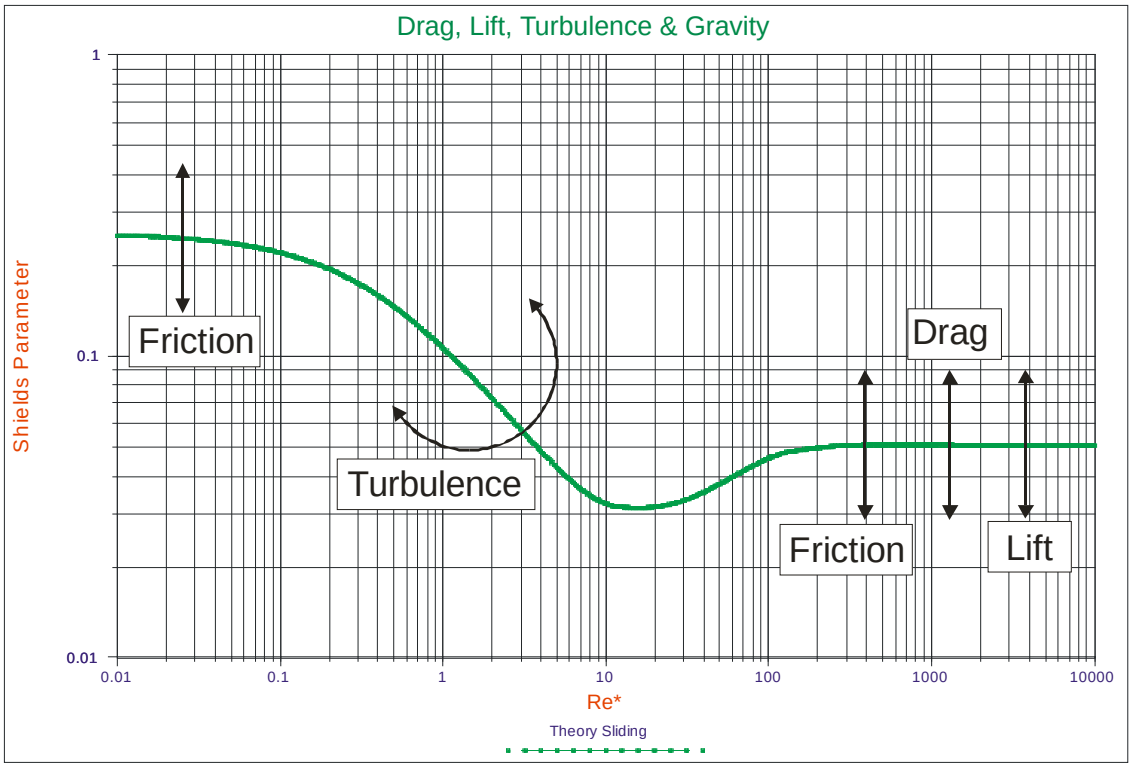

Figure 25: The influence of friction, drag, lift and turbulence on the shape of the Shields curve

Exposure and Protrusion Levels

To determine the influence of exposure and protrusion levels, exposure levels from 0.2 up to 1.2 will be investigated as is shown in **Figure 26** and **Figure 27**. In the laminar region the virtual bed level is chosen at $\mathbf{0.2 \cdot d}$ below the top of the bed, while in the turbulent region this is corrected with $\mathbf{0.2 \cdot d + y_0 = 0.233 \cdot d}$, still giving an exposure level starting at $\mathbf{0.2 \cdot d}$ below the top of the bed, assuming the roughness $\mathbf{k_s = d}$.

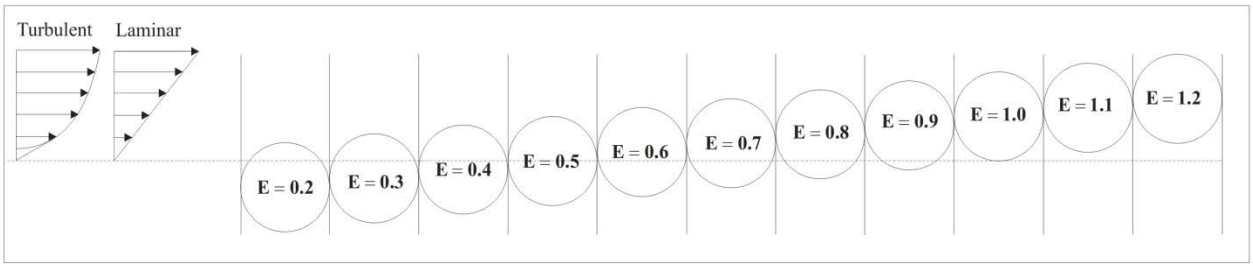

Figure 26: The exposure levels from 0.2 to 1.2

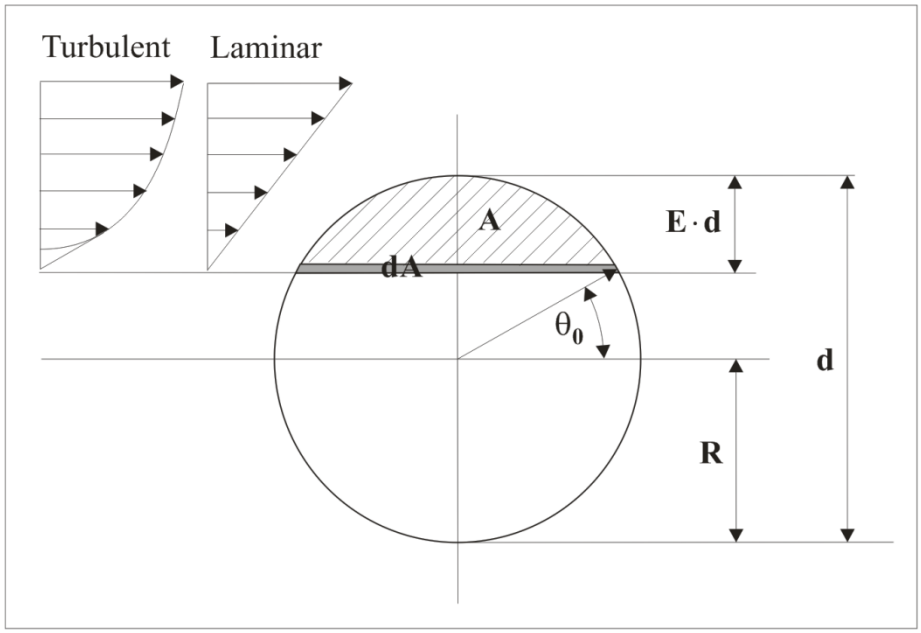

Figure 27: The area subjected to the flow

To determine the cross section subjected to the flow and the effective velocity on the cross section subjected to the flow, first the relation between the exposure level and the initial angle θ_0 for integration has to be determined, this relation is:

$$\sin(\theta_0) = 1 - 2 \cdot E$$

$$\theta_0 = \arcsin(1 - 2 \cdot E) \qquad \textbf{(86)}$$

To determine the cross section subjected to the flow we must integrate from the initial angle θ_0 for integration to an angle of $\pi/2$ according to:

$$dA = 2 \cdot R \cdot \cos(\theta) \cdot R \cdot d\theta \cdot \cos(\theta)$$

$$A = \int_{\theta_0}^{\pi/2} 2 \cdot R^2 \cdot \cos(\theta) \cdot \cos(\theta) \cdot d\theta \qquad \textbf{(87)}$$

The Drag Surface Factor

To determine the fraction f_{Drag} of this cross section with respect to the cross section of the whole sphere, equation **(87)** must be divided by $\pi \cdot R^2$ as is shown in equation **(88)**.

$$f_{Drag} = \frac{2 \cdot R^2 \cdot \int_{\theta_0}^{\pi/2} \cos^2(\theta) \cdot d\theta}{\pi \cdot R^2} \qquad \textbf{(88)}$$

The Lift Surface Factor

The lift surface factor is an empirical factor. One can imagine that the lift coefficient depends on the exposure level. At very low exposure levels, only the top of a sphere is affected by the flow and a smaller lift coefficient should be applied. At an exposure level of 0.5 the top half of the sphere is affected by the flow, but the bottom half is not. At an exposure level of 1.0 the whole sphere is surrounded by flow. Inspired by the work of Luckner (2002) the following empirical equation has been derived for the relation between the lift surface factor and the exposure level. The lift coefficient itself is chosen to be equal to the drag coefficient at high Reynolds numbers being $C_L = 0.445$.

$$f_{Lift} = 0.7125 + 0.4375 \cdot E \qquad \textbf{(89)}$$

The Pivot Angle

The pivot angles chosen are also inspired by the work of Luckner (2002) and corrected for the difference between exposure level and protrusion level.

The resulting values for the protrusion level (laminar), the drag surface factor, the lift surface factor, the pivot angle and the integration starting angle can be found in **Table 1** as a function of the exposure level. For exposure levels above 1.0, the surface factors and the integration angles are chosen to be equal to the ones at an exposure level of 1.0.

Table 1: Protrusion level, surface factors and pivot angle as a function of the exposure level

E	p/d	f_{Drag}	f_{Lift}	ψ	Θ_0
0.2	0.0	0.133	0.800	90	36.89
0.3	0.1	0.252	0.844	80	23.59
0.4	0.2	0.373	0.888	68	11.54
0.5	0.3	0.500	0.932	59	00.00
0.6	0.4	0.632	0.975	49	-11.54
0.7	0.5	0.759	1.019	40	-23.59
0.8	0.6	0.867	1.062	34	-36.89
0.9	0.7	0.954	1.106	27	-53.16
1.0	0.8	1.000	1.150	20	-90.00
1.1	0.9	1.000	1.150	12	-90.00
1.2	1.0	1.000	1.150	00	-90.00

The Drag Point of Action

To determine exactly which velocity to use for calculating the drag force, the surface averaged drag force has to be calculated. Since the drag force depends on the square of the local velocity, the surface averaged square of the velocity has to be determined. To find the drag point of action, the square of the local velocity has to be integrated over the surface exposed to the flow, the result has to be divided by the square of the velocity at the top of the sphere and divided by the surface. Taking the square root of this gives the drag point of action as a fraction of the exposure level. Equation **(90)** gives the general equation for this, while equation **(91)** and equation **(92)** show this for laminar flow in the viscous sub layer and turbulent flow in the turbulent region.

$$\ell_{Drag} = \sqrt{\frac{\int_{\theta_0}^{\pi/2} \overline{u(y)}^2 \cdot dA}{\overline{u(y)}_{top}^2 \cdot A}} \qquad \textbf{(90)}$$

$$\ell_{Drag-Lam} = \sqrt{\frac{2 \cdot R^2 \int_{\theta_0}^{\pi/2} \left(\frac{2 \cdot E - 1 + \sin(\theta)}{2}\right)^2 \cdot \cos(\theta)^2 \cdot d\theta}{E^2 \cdot 2 \cdot R^2 \cdot \int_{\theta_0}^{\pi/2} \cos^2(\theta) \cdot d\theta}} \qquad \textbf{(91)}$$

$$\ell_{Drag-Turb} = \sqrt{\frac{2 \cdot R^2 \int_{\theta_0}^{\pi/2} \left(\ln\left(\frac{\left(\frac{2 \cdot E - 1 + \sin(\theta)}{2} \right)}{0.033} + 1 \right) \right)^2 \cdot \cos^2(\theta) \cdot d\theta}{\left(\ln\left(\frac{E}{0.033} + 1 \right) \right)^2 \cdot 2 \cdot R^2 \cdot \int_{\theta_0}^{\pi/2} \cos^2(\theta) \cdot d\theta}} \quad \textbf{(92)}$$

The Additional Lever Arms

The additional lever arms, necessary for the pivoting mechanism, are related to the drag point of action according to equation **(93)** for laminar flow and equation **(94)** for turbulent flow. It is obvious that these additional lever arms for laminar and turbulent flow are not equal.

$$\ell_{Lever-Lam} = 1 - 2 \cdot E \cdot (1 - \ell_{Drag-Lam}) \quad \textbf{(93)}$$

$$\ell_{Lever-Turb} = 1 - 2 \cdot E \cdot (1 - \ell_{Drag-Turb}) \quad \textbf{(94)}$$

Table 2 gives the values of the drag point of action and the additional lever arms for laminar and turbulent flow as a function of the exposure and the protrusion level. In general, the drag point of action is located higher for turbulent flow than for laminar flow, also resulting in a larger additional lever arm.

Table 2: The drag point of action and the additional lever arms

E	p/d	$\ell_{Drag-Lam}$	$\ell_{Lever-Lam}$	$\ell_{Drag-Turb}$	$\ell_{Lever-Turb}$
0.2	0.0	0.485	0.794	0.541	0.816
0.3	0.1	0.490	0.694	0.586	0.752
0.4	0.2	0.494	0.596	0.623	0.698
0.5	0.3	0.500	0.500	0.655	0.655
0.6	0.4	0.505	0.405	0.682	0.618
0.7	0.5	0.511	0.315	0.706	0.588
0.8	0.6	0.522	0.235	0.730	0.568
0.9	0.7	0.537	0.166	0.754	0.557
1.0	0.8	0.559	0.118	0.784	0.568
1.1	0.9	0.591	0.100	0.788	0.533
1.2	1.0	0.619	0.086	0.792	0.501

CALCULATIONS

Spheres

Based on the basic equations for sliding, rolling and lifting, the surface factors, pivot angle, the calculated values for the drag point of action, the additional lever arms and the assumptions of an angle of repose of $\phi = 30°$ and a lift coefficient $C_L = 0.445$, the values of the Shields parameter can be calculated as a function of the exposure level and the mechanism. **Table 3** gives these values for the laminar region, the turbulent region and the minimum in the transition region and for pure lift in the turbulent region.

Table 3: Shields values for 3 mechanisms at different exposure levels

E	p/d	Sliding Laminar	Sliding Turbulent	Sliding Minimum	Rolling Laminar	Rolling Turbulent	Rolling Minimum	Lift
0.1	-0.1	9.5117	0.3344	0.3344	20.4147	0.3399	0.3399	0.3462
0.2	0.0	2.4783	0.1535	0.1340	5.0364	0.1596	0.1561	0.1664
0.3	0.1	0.8634	0.0958	0.0727	1.6287	0.1025	0.0988	0.1128
0.4	0.2	0.4327	0.0674	0.0458	0.7440	0.0731	0.0677	0.0865
0.5	0.3	0.2551	0.0505	0.0314	0.3926	0.0543	0.0461	0.0706
0.6	0.4	0.1665	0.0393	0.0228	0.2253	0.0408	0.0306	0.0598
0.7	0.5	0.1172	0.0316	0.0174	0.1359	0.0305	0.0202	0.0519
0.8	0.6	0.0878	0.0262	0.0140	0.0836	0.0225	0.0133	0.0459
0.9	0.7	0.0690	0.0226	0.0117	0.0507	0.0159	0.0086	0.0412
1.0	0.8	0.0568	0.0194	0.0103	0.0287	0.0103	0.0052	0.0373
1.1	0.9	0.0488	0.0179	0.0094	0.0127	0.0058	0.0024	0.0341
1.15	0.95	0.0456	0.0173	0.0090	0.0065	0.0034	0.0013	0.0327
1.2	1.0	0.0427	0.0167	0.0086	0.0012	0.0007	0.0002	0.0313

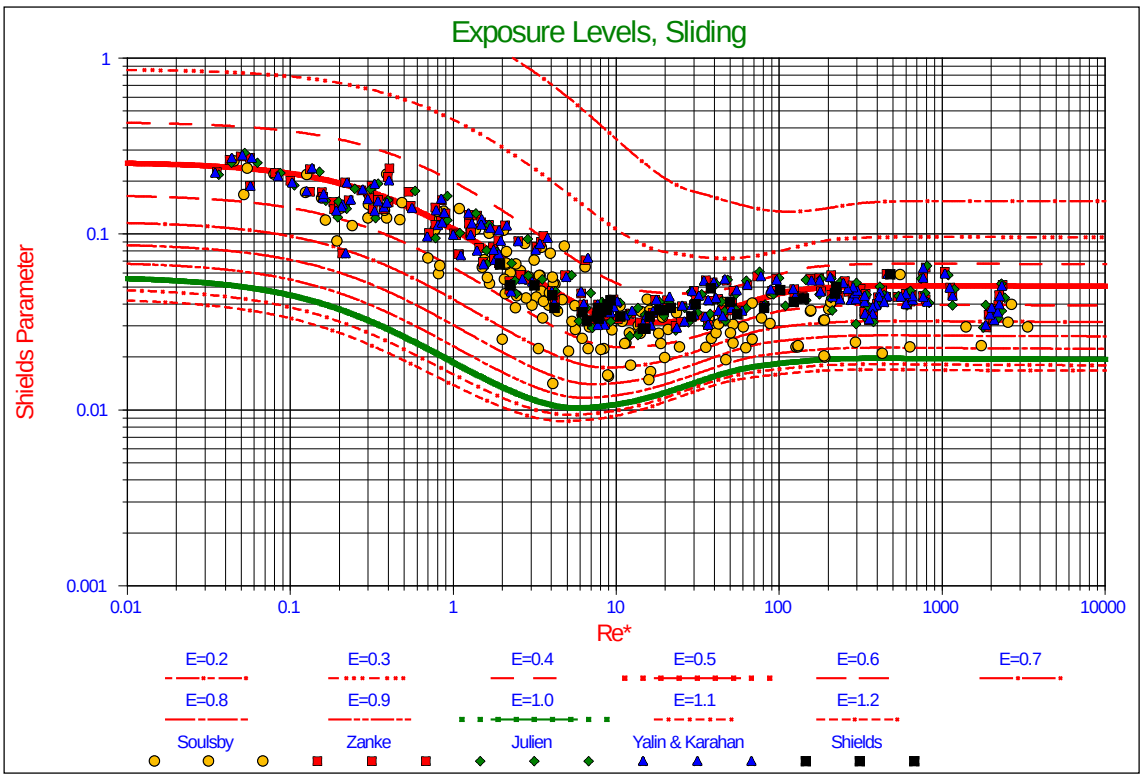

Figure 28: The Shields curves for the sliding mechanism

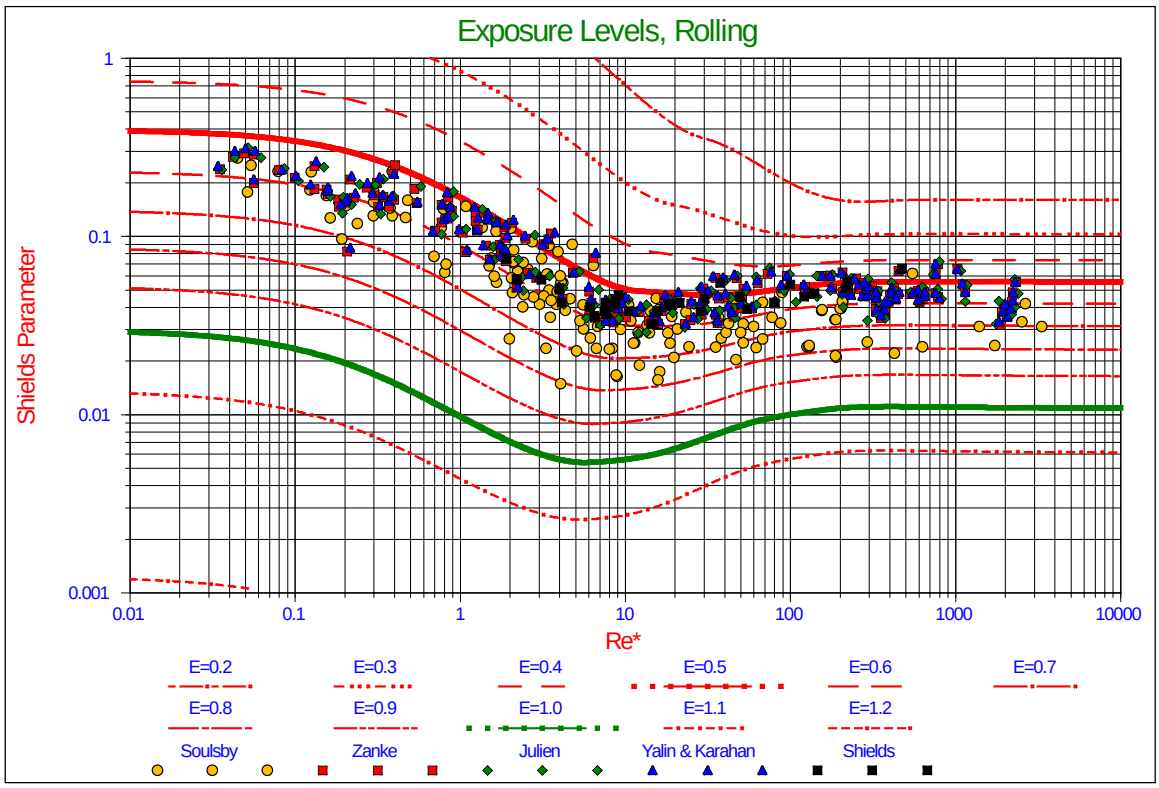

Figure 29: The Shields curves for the rolling mechanism

In the laminar region, the Shields values for sliding are smaller than the Shields values for rolling for exposure levels smaller than 0.6. Above an exposure level of 0.6 the Shields values for rolling are smaller. In the turbulent region this transition occurs at an exposure level somewhere between 0.6 and 0.7. The Shields values for pure lifting are always bigger than sliding and rolling, but at the smallest exposure level considered of 0.1, the value is almost equal to sliding and rolling. The conclusion can be drawn here that for exposure levels up to 0.6 the main mechanism for entrainment is sliding, which will occur for many particles at many locations simultaneously, while at higher exposure levels rolling will be the main mechanism, which will occur for single particles. **Figure 28** and **Figure 29** show the resulting curves for exposure levels from 0.2 up to 1.2 for sliding and rolling for spheres.

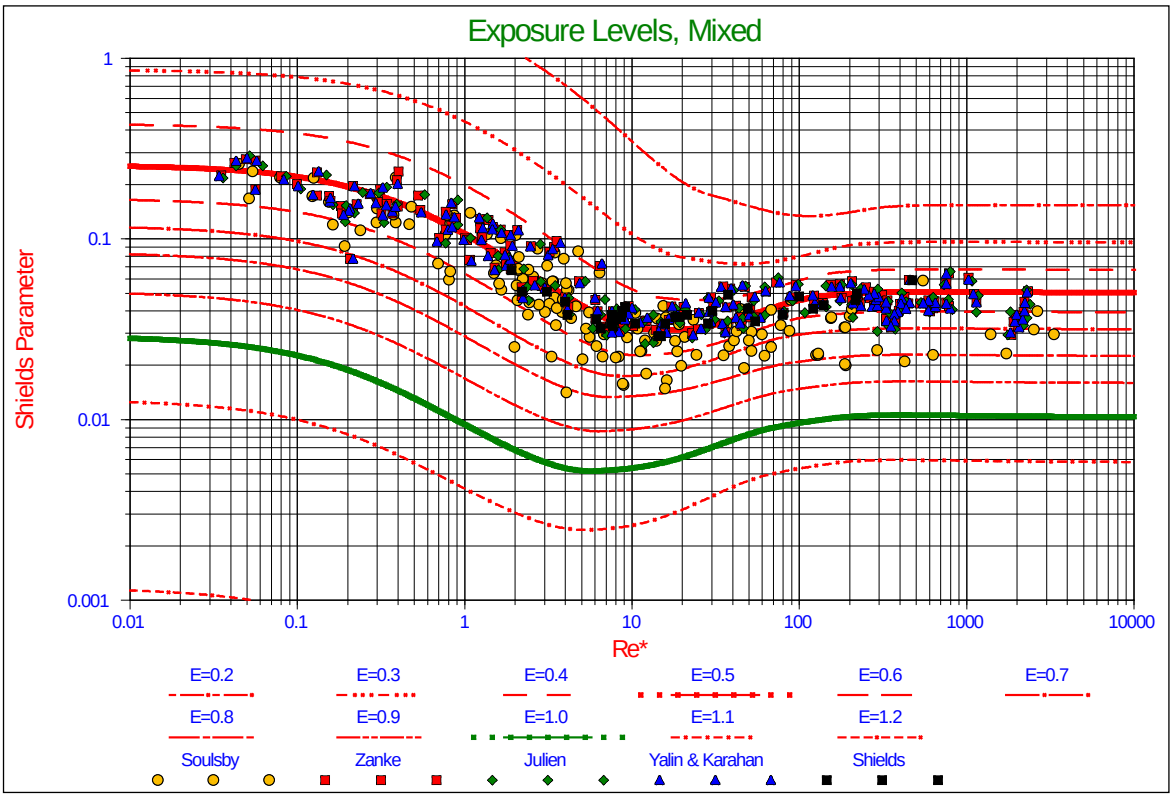

Figure 30: The Shields curves for sliding and rolling

Figure 30 shows the Shields curves for sliding for an exposure level of 0.2 up to an exposure level of 0.6 and rolling from an exposure level of 0.7 up to 1.2. **Figure 31** shows the same set of curves, but now as a function of the non-dimensional particle diameter (the Bonneville parameter). The advantage of using the Bonneville parameter is that this diagram is explicit. There is an explicit relation between the Shields parameter and the particle diameter, while this relation is implicit in the original Shields diagram where the friction velocity is part of both the boundary Reynolds number on the horizontal axis and the Shields parameter on the vertical axis. Dividing the Bonneville parameter by about 20 will give the particle diameter in mm for quarts with a density of 2650 kg/m^3 in a fluid with a viscosity of about 10^{-6} m^2/sec.

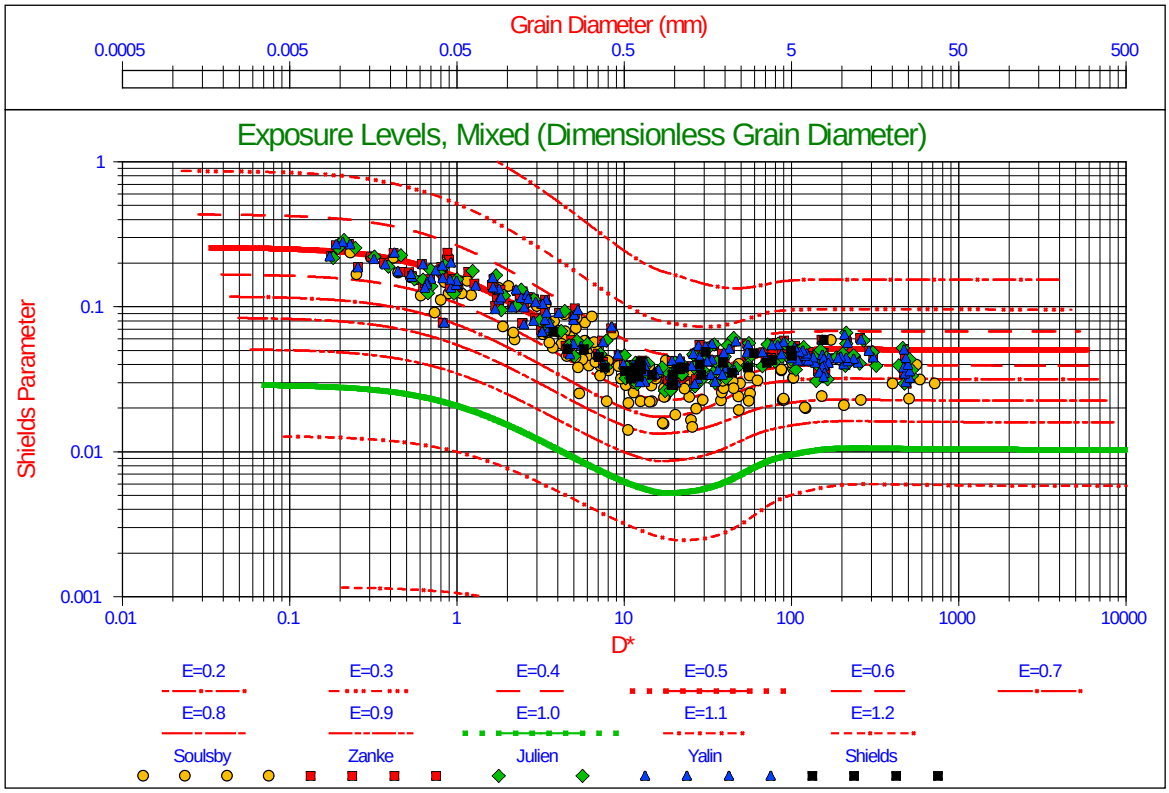

Figure 31: The Shields curves as a function of the Bonneville parameter

Natural Sands and Gravels

As has been described in Part A of this publication, the drag coefficient of natural sands and gravels differs from the drag coefficient of spheres. For rounded grains this difference is probably not too big, but for angular grains it is. In the laminar region at low Reynolds numbers both spheres and natural particles follow (or almost follow) the Stokes law, giving a drag coefficient of $\mathbf{C_D = 24 / Re}$, while some researchers use $\mathbf{C_D = 32 / Re}$ for natural sands. In the turbulent region however the difference is much larger. At large Reynolds numbers the drag coefficient for spheres is about $\mathbf{C_D = 0.445}$, while for natural sands and gravels values of $\mathbf{C_D = 1 - 2}$ are used. Using the equation as mentioned in Julien (1995) gives Shields curves as shown in **Figure 32**. In the laminar region the curves are almost identical to the curves for spheres, but in the turbulent region the curves gives values of 50% to 60% of the curves for spheres. The curves in **Figure 32** are for the sliding mechanism for exposure levels up to 0.6 and the rolling mechanism for larger exposure levels.

$$\mathbf{C_D = \frac{24}{Re_D} + 1.5} \qquad \textbf{(95)}$$

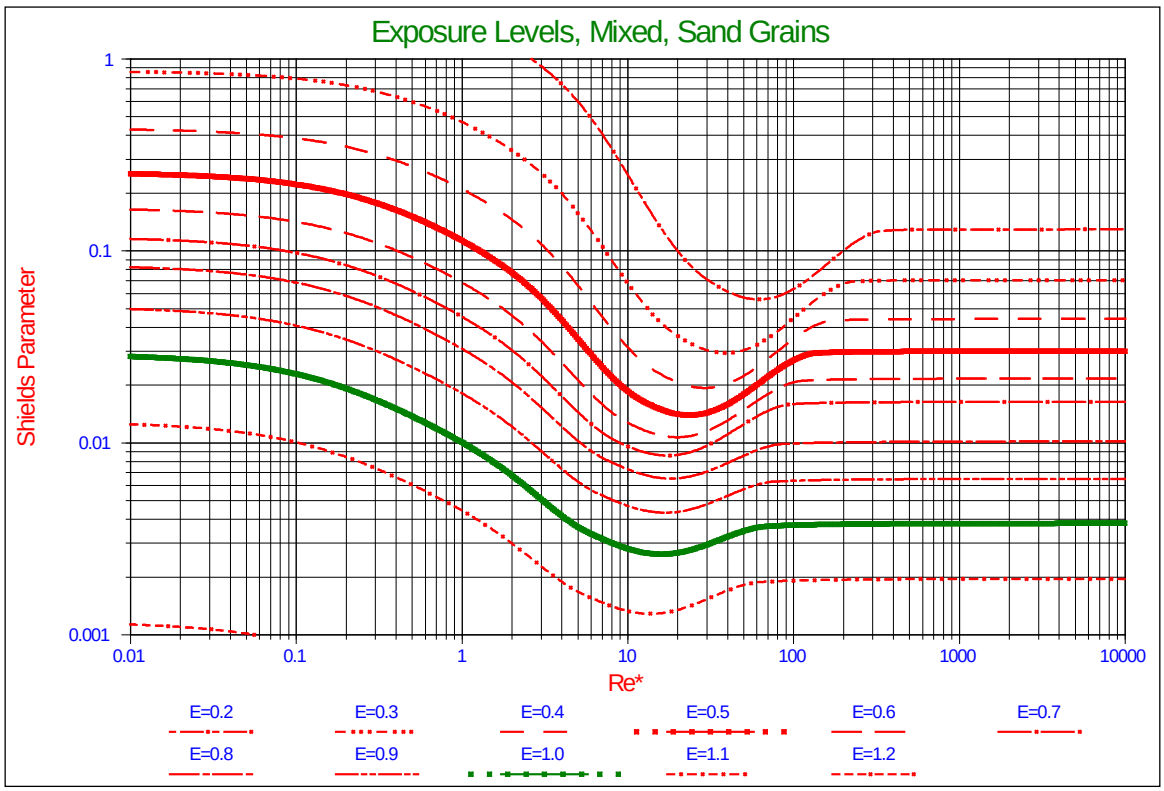

Figure 32: The Shields curves for natural sands and gravels

EXPOSURE & PROTRUSION LEVELS

The model developed here is now capable of predicting the non-dimensional shear stress or Shields parameter as a function of the exposure and protrusion level, so it is interesting to see how this correlates with experiments. The most cited experiments are those from Fenton & Abbot (1977) and Chin & Chiew (1993), who performed their experiments with spheres, where the bed consisted of fixed spheres, having a single loose sphere at a certain protrusion level. The only possible entrainment mechanism is rolling (pivoting), so their results will be compared with the curves calculated for rolling. Fenton & Abbot (1977) also re-analyzed the tests carried out by Coleman (1967) but the Shields values found should only be used as an indication of the magnitude of the Shields parameter. **Figure 33** shows all the measurements as a function of the boundary Reynolds number, grouped by protrusion level according to **Table 4**. The measurements of Coleman (1967) were carried out with spheres on top of the bed having a protrusion level of about 0.8 and an exposure level of 1.0, assuming a virtual bed level of 0.2 times the diameter below the actual bed level.

It is clear from **Figure 33** that the magnitude of the Shields values of the Coleman (1967) experiments match the Shields curve for an exposure level of 1.0 very well, although the minimum for these experiments tends to occur at a higher boundary Reynolds number than in the calculated curve. It should be mentioned that the experimental results of Coleman (1967) were calculated by Fenton & Abbot (1977) assuming full turbulent flow, while a number of these experiments are inside the transition region. Using the assumption of laminar flow for these

experiments would increase the value of the Shields parameter to values between 0.005 and 0.01, still being close to the calculated curve. For large boundary Reynolds numbers, the Coleman (1967) experiments gives value between 0.01 and 0.015, on average a bit higher than the theoretical curve.

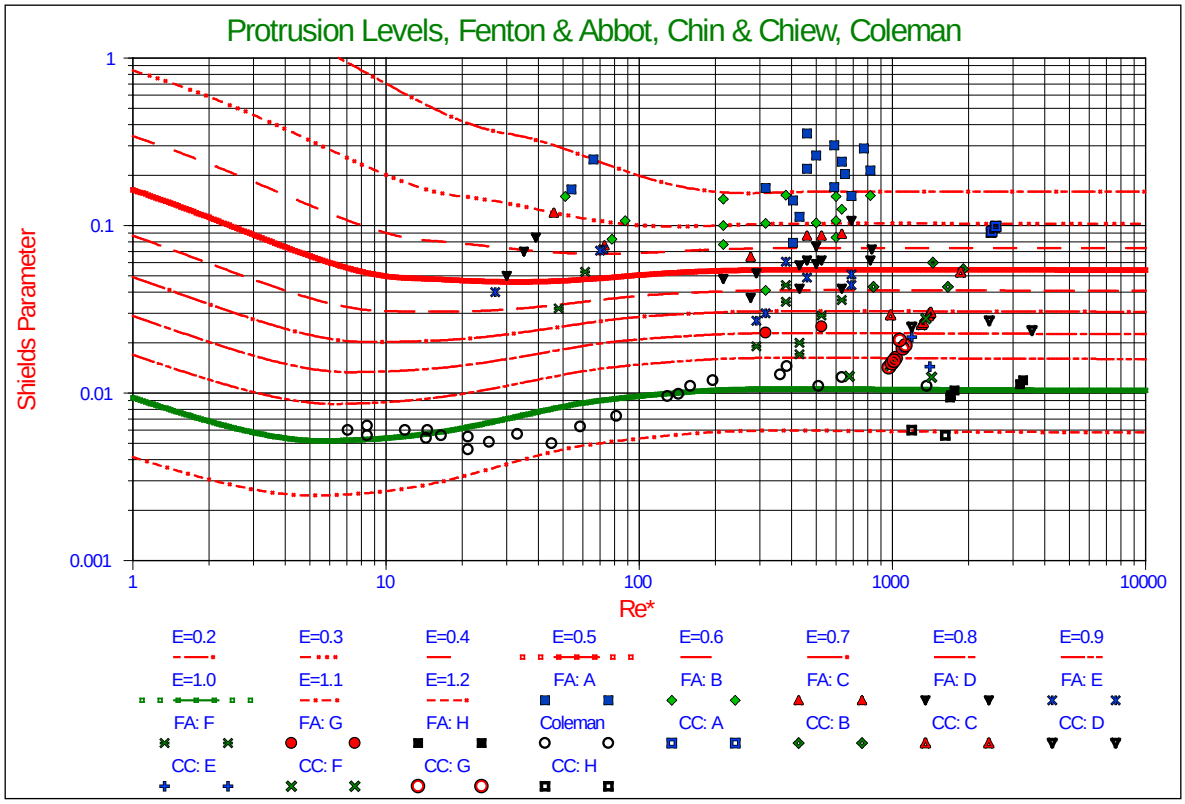

Figure 33: The measurements of Fenton & Abbot, Chin & Chiew and Coleman

Table 4: Explanation of the legend of Figure 33.

Fenton & Abbot	p/d	Chin & Chiew	p/d
FA: A	-0.3 – 0.0	CC: A	-0.3 – 0.1
FA: B	0.0 – 0.1	CC: B	0.1 – 0.3
FA: C	0.1 – 0.2	CC: C	0.3 – 0.5
FA: D	0.2 – 0.3	CC: D	0.5 – 0.6
FA: E	0.3 – 0.4	CC: E	0.6 – 0.7
FA: F	0.4 – 0.5	CC: F	0.7 – 0.8
FA: G	0.5 – 0.6	CC: G	0.8 – 0.9
FA: H	0.6 – 1.0	CC: H	0.9 – 1.0

Figure 34 and **Figure 35** show the measurements of Fenton & Abbot (1977) and Chin & Chiew (1993) in a linear-linear graph and a logarithmic-linear graph. Both graphs also show the calculated values for rolling at very high boundary Reynolds numbers, the minimum for rolling in the transition zone and the values for lifting. Most of the experiments of Fenton & Abbot (1977) were carried out at protrusion levels below 0.5 (exposure levels below 0.7), while

Chin & Chiew (1993) wanted to observe what would happen at higher protrusion levels. **Figure 34** shows that the theoretical values for protrusion levels from 0.1 up to 0.7 match very well with the experiments. At protrusion levels below 0.1 the theoretical values still match, but also many experiments have values below the theoretical ones. In general, the theory overestimates the Shields values compared with the experiments in this region. For protrusion levels above 0.7 its better to use the logarithmic-linear graph of **Figure 35**. The measurements carried out at a protrusion level of 0.82, which is the maximum protrusion level of a sphere resting on other spheres, show Shields values between 0.01 and 0.02, where Fenton & Abbot (1977) give values close to 0.01 and Chin & Chiew (1993) give the higher values. The theoretical value is about 0.01. Chin & Chiew (1993) also carried out experiments at protrusion levels of 0.90 and 0.94 and the theoretical value matches the measurement at the protrusion level of 0.90, but underestimates the protrusion level of 0.94. Still in general it can be concluded that the theoretical values match the measurements well enough, being evidence for the way the lift coefficient is used in the theoretical model. At the very low protrusion levels, -0.3 to -0.1, most probably another mechanism is occurring, since these protrusion levels are near the virtual bed level and without having enough velocity, entrainment can never be explained.

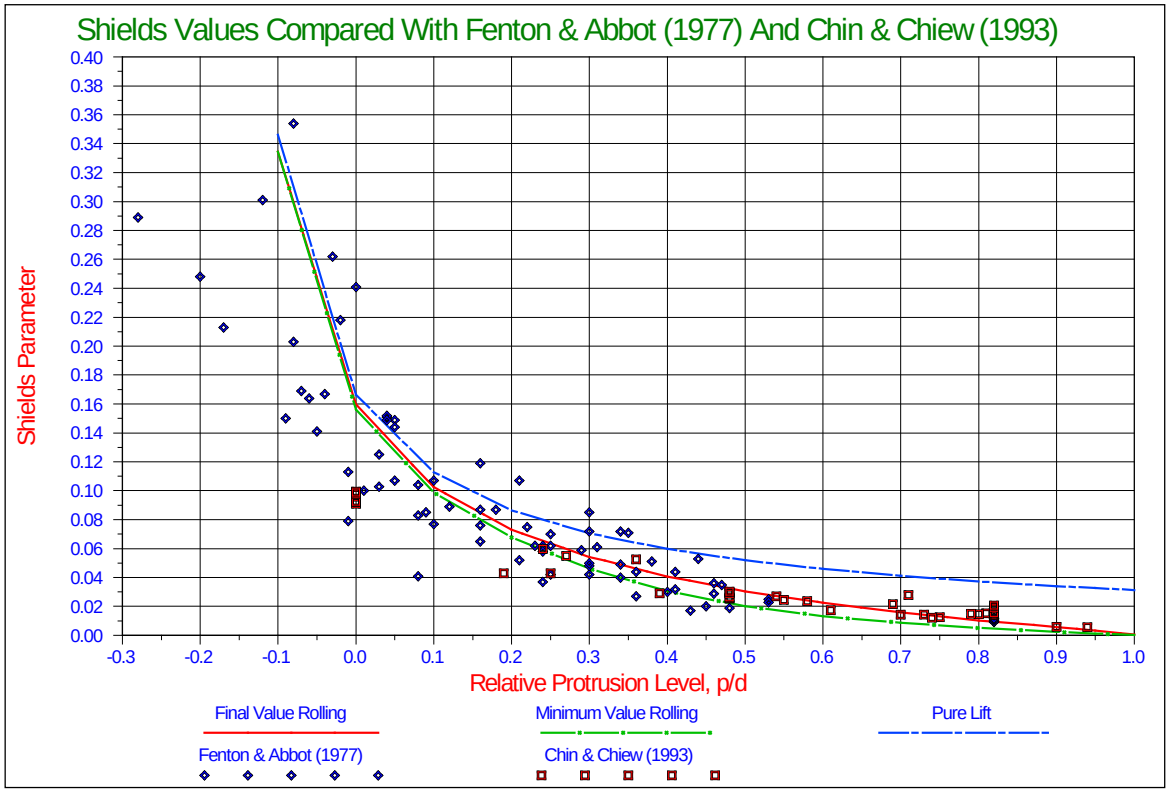

Figure 34: The experimental results of Fenton & Abbot (1977) and Chin & Chiew (1993) compared with the theory for rolling

SHEAR VELOCITY AND SHEAR STRESS

For the verification of the model to predict the initiation of motion, it is good to look at this physical phenomenon from different points of view. The first point of view is comparing the calculated Shields curve with the available data with the boundary Reynolds number at the horizontal axis and the non-dimensional shear stress on the vertical axis. A second point of view is to compare the theory with measurements of the Shields parameter for different protrusion levels. A third point of view is to compare the theory with measurements of the critical shear velocity (friction velocity) or with the critical shear stress. Wiberg & Smith (1987A) used the data selected by Miller, McCave & Comar (1977) that employed a consistent definition of critical motion. In addition, they required that the measurements were made in parallel sided flumes with an initially flat bed, using rounded, non-cohesive particles of nearly uniform size. The data satisfying these criteria are given by Casey (Tison, 1953), Neil (1967), Grass (1970), White (1970), Everts (1973) and Paintal (1971), complemented with data from Julien (1995) Fig. 7.7. Sundborg (1956) also used these data. The data are shown as the friction velocity as a function of the grain diameter in **Figure 36** and as the shear stress as a function of the grain diameter in **Figure 37**. In both figures the calculated Shields curves are plotted for exposure levels ranging from 0.2 up to 1.2 (protrusion levels from 0.0 up to 1.0). The calculated curve for an exposure level of 0.5 matches very well with the measurements, while most measurements lie in the range of exposure levels ranging from 0.4 to 0.6. Some of the scatter is caused by the fact that, although each researcher used a consistent definition of initial motion in their own experiments, some discrepancy exists among the different researchers regarding this definition. Wiberg & Smith (1987A) go more in to detail regarding this definition.

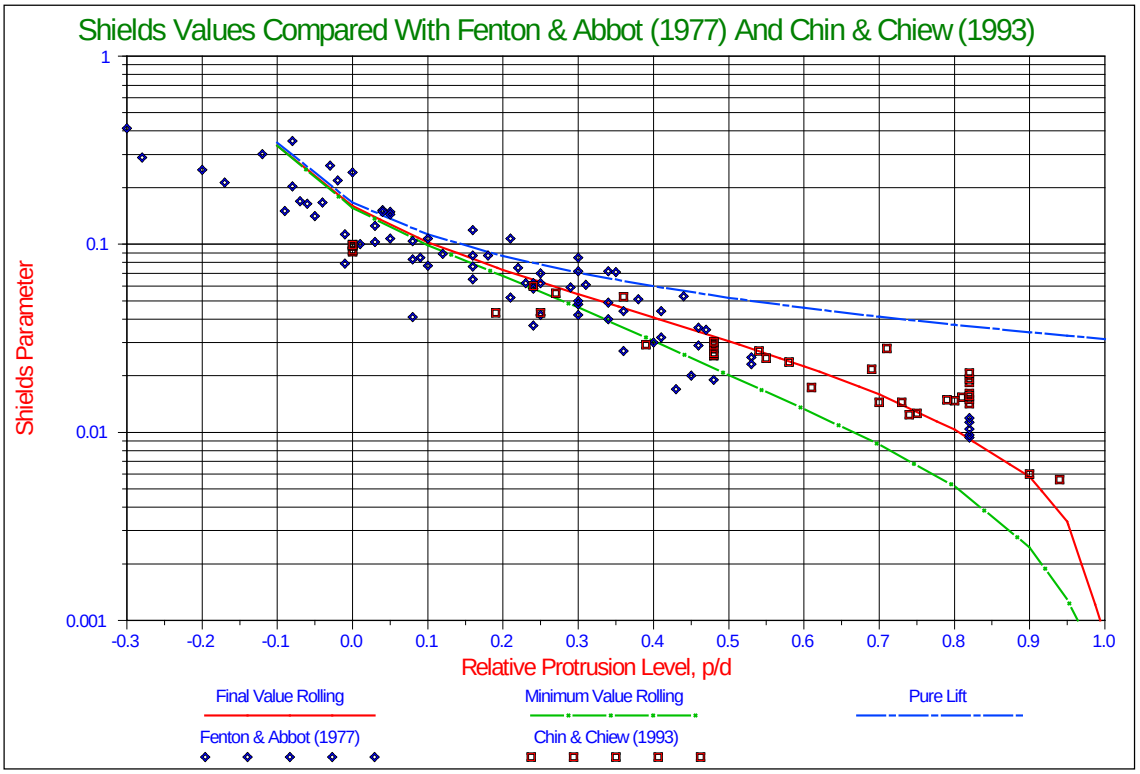

Figure 35: The experimental results of Fenton & Abbot and Chin & Chiew compared with the theory for rolling

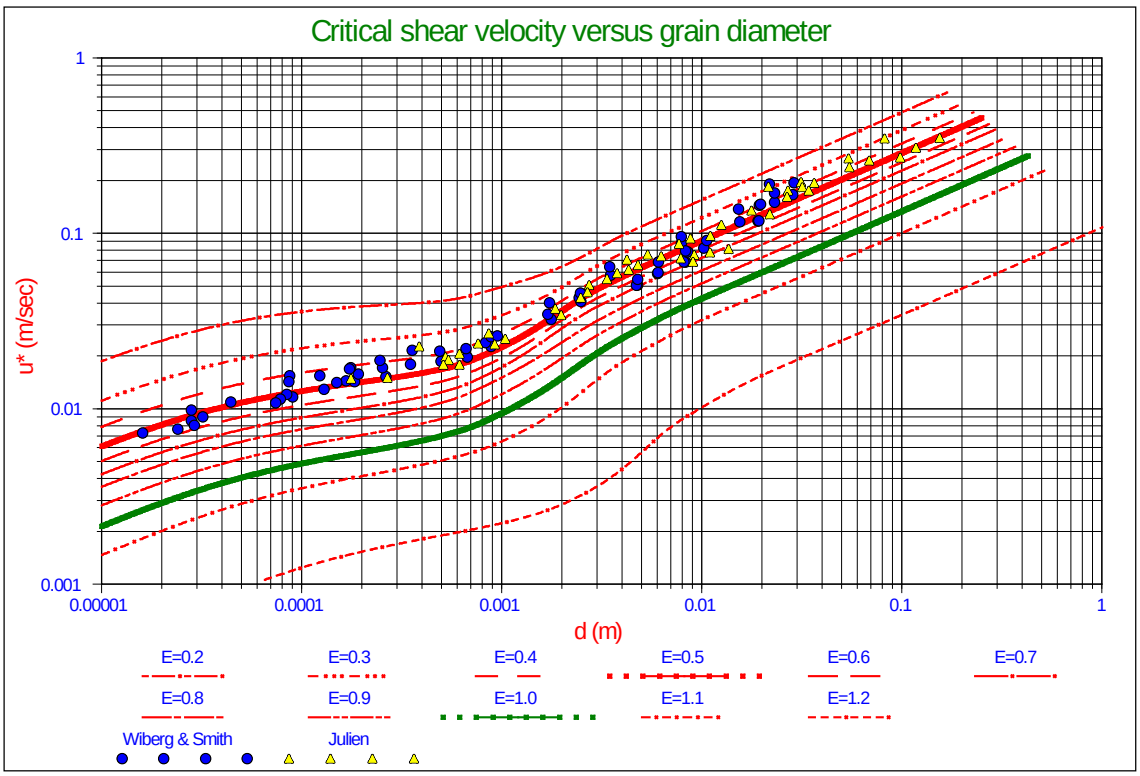

Figure 36: The critical shear velocity (friction velocity) as a function of the grain diameter

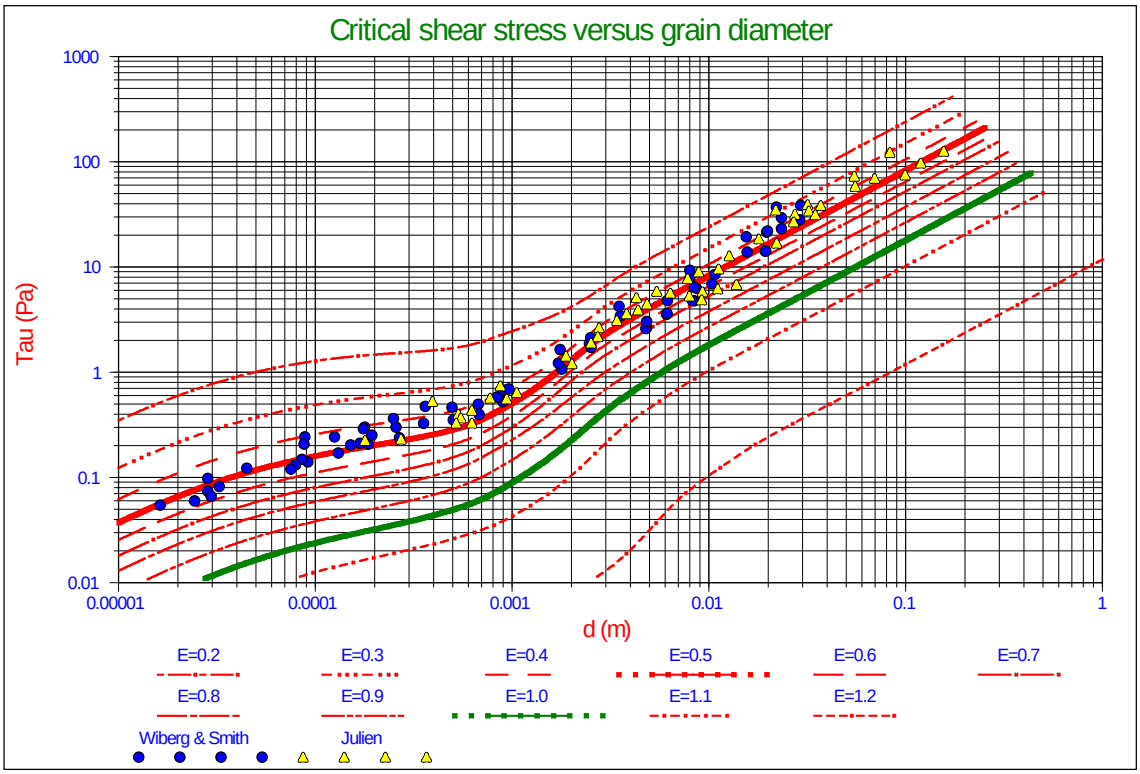

Figure 37: The critical shear stress as a function of the grain diameter

THE TERMINAL SETTLING VELOCITY

A fourth point of view is comparing the friction velocity with the terminal settling velocity. The settling velocity of grains depends on the grain size, shape and specific density. It also depends on the density and the viscosity of the fluid the grains are settling in, and it depends upon whether the settling process is laminar or turbulent. Discrete particles do not change their size, shape or weight during the settling process (and thus do not form aggregates). A discrete particle in a fluid will settle under the influence of gravity. The particle will accelerate until the frictional drag force of the fluid equals the value of the gravitational force, after which the vertical (settling) velocity of the particle will be constant (Figure 38).

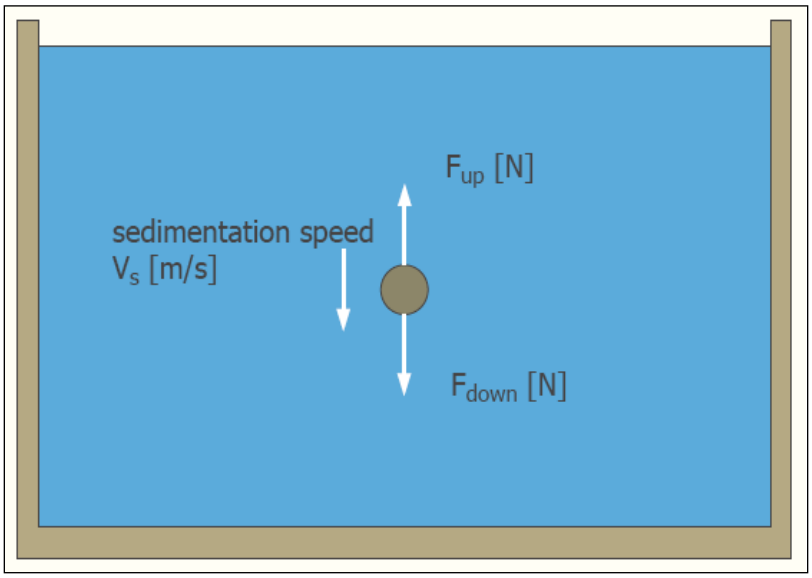

Figure 38: Forces on a settling particle

The upwards directed force on the particle, caused by the frictional drag of the fluid, can be calculated by:

$$\mathbf{F_{up} = C_D \cdot \frac{1}{2} \cdot \rho_w \cdot v_s^2 \cdot A} \qquad \mathbf{(96)}$$

The downward directed force, cause by the gravitational difference in density between the particle and the water, can be calculated by:

$$\mathbf{F_{down} = (\rho_q - \rho_w) \cdot g \cdot V} \qquad \mathbf{(97)}$$

The projected surface of the particle is:

$$\mathbf{A = \frac{\pi}{4} \cdot d^2} \qquad \mathbf{(98)}$$

The volume of the particle is:

$$\mathbf{V = \frac{\pi}{6} \cdot d^3} \qquad \textbf{(99)}$$

In general, the settling velocity $\mathbf{v_s}$ can now be determined with the following equation:

$$\mathbf{v_s = \sqrt{\frac{4 \cdot g \cdot (\rho_q - \rho_w) \cdot d}{3 \cdot \rho_w \cdot C_d}}} \qquad \textbf{(100)}$$

The settling velocity is thus dependent on the density of the particle and the fluid, the diameter and the flow pattern around particle. The Reynolds number of the settling process determines whether the flow pattern around the particle is laminar or turbulent. The Reynolds number can be determined by:

$$\mathbf{Re_p = \frac{v_s \cdot d}{\nu}} \qquad \textbf{(101)}$$

The settling of particles occurs in one of 3 regions, the laminar region, a transitional region or the turbulent region.

The laminar region, $\mathbf{Re_p < 1}$ (Stokes flow):

The upward flow of water along downward moving particles occurs under streamline conditions. The frictional resistance is only due to viscous forces and $\mathbf{C_D}$ varies inverse proportional to $\mathbf{Re_p}$.

The turbulent region, $\mathbf{Re_p > 2000}$**:**

The flow of water along the settling particles takes place under fully developed turbulent conditions. Compared with the eddying resistance, the viscous forces are negligible and $\mathbf{C_D}$ is virtually constant.

The transition region, $\mathbf{1 < Re_p < 2000}$**:**

The viscous and eddying resistances are of equal importance. An exact equation for $\mathbf{C_D}$ cannot be given, but there are several approximations.

Liu (1957) carried out measurements for the initiation of motion based on the ratio of the friction velocity and the terminal settling velocity. To compare these measurements with the Shields curve calculated, first the diameter of the grain considered has to be determined. This can be achieved by first determining the Bonneville parameter from the boundary Reynolds number and the Shields parameter:

$$D_* = \left(\frac{Re_*}{\sqrt{\theta}} \right)^{2/3} \quad (102)$$

The second step is to determine the grain diameter from the Bonneville parameter, using a factor 0.7, since an exposure level of 0.5 implies that half the grain cross section is exposed to the flow, resulting in an equivalent grain diameter of about 0.7 times the real diameter.

$$d = \frac{0.7 \cdot D_*}{\sqrt[3]{\frac{R_d \cdot g}{\nu^2}}} \quad (103)$$

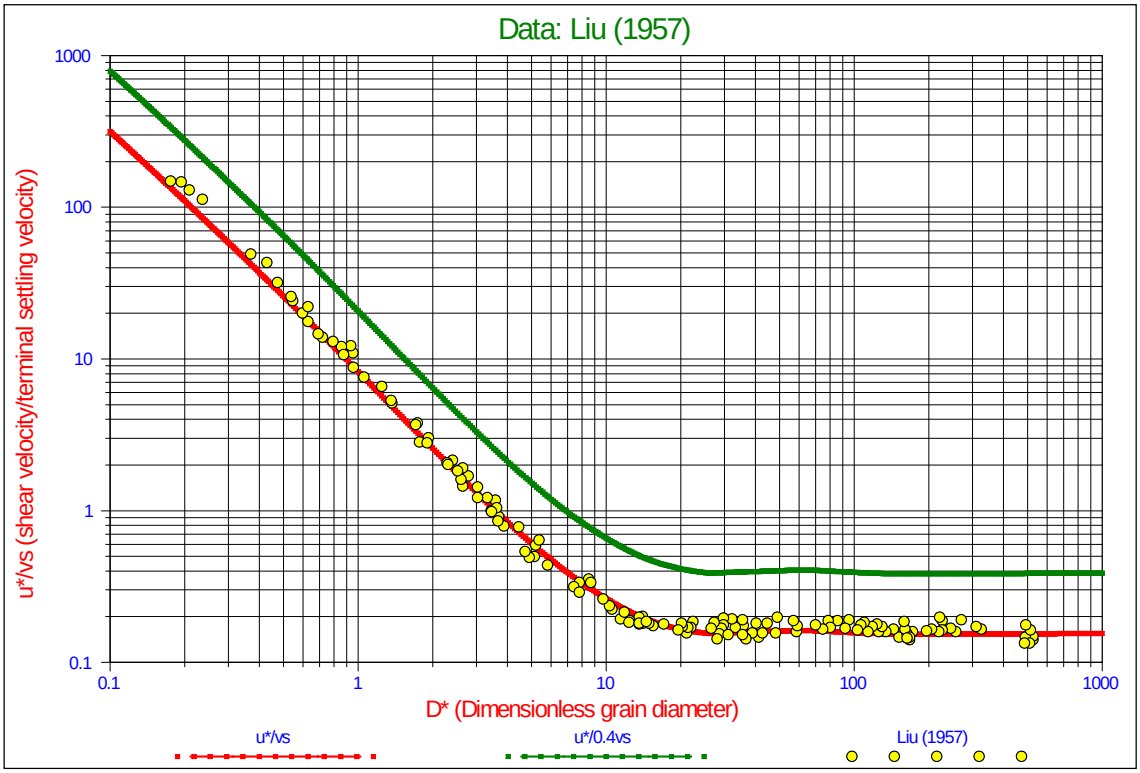

Figure 39: The ratio between the friction velocity and the terminal settling velocity

Figure 39 shows the converted Shields curve compared with the data of Liu (1957). The converted calculated Shields curve correlates almost perfectly with the data. It is remarkable how the curve of $u_* / 0.4 \cdot v_s$ matches the findings of Nino, Lopez & Garcia (2003) regarding the initiation of suspension as mentioned in van Rijn (2006). It should be mentioned here that, in order to get the good fit as is shown in **Figure 39**, exactly the same drag coefficient is applied for calculating the horizontal drag force, as is used for calculating the terminal settling velocity, while the equivalent grain diameter derived from the Bonneville parameter has been multiplied by 0.7, since at an exposure level of 0.5 only 50% of the cross section of the grain is exposed to the flow and this cross section is proportional to the square of the grain diameter.

STAGES OF ENTRAINMENT

A fifth point of view is the stage of entrainment. Several researchers investigated different stages of entrainment, usually starting with a single particle being entrained and ending with general transport. Vanoni (1975) investigated small particles (0.037 mm, 0.102 mm) in the laminar sub layer with boundary Reynolds numbers ranging from 0.2 to 2. Delft Hydraulics (1976), see van Rijn (1993), carried out tests on particles of 7 diameters with boundary Reynolds numbers ranging from 1 to 150. Graf & Pazis (Rijn, 1993) carried out tests in the boundary Reynolds range of 50 to 150, while more recently experiments were carried out by Dey & Raikar (2007) in the turbulent region with boundary Reynolds numbers ranging from 200 to 2000. Ziervogel (2003) carried out experiments on sediments in the Baltic Sea. **Figure 40** shows the results of these researchers as a function of the boundary Reynolds number. **Figure 41** shows the same measurements, but now as a function of the Bonneville parameter.

The Delft Hydraulics (1972) defined 7 levels of erosion according to:

1. Occasional particle movement at some locations (DHL7).
2. Frequent particle movement at some locations (DHL6).
3. Frequent particle movement at many locations (DHL5).
4. Frequent particle movement at nearly all locations (DHL4).
5. Frequent particle movement at all locations (DHL3).
6. Permanent particle movement at all locations (DHL2).
7. General transport (initiation of ripples) (DHL1).

Graf & Pazis (1977) defined 4 levels for the threshold of motion, based on experiments with 6 particle sizes ($0.5 <= d_{50} <= 3.0$ mm). They calculated the average number, N, of particles in motion per unit area as a function of bed stress.

1. GP1: N=1.
2. GP2: N=10.
3. GP3: N=100.
4. GP4: N=1000.

Vanoni (1964) distinguishes 4 levels for the threshold of motion, for runs with two sediments in a turbulent shear flow (0.0037 mm, 0.102 mm).

1. General
2. Critical
3. Small
4. Negligible

Originally all the measurements with the 0.037 mm sand were below the original Shields curve, which would continue to increase with a decreasing boundary Reynolds number. From **Figure 40** and **Figure 41** it is clear that the Vanoni (1975) measurements also match very well with the new calculated curve for an exposure level of 0.5.

Dey & Raikar (2007) investigated the entrainment of gravel and distinguished 3 levels.

1. Lower threshold level (DL: a few surface particles are disturbed)
2. Medium threshold level (DM: many surface particles are disturbed)
3. Upper threshold level (DU: almost all the surface particles are disturbed, a weakly mobile boundary)

It should be mentioned that the angle of repose (friction angle) is increasing slightly with increasing grain diameter (from 32.5° to 39°), which probably is the reason for a higher transition between the three threshold levels for bigger particles as is also shown in the sensitivity analysis.

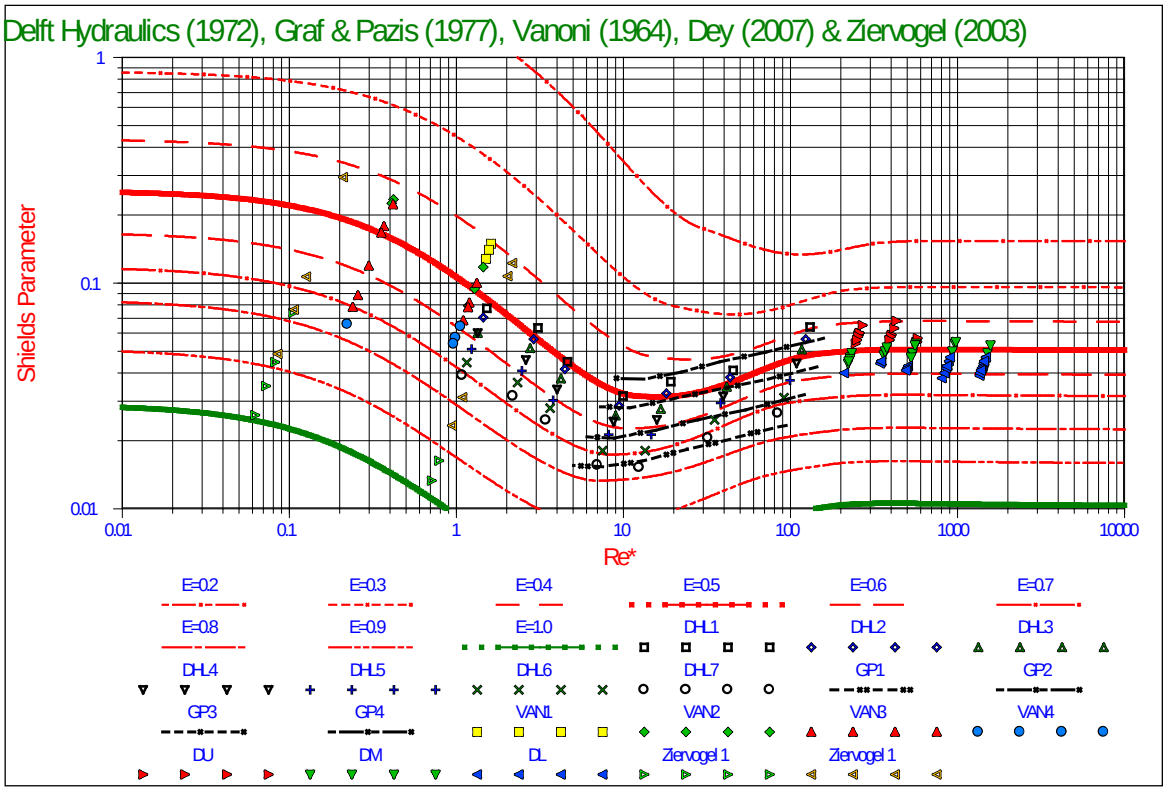

Figure 40: Stages of entrainment

Ziervogel (2003) only distinguished no-erosion (Ziervogel 1) or erosion (Ziervogel 2), his experiments were carried out on sediments with a d_{50} of 20 µm and 130 µm.
From Figure 41 the conclusion can be drawn that incipient motion starts incidentally for exposure levels between 0.65 and 0.85 (protrusion levels between 0.45 and 0.55). Although it would be expected to find incidental incipient motion at higher exposure levels sooner. However these exposure levels will occur much less frequent in a bed of natural grains and may not have been present in the beds used, since often the bed is prepared by a flow over the bed at a low flow rate, until no particles move anymore, moving the grains with the highest protrusion levels to spots in the bed where they will have a lower protrusion rate and thus more resistance to the flow. General transport occurs at exposure levels between 0.4 and 0.5 (protrusion levels between 0.2 and 0.3). On average the general transport occurs at an exposure level of 0.45 which is lower

than the 0.5 on which the theoretical Shields curve is based, the resulting Shields parameter values are thus higher. Combining the data of Delft Hydraulics (1972), Graf & Pazis (1977), Vanoni (1964), Dey & Raikar (2007) and Ziervogel (2003) gives information over a broad range of boundary Reynolds numbers (0.06 to 2000) or as a function of the Bonneville parameter (0.5 to 400).

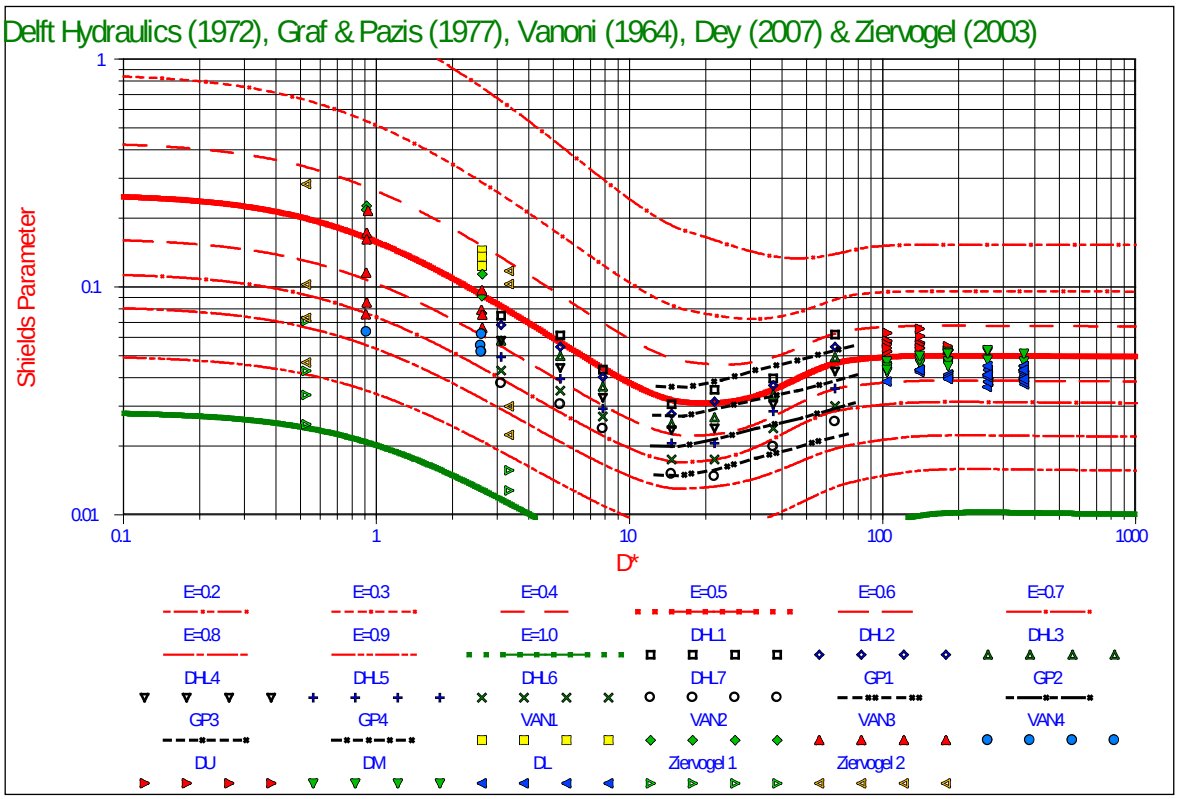

Figure 41: Stages of entrainment as a function of the Bonneville parameter

LAMINAR MAIN FLOW

A sixth point of view is laminar main flow. In the previous paragraphs the words laminar flow and laminar region have always been used for the flow around the top of a particle causing drag, lift and local eddies. The words turbulent flow and turbulent region have been used in the same way. The main flow has always been considered to be turbulent with either a smooth or a rough wall. But the main flow could also be laminar, implying that a viscous sub layer does not exist, since the whole main flow is viscous. This means that theoretically turbulence does not exist. The fact whether the flow is laminar or turbulent depends on the Reynolds number of the main flow. For Reynolds numbers below 2000 (literature also often mentions 2300) the flow is considered laminar, above 2000 it is considered turbulent. Around 2000 a transition zone exists having some turbulence, but not fully developed. The velocity profile in a laminar flow can be determined with:

$$u^+ = \frac{u(y)}{u_*} = \frac{u_* \cdot y}{\nu} \cdot \left(1 - \frac{y}{2 \cdot h}\right) \quad \textbf{(104)}$$

The average flow velocity can be derived from the friction velocity according to:

$$\overline{u(y)} = \frac{1}{3} \cdot \frac{u_*^2 \cdot h}{\nu} \quad \textbf{(105)}$$

Thus, the friction velocity can also be determined from the average flow velocity:

$$u_* = \sqrt{\frac{3 \cdot \overline{u(y)} \cdot \nu}{h}} \quad \textbf{(106)}$$

For small values of **y**, the distance to the wall, equation **(104)** gives the same velocity profile as the one found in the viscous sub layer. This means that the same equations can be applied for calculating the drag forces, while turbulence should be almost absent. Almost, because many of the measurements found in literature are in the transition zone between laminar and turbulent main flow, so some turbulent eddies might exist. The measurements found in literature are those of White (1940), Mantz (1977), Yalin & Karahan (1979), Pilotti & Menduni (2001), Charru et all (2004), Loiseleux et all (2005) and Ourimi et all (2007).

Most measurements were carried out in the 'laminar' region with natural sands, while Pilotti & Menduni (2001) also carried out some tests in the 'turbulent' region with Reynolds numbers of the main flow up to about 3500. **Figure 42** shows the measurements and a number of calculated Shields curves for natural sands, while **Figure 43** shows the results for spheres. The calculated Shields curves are for 0, 1, 2, 3 and 4 times the effect of turbulence intensity (the turbulence intensity factor) based on Nezu & Rodi (1986) for natural sands and one curve for an exposure level of 0.6 and 0.5 times the turbulence intensity for spheres. Analyzing the data points shows that the data points can be grouped in 3 sub-groups. The first sub group are the data points of Pilotti & Menduni (2001) for boundary Reynolds numbers below 1. On average, these data points are below the calculated curves and below the asymptotic value of 0.255 for very small boundary Reynolds numbers. It is difficult to draw any reasonable conclusion from these data points, except that they are not too far from the theoretical curves. The second sub group also consists of data points from Pilotti & Menduni (2001) for boundary Reynolds numbers above 1. These data points are mainly located between the theoretical Shields curves with a turbulence intensity factor of 0 and 1, with a best fit at a turbulence intensity factor of 0.5 to 0.6. The Shields curve for full turbulent main flow has a turbulence intensity factor of 3. There is no real difference between the data points of laminar and turbulent main flow of Pilotti & Menduni (2001) in this region. The third sub group of data points are the data points measured by White (1940), Mantz (1977), Yalin & Karahan (1979) and Loiseleux et all (2005). Loiseleux et all (2005) used spherical particles and observed rolling of many particles at many locations, matching an exposure level of 0.6 (see stages of entrainment) as is shown in **Figure 43**.

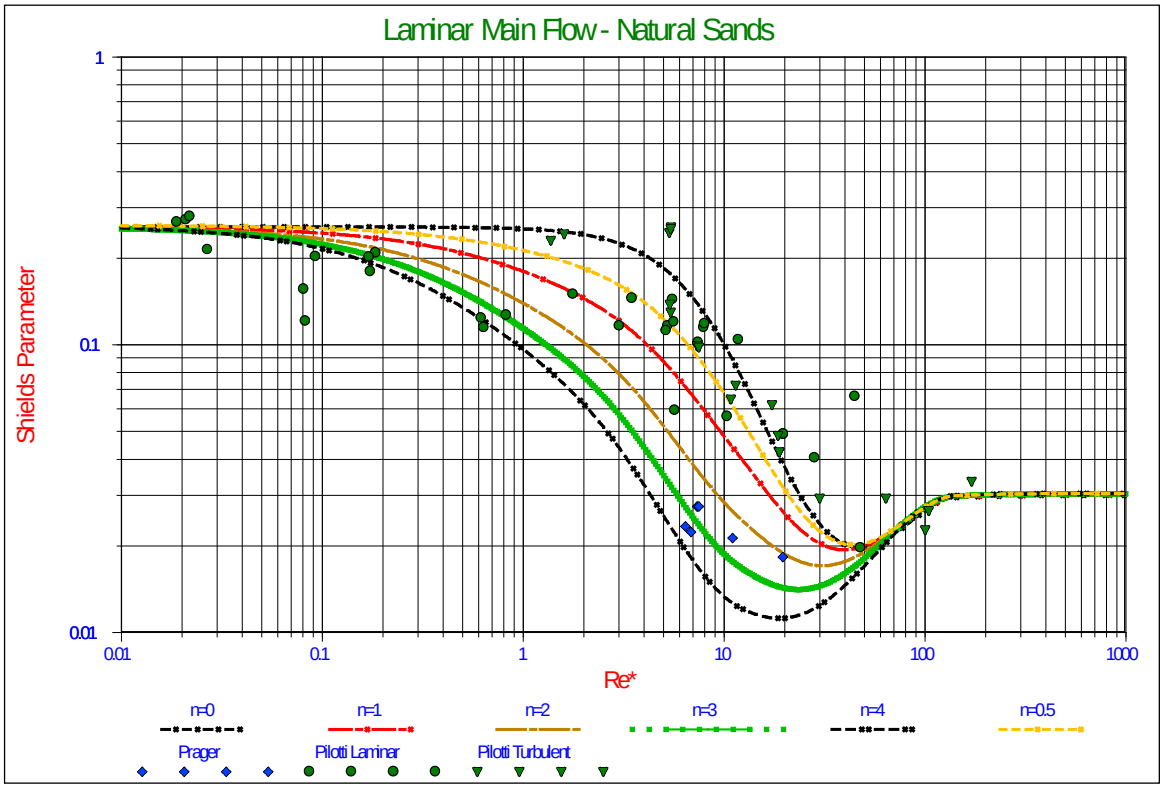

Figure 42: Measurements and calculation in a laminar main flow

For the small boundary Reynolds numbers these measurements tend to have an asymptotic value of about 0.17 which matches the exposure level of 0.6. With a turbulence intensity factor of 0.5 a good fit of the theoretical Shields curve for spheres and the data points is achieved. In general it can be concluded that the measurement of the Shields parameter in a laminar main flow match the calculated curves with a turbulence intensity factor of 0.5 well, while a turbulence intensity factor of 3 should be used for turbulent main flow. Again a good fit has been found between measurements and the calculated Shields curves, but laminar and turbulent main flow should never be mixed in one graph, just like spheres and natural sands and gravels should not be mixed. To show this, the measurements of Prager et all (1996) in turbulent flow, using angular carbonate sands, are shown in **Figure 42** as well. These measurements range for boundary Reynolds numbers from 7 to 20 and Shields numbers from 0.018 to 0.028, matching the Shields curve for natural sands with a turbulence intensity factor of 3. Govers (1987) carried out experiments in both laminar and turbulent main flow. The data can be found in **Figure 43**. The data points for laminar flow tend to give slightly higher Shields values than the data points of White (1940), Mantz (1977), Yalin & Karahan (1979) and Loiseleux et al. (2005). The data fit very well using an exposure level of 0.53 and a turbulence intensity of 0.50. The data points for turbulent flow match very well with the Shields curve using an exposure level of 0.53 and a turbulence intensity of 2.3. The latter can be explained by the fact that the Reynolds numbers of the main flow were not high and turbulence might not have been fully developed.

For large boundary Reynolds numbers (above 30), still the model for turbulent main flow is applied for calculating the Shields curves, since the main flow Reynolds numbers of the measurements in this range were above 2300.

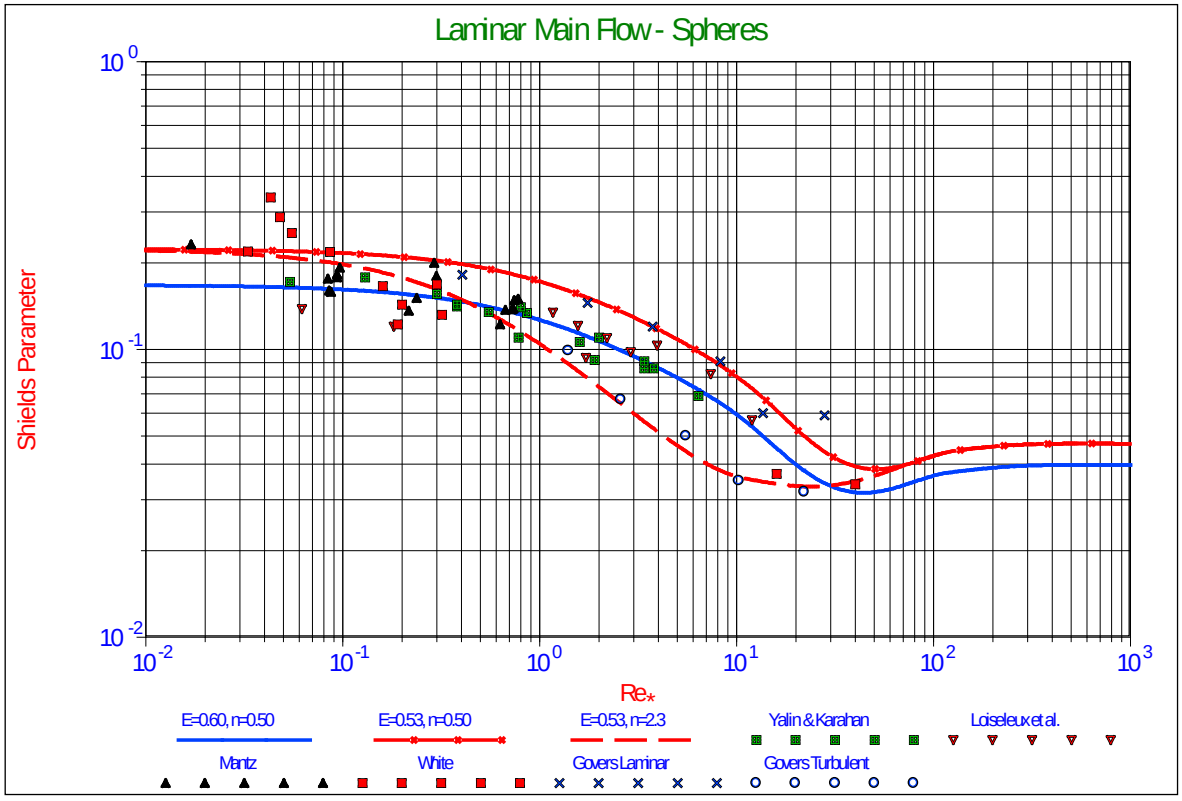

Figure 43: Spheres in a laminar main flow

CONCLUSIONS AND DISCUSSION

The model developed in Part A has been verified and validated from 6 points of view.

1. The traditional Shields diagram, a sensitivity analysis
2. Exposure and protrusion levels
3. Shear velocity and shear stress
4. The ratio between the friction velocity and the terminal settling velocity
5. Stages of entrainment
6. Laminar main flow

The 3 possible mechanisms for the entrainment of particles, sliding, rolling and lifting, are considered, based on a set of equations where the exposure level and the surface averaged drag force acting point are an integral part of these equations. The sensitivity analysis shows that most of the scatter of the measured data points in the Shields diagrams can be explained by applying a range of the friction angle from 25° to 35°, a turbulence intensity factor from n=2 to n=4 for the laminar region (particles in the viscous sub layer), a lift coefficient from $\mathbf{C_L = 0.7 \cdot 0.445}$ to $\mathbf{C_L = 0.445}$ in the turbulent region and applying a drag coefficient for spheres and natural sands and gravels. It must be mentioned here that some of the measured Shields values used in the sensitivity analysis were the result of laminar main flow, resulting in more scatter. Applying the drag coefficient of natural sands and gravels may reduce the value of the Shields parameter to

about 50%-60% in the transition and the turbulent region, explaining for the statement found in literature that for engineering purposes in real sands and gravels the Shields parameter should be divided by 2. In the laminar region however this is not the case, since the drag coefficient follows or almost follows the Stokes law for very small boundary Reynolds numbers. The Shields curves calculated for different exposure and protrusion levels match the findings of Fenton & Abbot (1977), Chin & Chiew (1993) and Coleman (1967) well, assuming a sliding mechanism of entrainment for exposure levels up to 0.6 and a rolling mechanism for larger exposure levels. The lifting mechanism might occur for single particles in a bed where all the other particles are fixed (glued) and the rolling mechanism cannot occur. The surface factor used for the dependency of the lift coefficient in relation to the exposure level has proven to give correct results in the turbulent region. Additional measured data, as also being used by Wiberg & Smith (1987A) and Julien (1995) , of the shear velocity (friction velocity) and the bottom shear stress, give a high correlation with the calculated curve for an exposure level of 0.5 and the sliding entrainment mechanism for spheres. Other additional measurements, as carried out by Liu (1957), of the ratio between the friction velocity and the terminal settling velocity give an almost perfect match with the Shields curve as calculated with an exposure level of 0.5 and the sliding entrainment mechanism. There has always been discussion amongst the different researchers about the definition of the stage of entrainment related to the Shields curve. In the past, when the extrapolated curve based on the original data of Shields was used, the measured data did not always match with this curve, because this extrapolated curve did not have an asymptotic value for very small boundary Reynolds numbers. Especially the measurements of Vanoni (1975) with the 0.037 mm grains fell below the extrapolated Shields curve. The new model as explained in this paper has an asymptotic value of about 0.25 for very small boundary Reynolds numbers, resulting in a different shape of the Shields curve. The different measurements all give the same conclusion, the Shields curve describes critical to general transport, with general transport at an exposure level of about 0.45, whilst a measurable incipient motion starts at an exposure level of about 0.7. Most experiments on the entrainment of particles have been carried out in a turbulent main flow, however some experiment were carried out in a laminar main flow. Buffington & Montgomery (1997) give a nice overview of most of the experiments carried out until 1997 and show the data of White (1940) and Yalin & Karahan (1979) of experiments carried out in a laminar main flow. Later Pilotti & Menduni (2001) carried out experiments in a laminar main flow and in the transition region between laminar and turbulent main flow. From these data it is clear that entrainment in a laminar main flow differs from entrainment in a turbulent main flow. Although for very small boundary Reynolds numbers there is not much difference theoretically, in the region of boundary Reynolds numbers from 0.1 to around 70 there is a big difference and the two regimes should not be mixed. Yalin & Karahan (1979) already proposed a separate equation for laminar main flow, but their measurements were limited to boundary Reynolds numbers of about 7. The Pilotti & Menduni (2001) experiments extended to boundary Reynolds numbers of about 70 and show the difference between the laminar and turbulent regimes clearly. Comparing the measured data with the theory developed results in a good correlation between the theory and the data if a turbulence intensity factor of 0.5 is applied for an exposure level of 0.5 and the sliding entrainment mechanism. Using the data from laminar main flow experiments to validate a turbulence based theory like Luckner & Zanke (2007) did in their fig. 1 (the laminar experiments of Pilotti & Menduni and Yalin & Karahan are used), gives a lot of scatter and a low correlation, which is obvious. It is proposed to distinguish 4 different Shields curves:

1. The Shields curve based on spheres in a turbulent main flow.
2. The Shields curve based on natural sands and gravels in a turbulent main flow.
3. The Shields curve in a laminar main flow for spheres (n=0.5).
4. The Shields curve in a laminar main flow for natural sands and gravels (n=0.5).

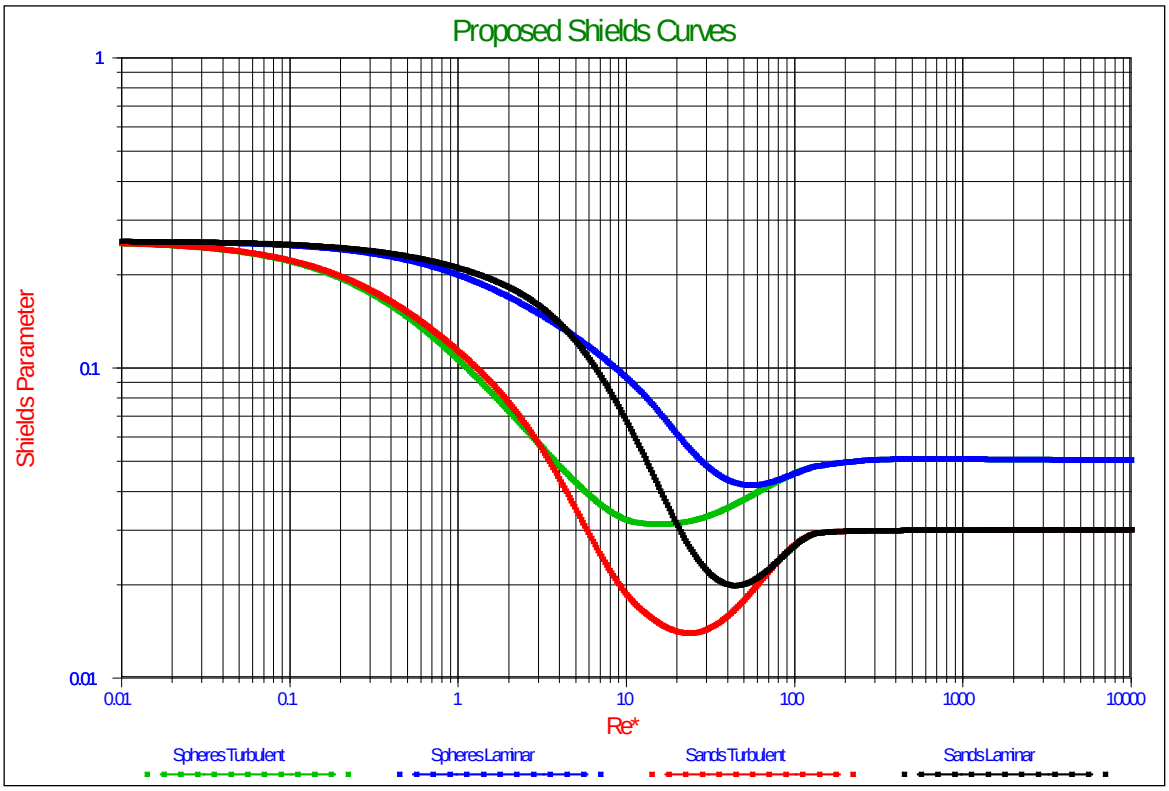

Figure 44: The proposed Shields curves

The two curves for laminar flow exist for boundary Reynolds numbers of about 70, for Reynolds numbers above 70 a normal turbulent rough flow is assumed, since the Reynolds numbers of the main flow will be far above 2300. The general conclusions of this research are:

- The basic Shields curve can be determined by applying the sliding entrainment mechanism, with a friction angle of 30°, an exposure level of 0.5 (protrusion level of 0.3), a turbulence intensity factor of n=3, a lift coefficient of 0.415 and the drag coefficient of spheres.
- Using a reasonable bandwidth for the different properties, a lower, medium and upper level for the Shields curve have been formed, explaining for most of the scatter of the data used.
- For natural sands and gravels a modified drag coefficient should be applied, based on the angularity of the particles.
- In the laminar region entrainment is dominated by drag and turbulence, while in the turbulent region this is dominated by drag and lift.
- Up to an exposure level of 0.6 sliding is the main entrainment mechanism, while for higher exposure levels rolling will occur.

- Laminar and turbulent main flow result in two different entrainment curves, based on the presence of turbulence. For laminar main flow a turbulence intensity factor of 0.5 has been found to correlate with the measurements.
- The new model developed correlates well with datasets of many independent researchers.

ACKNOWLEDGEMENTS

The author wishes to thank Ulrich Zanke and Thomas Luckner for their explanations and sending papers and a thesis, Pierre Julien and Junke Guo for their explanations, Arno Talmon for the many discussions on the subject of erosion and velocity distributions, Jerry Westerweel and Wim Paul Breugem for their point of view on turbulence and last but not least my wife Thi Kim Thuy for being very patient every time I was very absent minded ☺.

LIST OF SYMBOLS USED

$\mathbf{A}$	Surface or cross section	m^2
$\mathbf{A_{Lam}}$	Interpolation constant for the laminar region	-
$\mathbf{A_{Turb}}$	Interpolation constant for the turbulent region	-
$\mathbf{C_D}$	Drag coefficient	-
$\mathbf{C_L}$	Lift coefficient	-
$\mathbf{d}$	Sphere, particle or grain diameter	m
$\mathbf{D_*}$	The Bonneville parameter or non-dimensional grain diameter	-
$\mathbf{E}$	Exposure level	-
$\mathbf{f_D, f_{Drag}}$	Fraction of cross section exposed to drag	-
$\mathbf{f_L, f_{Lift}}$	Fraction of top surface exposed to lift	-
$\mathbf{F_D}$	Drag force	N
$\mathbf{F_L}$	Lift force	N
$\mathbf{F_w}$	Weight of a particle	N
$\mathbf{g}$	Gravitational constant	9.81 m/sec^2
$\mathbf{h}$	Thickness of the layer of water	m
$\mathbf{k_s}$	Roughness often chosen equal to the particle diameter	m
$\mathbf{k_s^+}$	The non-dimensional roughness or roughness Reynolds number	-
ℓ	The point of action of the drag force	-
ℓ	Mixing length	m
$\ell_{\mathbf{Drag}}$	Drag point of action	-
$\ell_{\mathbf{Lift}}$	Lift point of action	-

$\ell_{\mathbf{Lever-D}}$	Additional lever arm for drag	-
$\ell_{\mathbf{Lever-L}}$	Additional lever arm for lift	-
n	Turbulence intensity factor	-
P	Probability used in interpolation	-
p/d	Relative protrusion level	-
Q	Factor used in interpolation	-
R	Radius of sphere, particle or grain	m
$\mathbf{R_d}$	The relative submerged specific density	-
$\mathbf{Re_D}$	The particle drag Reynolds number	-
$\mathbf{Re_*}$	Boundary Reynolds number	-
$\mathbf{Re_p}$	The particle Reynolds number	-
$\mathbf{S_*}$	The Grant & Madsen parameter	-
u	Time and surface averaged velocity	m/sec
$\mathbf{u_*}$	Friction velocity	m/sec
$\mathbf{u^+}$	Non dimensional time and surface averaged velocity	-
$\mathbf{u_{r.m.s.}}$	Turbulence intensity	m/sec
$\mathbf{u'_{r.m.s.}}$	Modified turbulence intensity	m/sec
$\mathbf{u'_{n\cdot r.m.s.}}$	The n^{th} moment of the modified turbulence intensity	m/sec
$\mathbf{u_{eff.}}$	The effective modified turbulence intensity	m/sec
$\mathbf{u^+_{r.m.s.}}$	Non dimensional turbulence intensity	-
$\mathbf{u^+_{total}}$	Non dimensional total velocity	-
V	Volume	m^3

y	Distance to the wall or virtual bed level	m
y_0	Integration constant	m
y^+	Non dimensional distance to the wall (Reynolds number)	-
α	The velocity factor at a certain exposure level	-
δ_v	Thickness of the viscous sub layer	m
δ_v^+	The non-dimensional thickness of the viscous sub layer	11.6
κ	Von Karman constant	0.412
ρ	Fluid density	kg/m^3
ρ_f	Fluid density	kg/m^3
ρ_s	Solids density	kg/m^3
ρ_w	The density of water or fluids	kg/m^3
ρ_q	The density of quarts or solids	kg/m^3
ϕ	Internal friction angle/angle of repose	°
ϕ_0	The Coulomb friction angle quarts-quarts	°
ϕ_0	Pivot angle in Wiberg & Smith (1987A)	°
ϕ_{Roll}	Friction angle for rolling resistance	°
Ψ	The dilatation angle	°
Ψ	The pivot angle	°
θ	The Shields parameter or non-dimensional shear stress	-
θ_5	The Shields parameter for $\xi = 5$	-
θ_{70}	The Shields parameter for $\xi = 70$	-
τ	Total shear stress	Pa

τ_t	Turbulent shear stress	Pa
τ_v	Viscous shear stress	Pa
τ_b	Bed shear stress	Pa
ν	Kinematic viscosity	m^2/sec
μ	Friction coefficient usually the tangent of the internal friction angle	-
μ_{Roll}	Equivalent friction coefficient for rolling	-
ξ	The non-dimensional distance of the top of the sphere to the virtual bed level	-

REFERENCES

Bonneville, R. (1963). *essais de synthese des lois debut d'entrainment des sediment sous l'action d'un courant en regime uniform.* Chatou: Bulletin Du CREC, No. 5.

Brownlie, W. (1981). *Compilation of alluvial channel data: laboratory and field, Technical Report KH-R-43B.* Pasadena, California, USA: California Institute of Technology.

Buffington, J. M. (1999). The legend of A.F. Shields. *Journal of Hydraulic Engineering, 125*, 376–387.

Buffington, J. M., & Montgomery, D. R. (1997). A systematic analysis of eight decades of incipient motion studies, with special reference to gravel-bedded rivers. *Water Resources Research, 33*, 1993-2029.

Charru, F., Mouilleron, H., & Eiff, O. (2004). Erosion and deposition of particles on a bed sheared by a viscous flow. *Journal of fluid mechanics, Vol. 519.*, 55-80.

Chepil, W. (1958). The use of evenly spaced hemispheres to evaluate aerodynamic force on a soil failure. *Transaction of the American Geophysics Union, Vol. 39(3)*, 397-404.

Chin, C. O., & Chiew, Y. M. (1993). Effect of bed surface structure on spherical particle stability. *Journal of Waterway, Port, Coastal and Ocean Engineering, 119(3)*, 231–242.

Coleman, N. L. (1967). A theoretical and experimental study of drag and lift forces acting on a sphere resting on a hypothetical stream bed. *International Association for Hydraulic Research,12th Congress, 3*, pp. 185-192.

Coleman, N. L., & Ellis, W. M. (1976). Model study of the drag coefficient of a streambed particle. *Federal Interagency Sedimentation Conference*, (pp. 4-12). Denver, Colorado.

Dey, S. (1999). Sediment threshold. *Applied Mathematical Modelling*, 399-417.

Dey, S., & Raikar, R. (2007). Characteristics of loose rough boundary streams at near threshold. *Journal of Hydraulic Engineering, ASCE.*, 288-304.

DHL. (1972). *Systematic Investigation of Two Dimensional and Three Dimensional Scour, Report M648/M863.* Delft, Netherlands: Delft Hydraulics Laboratory.

Dittrich, A., Nestmann, F., & Ergenzinger, P. (1996). Ratio of lift and shear forces over rough surfaces. *Coherent flow structures in open channels.*, 126-146.

Egiazarof, I. (1965). Calculation of non-uniform sediment concentrations. *Journal of the Hydraulic Division, ASCE, 91(HY4)*, 225-247.

Engelund, F., & Hansen, E. (1967). A monograph on sediment transport to alluvial streams. *Copenhagen: Technik Vorlag*.

Everts, C. (1973). Particle overpassing on flat granular boundaries. *Journal of Waterways, Harbors, & Coastal Engineering, ASCE Vol. 99(WW4).*, 425-438.

Fenton, J. D., & Abbott, J. E. (1977). Initial movement of grains on a stream bed: The effect of relative protrusion. *Proceedings of Royal Society, 352(A)*, pp. 523–537. London.

Garcia, M. H. (2008). *Sedimentation Engineering* (Vol. 110). ASCE Manuals & Reports on Engineering Practise No. 110.

Govers, G. (1987). Initiation of motion in overland flow. *Sedimentology (34)*, 1157-1164.

Graf, W. H., & Pazis, G. C. (1977). Les phenomenes de deposition et d'erosion dans un canal alluvionnaire. *Journal of Hydraulic Research, 15*, 151-165.

Grass, A. J. (1970). The initial instability of fine bed sand. *Journal of Hydraulic Division, ASCE, 96(3)*, 619-632.

Guo, J., & Julien, P. (2007). Buffer law and transitional roughness effects in turbulent open-channel flows. *5th International Symposium on Environmental Hydraulics, 4-7 December 2007.* Tempe, Arizona, USA: ISEH.

Hinze, J. (1975). *Turbulence.* McGraw Hill Book company.

Hjulstrøm, F. (1935). Studies of the morphological activity of rivers as illustrated by the River Fyris. *Bulletin of the Geological Institute, 25*, 221–527. University of Uppsala.

Hjulstrøm, F. (1939). Transportation of debris by moving water, in Trask, P.D., ed., Recent Marine Sediments. *A Symposium: Tulsa, Oklahoma, American Association of Petroleum Geologists*, (pp. 5-31). Tulsa, Oklahoma.

Hofland, B. (2005). *Rock & Roll.* Delft, The Netherlands: PhD Thesis, Delft University of Technology.

Ikeda, S. (1982). Incipient motion of sand particles on side slopes. *Journal of the Hydraulic division, ASCE, 108*(No. HY1).

Iwagaki, Y. (1956). Fundamental study on critical tractive force. *Transactions of the Japanese Society of Civil Engineers, Vol. 41*, 1-21.

Julien, P. (1995). Erosion and sedimentation. *Cambridge University Press*.

Kim, J., Moin, P., & Moser, R. (1987). Turbulence statistics in fully developed channel flow at low Reynolds number. *Journal of Fluid Mechanics, 177*, 133-166.

Kirkby, M., & Statham, I. (1975). Surface stone movement and scree formation. *Journal of Geology, Vol. 83.*, 349-362.

Kramer, H. (1935). Sand mixtures and sand movement in fluvial levels. *Transaction of ASCE 100.*, 798-838.

Kurihara, M. (1948). On the critical tractive force. *Research Institute for Hydraulic Engineering*, Report No. 3, Vol. 4.

Liu, H. (1957). Mechanics of sediment ripple formation. *Journal of the Hydraulics Division, Vol. 83, No. 2, March/April.*, 1-23.

Liu, Z. (2001). Sediment Transport. *Lecture notes*. Aalborg University.

Loiseleux, T., Gondret, P., Rabaud, M., & Doppler, D. (2005). Onset of erosion and avalanche for an inclined granular bed sheared by a continuous laminar flow. *Physics of fluids, Vol. 17*, 1-9.

Luckner, T. (2002). Zum Bewegungsbeginn von Sedimenten. *Dissertation.* Darmstadt, Germany: Technische Universitat Darmstadt.

Luckner, T., & Zanke, U. (2007). An analytical solution for calculating the initiation of sediment motion. *International Journal of sediment Research, Vol. 22, No. 2.*, 87-102.

Madsen, O., & Grant, W. (1976). *Sediment transport in the coastal environment.* Cambridge, Massachusetts, USA: Technical report 209, M.I.T.

Mantz, P. A. (1977). Incipient transport of fine grains and flakes by fluids—Extended Shields diagram. *Journal of Hydraulic Division, ASCE, 103(6)*, 601-615.

Marsh, N. A., Western, A. W., & Grayson, R. B. (2004, July 1). Comparison of Methods for Predicting Incipient Motion for Sand Beds. *Journal of Hydraulic Engineering, 130*(No. 7, July 1, 2004)).

Miedema, S. (2010A). Constructing the Shields Curve: Part A Fundamentals of the Sliding, Rolling and Lifting Mechanisms for the Entrainment of Particles. *Submitted to the Journal of Hydraulic Engineering*.

Miller, M., McCave, I., & Komar, P. (1977). Threshold of sediment motion under unidirectional currents. *Sedimentology, Vol. 24.*, 507-527.

Morsi, S., & Alexander, A. (1972). An investigation of particle trajectories in two-phase flow systems. *Journal of Fluid Mechanics, Vol. 55*, 193-208.

Naden, P. (1987). An erosion criterion for gravel bed rivers. *Earth Surface and Landforms, Vol. 12.*, 83-93.

Nakagawa, H., & Nezu, I. (1977). Prediction of the contribution to the Reynolds stress from the bursting events in open-channel flows. *Journal of Fluid Mechanics, 80*, 99–128.

Neil, C. (1967). Mean velocity criterion for scour of coarse uniform bed material. *Proceedings of the twelfth I.H.A.R. Congress.*, (pp. 46-54).

Nezu, I., & Nakagawa, H. (1993). *Turbulence in Open Channel Flows.* A. A. Balkema.

Nezu, I., & Rodi, W. (1986). Open-channel flow measurements with a laser Doppler anemometer. *Journal of Hydraulic Engineering . ASCE, 112*, 335–355.

Nino, Y., Lopez, F., & Garcia, M. (2003). Threshold of particle entrainment into suspension. *Sedimentology, Vol. 50.*, 247-263.

Ourimi, M., Aussillous, P., Medale, M., Peysson, Y., & Guazzelli, E. (2007). Determination of the critical Shields number for particle erosion in laminar flow. *Physics of fluids, Vol. 19.*, 1-4.

Paintal, A. S. (1971). Concept of critical shear stress in loose boundary open channels. *Journal of Hydraulic Research, 8*(1), 91-109.

Pilotti, M., & Menduni, G. (2001). Beginning of sediment transport of incoherent grains in shallow shear flows. *Journal of Hydraulic Research, Vol. 39, No. 2.*, 115-124.

Prager, E., Southard, J., & Vivoni-Gallart, E. (1996). Experiments on the entrainment threshold of well-sorted and poorly sorted carbonate sands. *Sedimentology, Vol. 43.*, 33-40.

Reichardt, H. (1951). Vollstandige Darstellung der Turbulenten Geswindigkeitsverteilung in Glatten Leitungen. *Zum Angew. Math. Mech., 3(7)*, 208-219.

Rijn, L. v. (1984). Sediment transport: Part I: Bed load transport. *Journal of Hydraulic Engineering, Vol. 110(10)*, 1431-1456.

Rijn, L. v. (1993). *Principles of sediment transport in rivers, estuaries and coastal seas.* Utrecht & Delft: Aqua Publications, The Netherlands.

Rijn, L. v. (2006). *Principles of sediment transport in rivers, estuaries and coastal areas, Part II: Supplement 2006.* Utrecht & Delft: Aqua Publications, The Netherlands.

Saffman, P. G. (1965). The lift on small sphere in a slow shear low. *Journal of Fluid Mechanics, 22*, 385-400.

Schlichting, H. (1968). *Boundary layer theory.* 6th ed. New York: McGraw-Hill.

Shields, A. (1936). Anwendung der Aehnlichkeitsmechanik und der Turbulenzforschung auf die Geschiebebewegung. *Mitteilung der Preussischen Versuchsanstalt fur Wasserbau und Schiffbau, Heft 26, Berlin.* Belin.

Simons, D. (1957). *Theory and design of stable channels in alluvial material.* PhD thesis: Colorado State University.

Soulsby, R., & Whitehouse, R. (1997). Threshold of sediment motion in coastal environment. *Proceedings Pacific Coasts and Ports.* (pp. 149-154). Christchurch, New Zealand: University of Canterbury.

Stevenson, P., Cabrejos, F. J., & Thorpe, R. B. (2002). Incipient motion of particles on a bed of like particles in hydraulic and pneumatic conveying. *Fourth World Congress of Particle Technology, Sydney, 21st–25th July (paper 400).* Sydney.

Stevenson, P., Thorpe, R. B., & Davidson, J. F. (2002). Incipient motion of a small particle in the viscous boundary-layer at a pipe wall. *Chemical Engineering Science, 57,* 4505–4520.

Sundborg, A. (1956). The River Klarålven: Chapter 2. The morphological activity of flowing water erosion of the stream bed. *Geografiska Annaler, 38,* 165-221.

Swamee, P. K. (1993). Critical depth equations for irrigation canals. *Journal of Irrigation and Drainage Engineering, ASCE.*, 400-409.

Tison, L. (1953). Studies of the critical tractive force of entrainment of bed materials. *Proceedings of the fifth I.A.H.R. Congress.*, (pp. 21-35).

Turton, R., & Levenspiel, O. (1986). A short note on the drag correlation for spheres. *Powder technology Vol. 47,* 83-85.

USWES. (1936). *Flume tests made to develop a synthetic sand which will not form ripples when used in movable bed models.* Vicksburg, Mississippi, USA: United States Waterways Experiment Station, tech. Memo 99-1.

Vanoni, V. A. (1975). *Sedimentation Engineering: American Society of Civil Engineers, Manuals and Reports on Engineering Practice. No. 54. P.745.*

White, C. M. (1940). The equilibrium of grains on the bed of a stream. *Proceedings Royal Society of London, A174,* pp. 322-338.

White, S. (1970). Plane bed thresholds of fine grained sediments. *Nature Vol. 228.*, 152-153.

Wiberg, P. L., & Smith, J. D. (1987A). Calculations of the critical shear stress for motion of uniform and heterogeneous sediments. *Water Resources Research, 23*(8), 1471–1480.

Wiberg, P., & Smith, J. (1987B). Initial motion of coarse sediment in streams of high gradient. *Proceedings of the Corvallis Symposium.* IAHS Publication No. 165.

Wikipedia. (n.d.). Retrieved from Wikipedia: http://en.wikipedia.org/wiki/Erosion

Wu, W., & Wang, S. (2006). Formulas for sediment porosity and settling velocity. *Journal of Hydraulic Engineering, 132(8),* 858-862.

Yalin, M. S., & Karahan, E. (1979). Inception of sediment transport. *ASCE Journal of the Hydraulic Division, 105,* 1433–1443.

Zanke, U. C. (2001). *Zum Einfluss der Turbulenz auf den Beginn der Sedimentbewegung.* Darmstadt, Germany: Mitteilungen des Instituts fur Wasserbau und Wasserwirtschaft der TU Darmstadt, Heft 120.

Zanke, U. C. (2003). On the influence of turbulence on the initiation of sediment motion. *International Journal of Sediment Research, 18*(1), 17–31.

Ziervogel, K. (2003). *Aggregation and transport behavour of sediment surface particles in Mecklenburg Bight, south western Baltic Sea affected by biogenic stickiness.* Rostock: PhD Thesis, Universitat Rostock, Germany.

NOTES FOR CONTRIBUTORS

General

The Journal of Dredging Engineering is a peer-reviewed practice periodical on dredging engineering topics. Prospective authors should **email an MS word version** of their manuscript to the following address:

Dr. Ram K. Mohan, Anchor QEA, LLC
6 Penns Trail, Suite 201, Newtown, PA 18940, USA
Phone: 267-753-6301; Fax: 267-753-6306
email: rmohan@anchorqea.com

Authors should obtain all necessary approvals for publication from employers or others involved, before submission of the paper. Submission of a manuscript implies that it is not under consideration for publication elsewhere and that original, previously unpublished work is being presented. **The paper should be free from evident commercialism or private interest** Copyright will be the property of the Western Dredging Association, but the author will be granted permission to reprint the paper and third party requests will be passed on to the authors. **Papers should be concisely written and not exceed 20 total printed pages including figures**. The papers will be reproduced directly from the camera-ready manuscripts provided by the authors and bound into a volume. Please give the manuscript preparation instructions to the person responsible for the preparation of the text.

Keywords

Please provide 5 keywords that are not already contained in the title, on a separate sheet of paper.

MANUSCRIPT PREPARATION

Order of contents

Title, author(s), affiliations, addresses, countries
Abstract (not to exceed 300 words).
Introduction, main body, and following text, conclusions, nomenclature (if necessary), and references. 5 keywords that are not already contained in the title (on a separate sheet of paper).
Refer to a previous issue of the journal for general guidelines on format.

Preparation of the text

The text should be submitted on unlined white 8½ x 11 inch paper with **single line spacing**, and top and side margins of 1 inch. Use full justification. **The image area or block of text will**

then be 6.5 x 9.0 inch. The bottom margin should be 1½ inch. Page numbers should be marked in pencil and placed at the bottom center of each page. **Do not leave additional margins. Do not use company letterhead paper.**

Fonts

If possible please use proportional, serif font such as Times New Roman 12 point. If such fonts are not available, use a 12 pitch typeface and work to the margins indicated above. Do not use headers or footers or draw a frame around your text. Use a letter quality or laser printer. **Do not use a dot matrix printer**. It may be possible for us to print your text directly from your disc. In this case we shall still require hard copies of your text. The preferred word processing program is Microsoft Word 6.0 or Word 97. If using other programs please also save your text as ASCII files. Discs should be labeled with the file name in both word processed and ASCII forms, the word processing package used, and the operating system.

Headings

Headings should be typed in bold capital letters centered and followed by a double space. Bold capitals and lower case letters should be used for subheadings, which should be preceded and followed by a double space as illustrated by these instructions. Sub-subheadings should use bold capitals and lower case letters and placed at the start of the paragraph.

Equations

All symbols must be defined in the nomenclature section that follows the conclusions. The SI system of units should be used. If units other than SI units are included, they should be given in parenthesis after the relevant SI unit. Equations should be successively numbered (in parenthesis) flush with the right-hand margin (see example below).

$$y = a + b + cx^2 \qquad (1)$$

References

References in the text should be given as: Smith (1988), (Smith, 1988) or (Jones et al., 1986). References should be listed alphabetically in the References section at the end of the paper. Give the names and initials of all authors, followed by the title of the article and publication, the publisher and the year of publication. References to conference papers or proceedings should include the name of the organizers. References to articles published in journals should also include the name of the journal, the number of the issue and page numbers (see example below). References to publications in a foreign language should give all details in the original language followed by a translation of the title.

Hunt, J.B. (1995). *"Environmental Dredging"*. Smith & Son, Inc., New York, NY.

Donegan, T.M., and Dinicola, W.J. (1986). *"Turbidity Associated With Dredging Operations"*. Technical Report, XYZ Consultants, Inc., Baltimore, MD., 60 p.

Jones, F., Doe, A., Hart, E.J.E., and Next, J.P.J. (1986). "*The Design of Dredged Material Disposal Sites.*"

Proceedings XIVth World Dredging Congress, CEDA, Amsterdam, The Netherlands, pp. 350-368.

White, F.K. and Jones, J.M. (1991). *"The Analysis of Flow Fields Around Dragheads.*" Journal of Waterway, Port, Coastal and Ocean Engineering, ASCE, Vol. 121, No. 5, pp. 1-16.

Page Numbers

Page numbers should be marked in pencil and placed at the bottom center of each page.

Figures and Tables

High quality figures and tables should be incorporated into the body of the text. Figures must not be placed at the end of the paper. Leave spaces for photographs. Figure captions should be below the figure; table captions should be above the table.

Line Drawings

The lines and lettering on the figures should be clearly legible. If originals cannot be supplied, ONLY BLACK AND WHITE COPIES OF VERY HIGH QUALITY are suitable for reproduction. PENCIL AND PHOTOCOPIES OR COPIES WITH A BACKGROUND COLOR ARE NOT SUITABLE.

Photographs

Photographs must be sharp, high contrast, glossy prints. Please use a pencil to indicate the title of the paper, figure number and title and top edge on the back of each photograph. Paste in the photographs where they should appear in the final manuscript. Place captions under the photograph as part of the text.

This page is intentionally left blank.

This page is intentionally left blank.

WEDA HOME PAGE INTERNET ADDRESS

WWW.WESTERNDREDGING.ORG

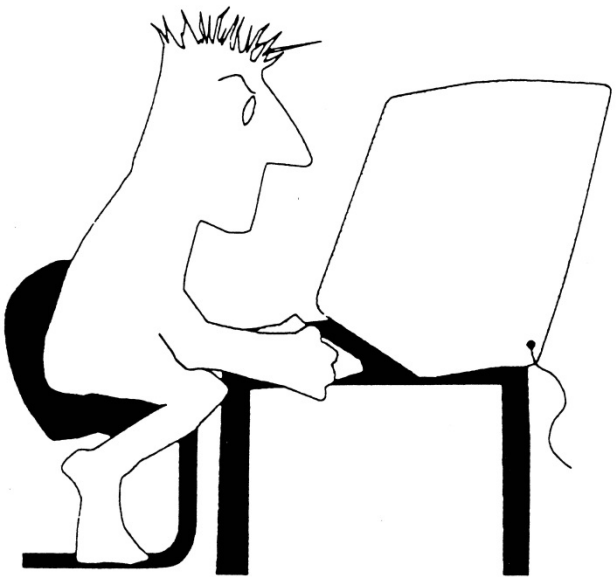

WEDA EMAIL ADDRESS

WEDA@COMCAST.NET

Dredging Creates a Strong Economy and Cleaner Environment